Eur. Phys. J. C (2025) 85:1441
https://doi.org/10.1140/epjc/s10052-025-14916-1

THE EUROPEAN PHYSICAL JOURNAL C

Regular Article - Experimental Physics

Estimation of backgrounds from jets misidentified as τ-leptons using the Universal Fake Factor method with the ATLAS detector

ATLAS Collaboration[⋆]

CERN, 1211 Geneva 23, Switzerland

Received: 7 February 2025 / Accepted: 13 October 2025

Abstract Processes with τ-leptons in the final state are important for Standard Model measurements and searches for physics beyond the Standard Model. The ATLAS experiment at the Large Hadron Collider observes τ-leptons produced in proton–proton collisions only through their decay products. Data analyses involving hadronically decaying τ-leptons face challenges due to backgrounds from jets misidentified as τ-leptons that are not modelled reliably by Monte Carlo simulations. Data-driven methods such as the fake-factor method allow such misidentified backgrounds to be predicted by measuring transfer factors, known as fake factors, in data from dedicated regions. This paper describes a refined technique for determining the fake factors, the Universal Fake Factor method. It evaluates the fake factors for a signal region by using fake factors from samples enriched in different sources of jets misidentified as τ-leptons (light-quark, gluon, b-quark, and pile-up jets). Each fake factor is calculated as a linear combination of fake factors measured in these different enriched samples. For the full Run 2 data set, the systematic uncertainty of the calculated fake factors, evaluated using $W(\mu\nu)$ enriched event sample, ranges from 15 to 35% depending on the τ-lepton's transverse momentum and charged-particle decay multiplicity.

Contents

1 Introduction

Due to their short lifetime, τ-leptons produced in proton–proton (pp) collisions at the Large Hadron Collider (LHC) can be observed in the ATLAS detector only in the form of their decay products. The τ-lepton decays either leptonically (τ_{lep}) or hadronically (τ_{had}), with corresponding branching fractions of 35% and 65%. Because neutrinos are not detected, only hadrons can be reconstructed as visible τ_{had} decay products ($\tau_{\text{had-vis}}$). In analyses with $\tau_{\text{had-vis}}$ in the final state, jets misidentified as $\tau_{\text{had-vis}}$ (fakes) constitute a sizeable source of background. Monte Carlo (MC) generators cannot properly model the 'fake' background because such modelling requires detailed simulation of soft jet properties and the detector's response to hadrons. It is also challenging to generate enough events with misreconstructed $\tau_{\text{had-vis}}$ from various sources to match the integrated luminosity of the data. Data-driven methods are therefore preferred. This paper describes and generalizes the fake-factor (FF) method [1] that has been applied successfully in many ATLAS and CMS analyses [2–15]. The FF method has also been used to estimate the background due to jets misidentified as electrons or muons [16].

The FF method estimates the fake background by measuring the transfer factors that allow the background in a signal region (SR) to be predicted by using data from a dedicated control region (CR). In this paper, the only difference between the SR and the CR is a single selection criterion: the $\tau_{\text{had-vis}}$ identification (ID), as described in Sect. 4, which

⋆ e-mail: atlas.publications@cern.ch

Published online: 19 December 2025

is inverted in the CR definition. Due to this similarity, the CR is treated as part of the SR and referred to as the antiID subregion of the SR. Its complement, where the $\tau_{\text{had-vis}}$ ID requirement is satisfied, is called the ID subregion of the SR. The transfer factors used to estimate the fake background are referred to as fake factors and are determined in dedicated regions, referred to as Determination Regions (DRs) in this paper.

In general, several types of jets are sources of fake $\tau_{\text{had-vis}}$. Four main sources of fake $\tau_{\text{had-vis}}$ are considered: jets originating from a b-quark (b), any lighter quark flavour (q), a gluon (g), or pile-up (p fakes), i.e. multiple pp interactions in the same and neighbouring bunch crossings. Jets originating from a c-quark are not treated as a separate category, as they are expected to form a small fraction of the total fakes in typical physics analyses. For example, the fraction of c-quark originated fake $\tau_{\text{had-vis}}$ is below 15% in all regions presented in this paper. The selected types of jets have different properties, and therefore they have different probabilities to be misidentified as a $\tau_{\text{had-vis}}$. The FF is different for each fake type, but generally it is not possible to measure the FF for each fake type separately because every region of phase space contains a mixture of different types. An ideal DR for the FF measurement would contain a sample of fakes with the same $q/g/b/p$ composition as in the SR, which is difficult to achieve. A solution to this problem is the Universal Fake Factor (UFF) method described in this paper. This method proposes that the FF for a particular SR can be obtained by knowing the fractions of $q/g/b/p$ fakes in the antiID subregion of the SR and using the FFs measured in samples enriched in each type of fake ($q/g/b/p$). The combined FF suitable for the SR is estimated as a linear combination of four FFs measured in the four fake-enriched regions. The combination coefficients are determined using a template fit. The dominant systematic uncertainty comes from differences in the FFs for different fake types, and it is estimated using MC simulation. The UFF method has one more advantage over more common ATLAS implementations of the FF method. The latter typically require many CRs or DRs, and an exhaustive validation of the predictions is often not possible. The UFF method does not require the analysis to define dedicated DRs to measure the FFs, as it defines its own fake-enriched regions for the FF measurement. Instead, regions that the analysis would define to measure the FFs can be used to validate the UFF-based fake-background prediction.

Preliminary versions of the UFF method were successfully used for fake-background estimation in three published ATLAS analyses. One searches for charged Higgs bosons in the τ_{had}+jets and τ_{had}+lepton final states [17], and the second for dark matter produced in association with a Higgs boson decaying into τ-leptons [18]. The third result measures the high-mass $\tau^+\tau^-$ production cross-section [19]. The CMS Collaboration has also developed and successfully applied a similar method [20–24].

The present version of the UFF method does not consider electrons, muons or photons misidentified as $\tau_{\text{had-vis}}$. These objects typically generate less background compared to the misidentified jets.

This paper is organized as follows. The ATLAS detector is described in Sect. 2. Section 3 introduces the data sets used in the present publication. Details of the reconstruction and identification of physical objects are provided in Sect. 4. After a summary of the FF method in Sect. 5, the UFF method is described in Sect. 6. The UFF method is tested in Sect. 7, its applicability and limitations are discussed in Sect. 8, and the conclusions are provided in Sect. 9.

2 ATLAS detector

The ATLAS detector [25] at the LHC covers nearly the entire solid angle around the collision point.[1] It consists of an inner tracking detector surrounded by a thin superconducting solenoid, electromagnetic and hadronic calorimeters, and a muon spectrometer incorporating three large superconducting air-core toroidal magnets.

The inner-detector system is immersed in a 2 T axial magnetic field and provides charged-particle tracking in the range $|\eta| < 2.5$. The high-granularity silicon pixel detector covers the vertex region and typically provides four measurements per track, the first hit generally being in the insertable B-layer installed before Run 2 [26,27]. It is followed by the silicon microstrip detector, which usually provides eight measurements per track. These silicon detectors are complemented by the transition radiation tracker (TRT), which enables radially extended track reconstruction up to $|\eta| = 2.0$. The TRT also provides electron identification information based on the fraction of hits (typically 30 in total) above a higher energy-deposit threshold corresponding to transition radiation.

The calorimeter system covers the pseudorapidity range $|\eta| < 4.9$. Within the region $|\eta| < 3.2$, electromagnetic calorimetry is provided by barrel and endcap high-granularity lead/liquid-argon (LAr) calorimeters, with an additional thin LAr presampler covering $|\eta| < 1.8$ to correct for energy loss in material upstream of the calorimeters.

[1] ATLAS uses a right-handed coordinate system with its origin at the nominal interaction point (IP) in the centre of the detector and the z-axis along the beam pipe. The x-axis points from the IP to the centre of the LHC ring, and the y-axis points upwards. Polar coordinates (r, ϕ) are used in the transverse plane, ϕ being the azimuthal angle around the z-axis. The pseudorapidity is defined in terms of the polar angle θ as $\eta = -\ln\tan(\theta/2)$ and is equal to the rapidity $y = (1/2)\ln[(E + p_z)/(E - p_z)]$ in the relativistic limit. Angular distance is measured in units of $\Delta R \equiv \sqrt{(\Delta y)^2 + (\Delta\phi)^2}$. Transverse momentum, p_{T}, is the magnitude of the momentum component in the transverse plane.

Hadronic calorimetry is provided by the steel/scintillator-tile calorimeter, segmented into three barrel structures within $|\eta| < 1.7$, and two copper/LAr hadronic endcap calorimeters. The solid angle coverage is completed with forward copper/LAr and tungsten/LAr calorimeter modules optimized for electromagnetic and hadronic energy measurements respectively.

The muon spectrometer (MS) comprises separate trigger and high-precision tracking chambers measuring the deflection of muons in a magnetic field generated by the superconducting air-core toroidal magnets. The field integral of the toroids ranges between 2.0 and 6.0 Tm across most of the detector. Three layers of precision chambers, each consisting of layers of monitored drift tubes, cover the region $|\eta| < 2.7$, complemented by cathode-strip chambers in the forward region, where the background is highest. The muon trigger system covers the range $|\eta| < 2.4$ with resistive-plate chambers in the barrel, and thin-gap chambers in the endcap regions.

The luminosity is measured mainly by the LUCID-2 [28] detector, which records Cherenkov light produced in the quartz windows of photomultipliers located close to the beampipe, complemented by measurements using the inner detector and calorimeters. Events are selected by the first-level (L1) trigger system implemented in custom hardware, followed by selections made by algorithms implemented in software in the high-level trigger [29]. The L1 trigger accepts events from the 40 MHz bunch crossings at a rate close to 100 kHz, which the high-level trigger further reduces in order to record complete events to disk at about 1.25 kHz. A software suite [30] is used in data simulation, in the reconstruction and analysis of data and simulated events, in detector operations, and in the trigger and data acquisition systems of the experiment.

3 Data and Monte Carlo samples

The present analysis uses data that the ATLAS experiment collected under stable-beam conditions in 2015–2018 at a pp centre-of-mass collision energy of $\sqrt{s} = 13$ TeV. After imposing data quality requirements to ensure that the ATLAS detector was operating normally [31], the integrated luminosity of the data sample is 140.1 ± 1.2 fb^{-1} [32].

The analysis uses two sets of MC samples called 'Default' and 'Powheg' in the following. Both of them include simulated events from $t\bar{t}$, single top, and $t\bar{t}V$ (where $V = W, Z$) production (collectively called 'Top'), quantum chromodynamics (QCD) and electroweak (EW) vector-boson production in association with jets (V + jets), pair production of vector bosons (VV), and dijet production. The Default set consists of the following MC samples. The V + jets events were generated with Sherpa2.2.1 [33]. The $t\bar{t}$ and single-top events were generated with Powheg Boxv2 [34–37] interfaced to Pythia8.230 [38], while the $t\bar{t}V$ events were modelled with MadGraph5_aMC@NLO2.3.3 [39] interfaced to Pythia8.210. Sherpa2.2.1 and Sherpa2.2.2 were used to generate the VV events. The dijet events were generated using Pythia8.230. The Powheg set differs from the Default set in two respects: QCD V + jets events in the Powheg set were generated with Powheg Boxv1 [35–37,40] interfaced to Pythia8.186, and dijet events were generated with Powheg Boxv2 interfaced to Pythia8.245. While the Default set provides more accurate modelling of final states with multiple jets, the Powheg set is used to estimate systematic uncertainties. Table 1 lists all the MC generators, the versions of parton distribution function (PDF) sets used in matrix element (ME) and parton shower (PS) computations, the set of tuned parameters ('tune') used for the underlying event, and the order in the strong coupling constant α_s to which the MEs and cross-sections are calculated.

MC simulation is used to model both τ-lepton production and the production of fake $\tau_{\text{had-vis}}$. Each generated event is passed through a detailed simulation of the ATLAS detector's response to particles [43], based on Geant4 [44]. The effect of pile-up was modelled by overlaying the simulated hard-scattering event with inelastic pp scattering events generated using Pythia8.186 [45] with the NNPDF2.3lo PDF set [46] and the A3 tune [47]. Simulated events are reweighted to match the pile-up conditions observed in the data.

4 Event reconstruction

In the data sample used for the present analysis, the number of pp collisions occurring simultaneously in a bunch crossing varies from about 20 to 70. The locations of individual pp collisions are called vertices, and each of them is reconstructed from the intersection of at least two tracks with $p_{\text{T}} > 500$ MeV. Additional requirements on the tracks guarantee that they originate from a region where the beams overlap in the transverse plane. The primary vertex is defined as the vertex with the largest sum of squared p_{T} of its matched tracks [48]. The present analysis considers events with electrons, muons, photons, $\tau_{\text{had-vis}}$, jets and b-jets in the final state.

Electron candidates consist of a track matched to a cluster of energy deposited in the electromagnetic calorimeter [49,50]. Selection criteria for the track impact parameters are imposed to guarantee that the track originates from the primary vertex. The transverse and longitudinal impact parameters, denoted by d_0 and z_0, are required to satisfy $d_0/\sigma(d_0) < 5$ and $|z_0 \sin\theta| < 5$ mm, where $\sigma(d_0)$ is the uncertainty in d_0 and θ is the track's polar angle. The pseudorapidity of the calorimeter energy cluster must satisfy $|\eta_{\text{cluster}}| < 1.37$ or $1.52 < |\eta_{\text{cluster}}| < 2.47$. The elec-

Table 1 List of MC generators, their settings, and the α_s-order of the cross-section (XS) calculation. MG5 v2.3.3 stands for MADGRAPH5_aMC@NLO2.3.3. The Sherpa, A14 and AZNLO underlying event (UE) tunes are described in Refs. [33,41,42], respectively

Process	Generator		PDF set		UE tune	ME order	XS order
	ME	PS	ME	PS			
V + jets QCD	SHERPA2.2.1		NNPDF3.0NNLO		Sherpa	NLO/LO	NNLO
V + jets EW	SHERPA2.2.1		NNPDF3.0NNLO		Sherpa	LO	LO
$t\bar{t}$	POWHEG BOXv2	PYTHIA8.230	NNPDF3.0NLO	NNPDF2.3LO	A14	NLO	NNLO
Single top	POWHEG BOXv2	PYTHIA8.230	NNPDF3.0NLO	NNPDF2.3LO	A14	NLO	NLO
$t\bar{t}V$	MG5 v2.3.3	PYTHIA8.210	NNPDF3.0NLO	NNPDF2.3LO	A14	NLO	NLO
VV	SHERPA2.2.1, 2.2.2		NNPDF3.0NNLO		Sherpa	NLO/LO	NNLO
Dijet	PYTHIA8.230		NNPDF2.3LO	NNPDF2.3LO	A14	LO	LO
V + jets QCD	POWHEG BOXv1	PYTHIA8.186	CT10NLO	CTEQ6L1	AZNLO	NLO	NLO
Dijet	POWHEG BOXv2	PYTHIA8.245	CT18NNLO	NNPDF2.3LO	A14	NLO	NLO

tron candidates are required to have $p_{\mathrm{T}} > 15$ GeV and satisfy the *Loose* ID selection criterion described in Ref. [51]. The *Loose* ID selection efficiency is greater than 88% for all considered electron candidates. A multivariate algorithm further suppresses non-isolated electrons arising from b-hadron decays [52]. The selection efficiency of the isolation criterion is greater than 70% for electron candidates with $p_{\mathrm{T}} > 20$ GeV.

Photon candidates are reconstructed from energy clusters in the electromagnetic calorimeter similarly to electrons [49,50]. Both converted (matched to a conversion vertex) and unconverted (not matched to an electron track or a conversion vertex) photons are considered. All photon candidates are required to have $p_{\mathrm{T}} > 15$ GeV. The identification criterion used in the present study is the *Tight* selection [49,51]. Its selection efficiency is greater than 92% (96%) for unconverted (converted) photons with $p_{\mathrm{T}} > 140$ GeV. The *Tight* isolation requirement defined in Ref. [53] is also used. The selection efficiency of this criterion is greater than 80% for photons with $p_{\mathrm{T}} > 140$ GeV.

Muon candidates consist of a track reconstructed in the inner detector matched to a track found in the muon spectrometer. Information about the two tracks is combined to measure the muon momentum more precisely [54]. The resulting track is then required to satisfy the same criteria for the impact parameters as electron tracks. Finally, muon candidates are selected if they have $p_{\mathrm{T}} > 7$ GeV, $|\eta| < 2.5$ and satisfy the *Loose* ID criterion described in Ref. [55]. The selection efficiency of the ID criterion is greater than 96% for all considered muon candidates. Muons are also required to satisfy isolation criteria similar to those for electrons. The selection efficiency of the isolation requirement is greater than 80% for muon candidates with $p_{\mathrm{T}} > 20$ GeV.

Jets are reconstructed from constituents built according to the particle-flow algorithm, which exploits both tracks and calorimeter energy clusters [56]. The particle-flow objects are passed to the anti-k_t algorithm [57,58] with a radius parameter of $R = 0.4$ to form jets via a four-momentum recombination scheme. Jet energy is calibrated to the hadronic scale with the effect of pile-up removed [59]. In-situ jet calibration is based on measurements of Z+jets, γ+jets and multijet events. Jets are required to have $p_{\mathrm{T}} > 20$ GeV and rapidity $|y| < 4.5$.

A multivariate b-tagging algorithm named DL1r [60] is used to tag jets from b-quarks. It exploits information about the impact parameters of tracks and properties of vertices in the jets. The algorithm tags jets with $p_{\mathrm{T}} > 20$ GeV and $|\eta| < 2.5$. A fixed 85%-efficiency working point is used, where the efficiency is evaluated in $t\bar{t}$ events from MC simulation. The flavour-tagging efficiency for jets from b, c, and lighter quarks is calibrated as described in Refs. [61–63].

Another multivariate algorithm, the jet-vertex tagger (JVT) [64], is used to veto jets with $p_{\mathrm{T}} < 60$ GeV and $|\eta| < 2.5$ if their constituent tracks are not consistent with the primary event vertex, as indicated by a low JVT output score. Similarly, a forward jet-vertex tagging (fJVT) algorithm [65] vetoes such jets with $p_{\mathrm{T}} < 60$ GeV and $|\eta| > 2.5$.

The $\tau_{\text{had-vis}}$ candidates [66–68] are seeded by jets formed using the anti-k_t algorithm with a radius parameter of $R = 0.4$. Three-dimensional clusters of calorimeter energy deposits called topo-clusters [69], calibrated using a local hadronic calibration (LC) [70], serve as inputs to the jet algorithm. The transverse momentum of a τ_{had} cannot be fully reconstructed because of an undetected neutrino. The energy scale of the visible decay products ($\tau_{\text{had-vis}}$) is measured using $Z(\tau\tau)$ events with one $\tau_{\text{had-vis}}$ and one τ-lepton decaying into a muon and neutrinos. Hadronic decay modes belonging to five categories are reconstructed [71]: decays with one matched track and either zero, one or more neutral pions, and decays with three matched tracks and either zero or more neutral pions. However, the present study groups the five categories into two to reduce the statistical uncertainties. The two categories consist of decays with either one or three matched tracks, referred to as 1-prong (1p) and 3-prong (3p)

decays respectively. Only $\tau_{\text{had-vis}}$ with reconstructed electric charge $|q| = 1$ are selected. Each $\tau_{\text{had-vis}}$ is required to have $p_{\text{T}} > 20$ GeV, $|\eta| < 1.37$ or $1.52 < |\eta| < 2.5$, and a score greater than 0.01 from an ID algorithm based on recurrent neural networks (RNN) [72]. In the present analysis, regions of phase space are often split into two parts according to the $\tau_{\text{had-vis}}$ ID score. The score value corresponding to the *Loose* ID working point is used for this purpose. Its efficiency is 85% (75%) for 1-prong (3-prong) $\tau_{\text{had-vis}}$ candidates regardless of their p_{T}. Its rejection power is 21 (90) for 1p (3p) $\tau_{\text{had-vis}}$ candidates in the dijet MC simulation.

Since particles are reconstructed by independent algorithms for each type of object, the same detector energy depositions are often reconstructed as more than one type of object. For example, a $\tau_{\text{had-vis}}$ is almost always reconstructed as a jet. It is necessary to remove this ambiguity and keep only one of the overlapping objects. The procedure for removing the redundant reconstructed objects is described in Ref. [3]. A $\tau_{\text{had-vis}}$ object is removed if an electron or muon is reconstructed within an angular distance of $\Delta R < 0.2$. A jet is removed if there is a $\tau_{\text{had-vis}}$ within $\Delta R < 0.2$.

The missing transverse momentum $\vec{p}_{\text{T}}^{\text{miss}}$ is defined as the negative vectorial sum of transverse momenta of electrons, muons, photons, $\tau_{\text{had-vis}}$, and jets. Soft particle tracks not matched to any object are taken into account via a separate 'soft term' [73]. The magnitude of the $\vec{p}_{\text{T}}^{\text{miss}}$ is denoted by $E_{\text{T}}^{\text{miss}}$.

When estimating the true τ-lepton, electron or muon contribution using the MC samples, each $\tau_{\text{had-vis}}$ candidate is required to geometrically match the generator-level τ-lepton, electron, or muon. In this situation, jets from the hadronization of quarks or gluons misidentified as $\tau_{\text{had-vis}}$ are not considered. The contamination of the fake-enriched samples by τ-leptons, electrons or muons is called real τ-lepton contamination in the following.

5 The fake-factor method

Assuming a SR with exactly one $\tau_{\text{had-vis}}$ candidate in the final state and assuming the candidate is a fake-$\tau_{\text{had-vis}}$, the number of events in the ID subregion of the SR, $N_{\text{ID}}^{\text{fake}}$, can be estimated as the number of events in the antiID subregion, $N_{\text{antiID}}^{\text{fake}}$, times a constant called a fake factor, FF:

$$N_{\text{ID}}^{\text{fake}} = N_{\text{antiID}}^{\text{fake}} \times \text{FF}. \tag{1}$$

The FF value can be estimated using an additional fake-enriched DR:

$$\text{FF} = \frac{N_{\text{ID DR}}^{\text{fake}}}{N_{\text{antiID DR}}^{\text{fake}}}. \tag{2}$$

The DR is split into two subregions, defined by the same selection criteria except for the $\tau_{\text{had-vis}}$ ID; $N_{\text{ID DR}}^{\text{fake}}$ ($N_{\text{antiID DR}}^{\text{fake}}$) stands for the number of DR events in which the $\tau_{\text{had-vis}}$ passes (fails) the ID selection. The DR selection criteria are typically very similar to the SR ones. Often, just one criterion is changed, e.g. the requirement on the $\tau_{\text{had-vis}}$ and a light lepton charges product in analyses targeting final states with two τ-leptons.

5.1 Details of the fake-factor method

The fake-enriched regions, the antiID subregion of the SR and the DR, also select a certain number of events where the reconstructed $\tau_{\text{had-vis}}$ candidate is not a jet originating from a QCD process. However, the FF method is defined just for fake-$\tau_{\text{had-vis}}$ events, and any contamination by real-τ-leptons must be removed. The real-τ-lepton contamination is estimated with MC simulation, by geometrically matching $\tau_{\text{had-vis}}$ candidates to generator-level objects as described in Sect. 4, and then subtracted from the data event yield, so that Eqs. (1) and (2) become:

$$N_{\text{ID}}^{\text{fake}} = \left(N_{\text{antiID}}^{\text{data}} - N_{\text{antiID}}^{\text{real}}\right) \times \text{FF},$$

$$\text{FF} = \frac{N_{\text{ID DR}}^{\text{data}} - N_{\text{ID DR}}^{\text{real}}}{N_{\text{antiID DR}}^{\text{data}} - N_{\text{antiID DR}}^{\text{real}}},$$

where the superscripts 'data' and 'real' label the data event yields and MC-estimated real-τ-lepton event yields, respectively.

Another feature of the method is that the FF is not a constant, but depends on the properties of the fakes. The present study takes into account its dependence on p_{T} and the number of matched tracks ('prongness'). A parameterization as a function of additional variables, such as η, was considered, but discarded because there were too few events. Section 7 shows that the fakes' η spectra are well modelled by the UFF method's predictions. The two-dimensional phase space is split into bins of p_{T} and prongness in which the FF method is used as described above. The final fake-background estimate for the SR is a sum of fake-background estimates coming from the individual phase-space bins.

The above fake-background estimation algorithm is thus easy to generalize for the case of multi-bin SRs. In each SR bin, the estimation is performed independently and as in the single-bin SR case.

5.2 Composition of fake-$\tau_{\text{had-vis}}$ samples

Ideally, the DR where the FF is determined should be defined to be as similar to the SR as possible in order to obtain fake-$\tau_{\text{had-vis}}$ samples with the same composition. In general, fake $\tau_{\text{had-vis}}$ can arise from several types of jets. Four main sources of fakes are considered: b-quarks (b); light quarks (q); glu-

ons, (g); and jets arising from pile-up (p). Fakes from these sources have different properties, and therefore these four types of jets have different probabilities of being misidentified as a $\tau_{\text{had-vis}}$. The FF varies among the types of fakes and, in general, it is not possible to measure the FF for each type of fake separately because every region of phase space contains a mixture of the different types. An ideal DR for the FF measurement would contain a sample of fakes with the same $q/g/b/p$ composition as in the SR, and fake-composition differences between the DR and SR are a source of systematic uncertainty.

5.3 Fake-factor method with two $\tau_{\text{had-vis}}$ in the final state

The FF method can be generalized for final states containing two $\tau_{\text{had-vis}}$. Often, there are two major sources of fakes, one producing a final state with a real $\tau_{\text{had-vis}}$ and a fake, and the other producing two fakes in the final state. In these cases, the dominant fake processes are typically $W(\tau\nu)$+jets and multijet production, and the FF method formula is:

$$N^{\text{fake}}_{2\text{ ID}} = \left(N^{\text{data}}_{1\text{ ID, }1\text{ antiID}} - N^{\text{real}}_{1\text{ ID, }1\text{ antiID}}\right) \times \text{FF} - \left(N^{\text{data}}_{2\text{ antiID}} - N^{\text{real}}_{2\text{ antiID}}\right) \times \text{FF}'_1 \times \text{FF}'_2, \quad (3)$$

where the event yields N have subscripts to denote ID and antiID $\tau_{\text{had-vis}}$ candidates, and superscripts to denote the data, real $\tau_{\text{had-vis}}$, and fake samples. In general, the fake-factor sets FF and FF$'$ are different from each other. FF'_1 and FF'_2 are taken from the same fake-factor set but they can have different values, depending on the p_{T} and prongness of the fakes. The subtraction of the two-fake yield in the second term of Eq. (3) is needed to cancel out the double counting of events with two fakes in the first term. The double counting occurs for combinatorial reasons: events where one $\tau_{\text{had-vis}}$ candidate passes the ID selection and the second one fails are as likely as events where the two $\tau_{\text{had-vis}}$ candidates are swapped. Since both groups provide the full estimate of the two-fake event yield, double counting occurs.

6 The Universal Fake Factor method

The UFF method provides a prescription for estimating the FFs suitable for the SR of an analysis. The method is a general solution to the major drawback of the FF method discussed in Sect. 5.2. The need to find a DR with the same $q/g/b/p$ composition as the SR is a serious limitation of the FF method. Rather than finding a suitable DR for each SR, the UFF method determines the fractions of the four main fake categories composing the antiID subregion of the SR, and uses them to evaluate the appropriate FF. Ideally, the categories would be q, g, b, and p fakes. However, it is impossible to find regions containing only one type of fake in order to measure the $q/g/b/p$-fake components for the UFF method. Instead, regions enriched in each type of fake are used.

6.1 Fake-enriched regions

Four selections are used to separate regions of phase space enriched in each category of fake background. The $Z(\mu\mu)$ region is enriched in q fakes, while the $t\bar{t}$ region is enriched in b fakes. Two multijet regions, called MJ hJVT and MJ lJVT, are enriched in g and p fakes, respectively. Each region's definition requires the presence of exactly one $\tau_{\text{had-vis}}$ candidate. The $\tau_{\text{had-vis}}$ must pass the *Tight* BDT-based electron veto, eBDT [3], to suppress electrons misidentified as $\tau_{\text{had-vis}}$. Its efficiency is 75% for $\tau_{\text{had-vis}}$ candidates passing the ID requirement. The veto is applied only to 1p $\tau_{\text{had-vis}}$ candidates.

The $Z(\mu\mu)$ region consists of events with exactly two opposite-charge muons. The muons must meet the *Tight* ID criterion [54] and have $p_{\text{T}} > 15$ GeV. The mass of the dimuon system, $m_{\mu\mu}$, is required to be within the range 76−106 GeV. The events are triggered by a logical OR of two single-muon trigger items [74,75]. One of them requires a muon with an online-reconstructed $p_{\text{T}} > 50$ GeV, while the other one has a lower p_{T} threshold of 26 GeV (20 GeV in 2015 data) but imposes an additional isolation requirement on the muon candidate. The leading muon is further required to have an offline $p_{\text{T}} > 28$ GeV. Events with an electron, photon or b-jet are vetoed. The seed jet of the $\tau_{\text{had-vis}}$ candidate must have a JVT score > 0.8.

The $t\bar{t}$ region is defined by the presence of one electron, one muon and at least one b-jet. The muon has to satisfy the *Tight* ID requirement and have $p_{\text{T}} > 10$ GeV. The electron is required to meet the *Tight* LLH ID criterion and have $p_{\text{T}} > 27$ GeV. The two leptons must have opposite charges. The events are triggered by a logical OR of three single-electron trigger items [75,76]. Their online p_{T} thresholds are 26, 60 and 140 GeV (24, 60 and 120 GeV in 2015 data), and they impose *Tight*, *Medium* and *Loose* (*Medium*, *Medium* and *Loose* in 2015 data) online ID requirements on the electron candidate, as well as an isolation requirement on the L1 objects. A photon veto is applied. The $\tau_{\text{had-vis}}$ candidate's seed jet must have a JVT score > 0.8.

Two multijet regions are defined by the presence of at least two jets that are back-to-back in the transverse plane. The events are triggered by a single-jet trigger [77] with an online p_{T} threshold of 420 GeV (360 GeV in 2015 data). Both jets must have $|\eta| < 3$, and the leading jet's p_{T} is required to exceed 450 GeV (390 GeV in 2015 data). The back-to-back topology is ensured by requiring the two leading jets to have an azimuthal separation of at least 2.7. The $\tau_{\text{had-vis}}$ candidate's p_{T} must be less than one-fourth of the two leading jets' average p_{T} to enrich the sample in g fakes.

Table 2 Selection criteria defining the $Z(\mu\mu)$, $t\bar{t}$, MJ hJVT, and MJ lJVT regions. The symbols μ, e, j, γ stand for a muon, an electron, a jet, and a photon, respectively. Their numerical subscripts refer to the ordering of that type of object in p_{T}. The symbol q stands for the electric charge. The azimuthal separation of the two leading jets is denoted by $\Delta\phi(j_1, j_2)$

$Z(\mu\mu)$	$t\bar{t}$	MJ	
$N_\mu = 2$	$N_\mu = 1$	$N_\mu = 0$	
$N_e = 0$	$N_e = 1$	$N_e = 0$	
$N_{b\text{-jet}} = 0$	$N_{b\text{-jet}} \geq 1$	$N_{b\text{-jet}} = 0$	
$N_\gamma = 0$	$N_\gamma = 0$	$N_\gamma = 0$	
Single-μ trigger	Single-e trigger	Single-jet trigger	
Tight μ ID	*Tight* LLH e ID		
	Tight μ ID		
$p_{\mathrm{T}}^{\mu_1} > 28$ GeV	$p_{\mathrm{T}}^{e} > 27$ GeV	$p_{\mathrm{T}}^{j_1} > 450$ GeV	
$p_{\mathrm{T}}^{\mu_2} > 15$ GeV	$p_{\mathrm{T}}^{\mu} > 10$ GeV		
		$\lvert\eta_{j_1}\rvert < 3$	
		$\lvert\eta_{j_2}\rvert < 3$	
$q_{\mu_1} q_{\mu_2} = -1$	$q_e q_\mu = -1$		
$m_{\mu\mu} \in (76, 106)$ GeV		$\Delta\phi(j_1, j_2) > 2.7$	
		$p_{\mathrm{T}}^{\tau} < \left(p_{\mathrm{T}}^{j_1} + p_{\mathrm{T}}^{j_2}\right) \Big/ 8$	
		$N_j = 2$ OR $p_{\mathrm{T}}^{j_3} < p_{\mathrm{T}}^{\tau}$	
Tight $\tau_{\text{had-vis}}$ eBDT	*Tight* $\tau_{\text{had-vis}}$ eBDT	*Tight* $\tau_{\text{had-vis}}$ eBDT	
$\mathrm{JVT}_{\tau_{\text{had-vis}}} > 0.8$	$\mathrm{JVT}_{\tau_{\text{had-vis}}} > 0.8$	MJ hJVT	MJ lJVT
		$\mathrm{JVT}_{\tau_{\text{had-vis}}} > 0.8$	$\mathrm{JVT}_{\tau_{\text{had-vis}}} < 0.8$

For a similar reason, a third-jet veto is applied. The events are required to have either exactly two jets or a third jet with p_{T} lower than the $\tau_{\text{had-vis}}$ candidate's p_{T}. Events with an electron, muon, photon or b-jet are vetoed. One multijet region, called MJ hJVT, is defined by imposing a requirement of JVT > 0.8 on the $\tau_{\text{had-vis}}$ candidate's seed jet. The other multijet region, called MJ lJVT, requires the $\tau_{\text{had-vis}}$ candidate's seed jet to have JVT < 0.8.

The purity of the target process in the $Z(\mu\mu)$, $t\bar{t}$, MJ hJVT and MJ lJVT regions is estimated using the Powheg MC sample set. In the $Z(\mu\mu)$ region, $Z(\mu\mu)$ production accounts for more than 95% of the events, while multijet production contributes more than 95% of the events in the MJ hJVT and MJ lJVT regions. In the $t\bar{t}$ region, $t\bar{t}$ production constitutes over 90% of the events. The contamination from real-τ-leptons, estimated with the Default MC sample set, is below 10% in the $Z(\mu\mu)$, MJ hJVT and MJ lJVT regions, and below 25% in the $t\bar{t}$ region.

Two regions are defined to estimate the systematic uncertainty of the UFF method, and to test the method. The $W(\mu\nu)$ region is defined by the presence of exactly one muon and one $\tau_{\text{had-vis}}$, with the same electric charge. The $\tau_{\text{had-vis}}$ candidate must satisfy the *Tight* eBDT criterion and be separated from the muon by $\Delta R(\mu, \tau) > 0.4$ in the $\eta{-}\phi$ plane. The muon is required to have $p_{\mathrm{T}} > 27.3$ GeV and satisfy the *Medium* ID criterion. The trigger strategy is the same as in the $Z(\mu\mu)$ region. Events with an electron or photon are vetoed. The $\mu 3j$ events form a subregion of the $W(\mu\nu)$ region. In addition to the $W(\mu\nu)$ requirements, the $\mu 3j$ region definition requires the presence of at least three jets, and at least one of them must be b-tagged.

One more region, called γ lJVT, is defined to estimate the systematic uncertainty of the UFF method and consists of events with a photon and a $\tau_{\text{had-vis}}$ candidate. A single-photon trigger with an online p_{T} threshold of 140 GeV and the *Loose* ID requirement [51] is used. The photon is required to have $p_{\mathrm{T}} > 145$ GeV. The $\tau_{\text{had-vis}}$ candidate must satisfy the *Tight* eBDT criterion, and its seed jet must have JVT < 0.8. The distance $\Delta R(\gamma, \tau)$ must exceed 0.2. Events with an electron or muon are vetoed.

Table 2 summarizes the selection criteria defining the $Z(\mu\mu)$, $t\bar{t}$, MJ hJVT, and MJ lJVT regions. Figure 1 shows the $q/g/b/p$ fake composition of the antiID $Z(\mu\mu)$, $t\bar{t}$, MJ hJVT, MJ lJVT, $W(\mu\nu)$, and $\mu 3j$ subregions, with an inclusive selection in p_{T} and prongness. The composition is determined with the Powheg set of MC samples. Regions $Z(\mu\mu)$, $t\bar{t}$, MJ hJVT, and MJ lJVT are each enriched in the type of fake they target. The γ lJVT region is not shown in the figure because it has a limited usage in the pile-up related systematic uncertainty estimation.

6.2 Evaluation of combined fake factors

The four fake-enriched regions, $Z(\mu\mu)$, $t\bar{t}$, MJ hJVT, and MJ lJVT, are split into p_{T} and prongness bins. The same is done for the antiID subregion of the SR of the analysis employing the UFF method. In each bin, the antiID subregion of the SR consists of four subregions. The fake population

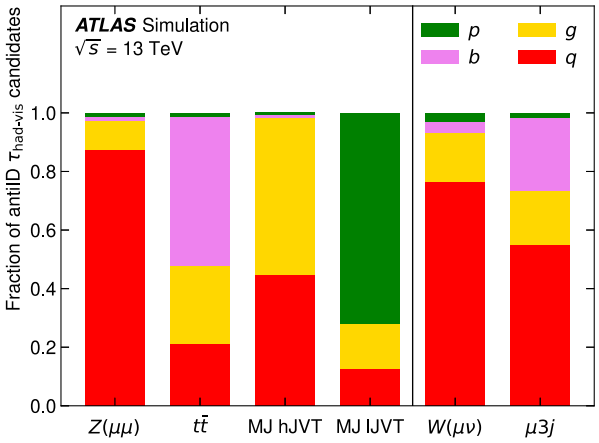

Fig. 1 The $q/g/b/p$ fake composition of the antiID $Z(\mu\mu)$, $t\bar{t}$, MJ hJVT, MJ lJVT, $W(\mu\nu)$, and $\mu 3j$ subregions, with an inclusive selection in p_{T} and prongness

in each of these subregions has a composition similar to that of a mixture of the fake populations in the antiID subregions of the $Z(\mu\mu)$, $t\bar{t}$, MJ hJVT, and MJ lJVT regions. The UFF method estimates this mixture of subregions contributing to the antiID subregion of the SR. This is done using a template fit of the ATLAS q/g tagger score [78] spectra, which will be discussed more in detail in Sect. 6.3. The combined FF suitable for the SR in question is then calculated as a weighted average of FFs measured in the $Z(\mu\mu)$, $t\bar{t}$, MJ hJVT, and MJ lJVT regions:

$$\begin{aligned}\mathrm{FF}_{\mathrm{UFF}} &= \mu_{Z(\mu\mu)} \times \mathrm{FF}_{Z(\mu\mu)} + \mu_{t\bar{t}} \times \mathrm{FF}_{t\bar{t}} \\ &\quad + \mu_{\text{MJ hJVT}} \times \mathrm{FF}_{\text{MJ hJVT}} \\ &\quad + \mu_{\text{MJ lJVT}} \times \mathrm{FF}_{\text{MJ lJVT}}, \end{aligned} \tag{4}$$

where the individual FFs and their weights in the combination are denoted by FF_X and μ_X, respectively, and $X = Z(\mu\mu), t\bar{t}$, MJ hJVT, MJ lJVT. The FFs are shown in Fig. 2. They decrease as a function of the $\tau_{\text{had-vis}}$ candidate's p_{T} because the fake rejection by the RNN algorithm improves with increasing p_{T} [72]. The FFs for the 1-prong fakes are higher than for the 3-prong fakes because the RNN's rejection power is higher for the latter. FFs determined in the MJ lJVT region tend to be lower than others, due to pile-up track rejection from the track matching and classification applied in the $\tau_{\text{had-vis}}$ reconstruction. MJ hJVT FFs are lower than $Z(\mu\mu)$ FFs because there is a higher admixture of g fakes in the MJ hJVT region, and the g fakes have lower FFs than the q fakes, as discussed in Sect. 6.4.

It should be noted that the FFs from the $Z(\mu\mu)$, $t\bar{t}$, MJ hJVT and MJ lJVT regions can be expressed as linear combinations of the $q/g/b/p$ FFs. The UFF method assumes that the same is true for the SR FFs. Therefore, there is no approximation in Eq. (4) when using the $Z(\mu\mu), t\bar{t}$, MJ hJVT and MJ lJVT FFs instead of the $q/g/b/p$ ones.

6.3 Template fit

In each p_{T} and prongness bin and each antiID subregion, a normalized template of the ATLAS q/g tagger score is built. The q/g tagger provides a multivariate-analysis score based on jet variables that are sensitive to the differences in radiation patterns, fragmentation, and hadronization between quark-initiated and gluon-initiated jets. Beside its sensitivity to q and g fakes, it also has a certain sensitivity to the properties of the b and p fakes. The q/g tagger score is evaluated on a particle-flow jet (see Sect. 4), closest to the $\tau_{\text{had-vis}}$ candidate in the $\eta{-}\phi$ plane in each event. If no particle-flow jet is found within a $\Delta R = 0.4$ distance from the $\tau_{\text{had-vis}}$ candidate, the candidate is added to the lowest q/g tagger score bin. Each template is built using data, as all the regions are fake-enriched. The residual real-τ-lepton contamination is subtracted from the $Z(\mu\mu), t\bar{t}$, MJ hJVT and MJ lJVT templates via MC simulation. Then, the four templates are normalized to the event yield in the antiID subregion of the SR minus the real-τ-lepton contamination in that region. The Default set of MC samples is used to estimate the real-τ-lepton contamination. As an example, Fig. 3 shows the four templates in the 1-prong and $p_{\mathrm{T}} \in (85, 100)$ GeV bin. For display purposes, the templates are normalized to unity. The sum of the $Z(\mu\mu)$, $t\bar{t}$, MJ hJVT, and MJ lJVT templates plus the histogram of the real-τ-lepton contamination in the antiID subregion of the SR is then fitted to the data in the antiID subregion of the SR using the maximum-likelihood method [79–83]. The fit is performed independently in each p_{T} and prongness bin. The normalization factors of the $Z(\mu\mu)$, $t\bar{t}$, MJ hJVT, and MJ lJVT templates are free parameters of the fit and their post-fit values are used as estimates of the combination coefficients μ_X in Eq. (4). No normalization factor is assigned to the real-τ-lepton contamination in the antiID subregion of the SR. The uncertainty due to the limited size of the samples for the $Z(\mu\mu)$, $t\bar{t}$, MJ hJVT and MJ lJVT templates and the real-τ-lepton contamination in the antiID subregion of the SR is taken into account in the fit. It is parameterized by nuisance parameters with Poisson constraints assigned to each bin of the q/g tagger score variable. An important feature of the UFF method is that the normalization factors are not constrained to be positive. This allows the method to provide an extrapolation in situations where the antiID subregion of the SR is more enriched in one type of fake than any antiID subregion of $Z(\mu\mu), t\bar{t}$, MJ hJVT, and MJ lJVT events. In these cases, the normalization factor corresponding to the region that is the most enriched in the given fake type can be larger than one. Consequently, at least one other normalization factor is usually negative so that the sum of the four normalization factors is close to one. Although the fit does not constrain the

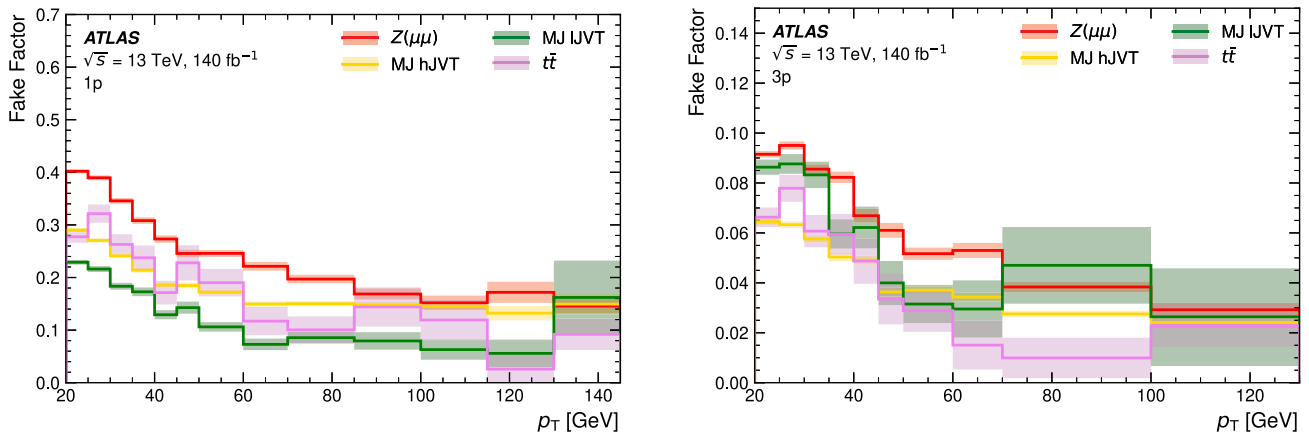

Fig. 2 FFs estimated in the $Z(\mu\mu)$, $t\bar{t}$, MJ hJVT and MJ lJVT regions for **a** 1-prong (1p) fakes and **b** 3-prong (3p) fakes as a function of the fake's p_{T}. The coloured bands display the statistical uncertainty of the FFs. The highest p_{T} bin contains events with fake-$\tau_{\text{had-vis}}$ with p_{T} of up to 300 GeV

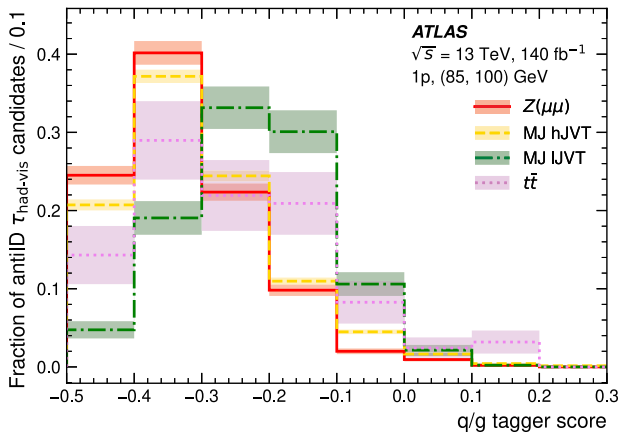

Fig. 3 Templates of the q/g tagger score distributions in the 1-prong (1p) and $p_{\mathrm{T}} \in (85, 100)$ GeV bin. They are determined in the $Z(\mu\mu)$, $t\bar{t}$, MJ hJVT and MJ lJVT antiID subregions. For display purpose, the templates are normalized to unity. The bands display the statistical uncertainty of the four templates

sum to one, its value is approximately one due to the absence of nuisance parameters substantially affecting the template normalization. As an example, Fig. 4a shows the results of the template fit in the 1-prong and $p_{\mathrm{T}} \in (85, 100)$ GeV bin of the $W(\mu\nu)$ region. In the figure, the q/g tagger score templates of the $Z(\mu\mu)$, $t\bar{t}$, MJ hJVT and MJ lJVT antiID subregions are shown, and they are scaled by their corresponding post-fit normalization factors. The contribution from real-τ-lepton background is also shown in the figure. Figure 4b shows the breakdown plot of the post-fit $Z(\mu\mu)$, $t\bar{t}$, MJ hJVT, and MJ lJVT templates whose sum is normalized to unity in each q/g tagger score bin.

6.4 Universal Fake Factor method uncertainties

The $Z(\mu\mu)$, $t\bar{t}$, MJ hJVT and MJ lJVT FFs and the coefficients μ_X from Eq. (4) are estimated using samples of finite size. The statistical uncertainties of the FFs are propagated to $\mathrm{FF}_{\mathrm{UFF}}$ assuming that these uncertainties are uncorrelated. On the other hand, the uncertainties of the coefficients μ_X are correlated, and the Hessian covariance matrix estimate, V, is taken into account in the uncertainty propagation. The total statistical uncertainty of $\mathrm{FF}_{\mathrm{UFF}}$ is estimated as the square root of the following expression:

$$\sigma^2_{\mathrm{UFF,\ stat.}} = \sum_X \mu_X^2 \sigma^2_{\mathrm{FF}_X} + \sum_{X,Y} \mathrm{FF}_X \mathrm{FF}_Y V_{XY},$$

where X and Y run over the $Z(\mu\mu)$, $t\bar{t}$, MJ hJVT and MJ lJVT regions.

The UFF method assumes that the FFs for $q/g/b/p$ fakes are the same in all regions of phase space. For $q/g/b$ fakes, this assumption is tested using MC simulation by comparing the FFs for a given fake type in five different regions. The regions are carefully chosen to represent common fake-production processes and kinematic regimes. Three of these five regions are $Z(\mu\mu)$, $t\bar{t}$ and MJ hJVT[2] defined in Sect. 6.1. The fourth region, $W(\mu\nu)$, targets q fake production in association with a W boson. The fifth region, $\mu 3j$, targets semileptonic $t\bar{t}$ events, containing q fakes from the decay of a colourless particle, the W boson.

In each region, the FFs for the q, g and b fakes are evaluated using the Powheg set of MC samples. To reduce the effective statistical uncertainty, MC samples corresponding to just the dominant process in each region are used, i.e.

[2] MJ lJVT is not in this list, as it targets p fakes, for which a dedicated systematic uncertainty is defined.

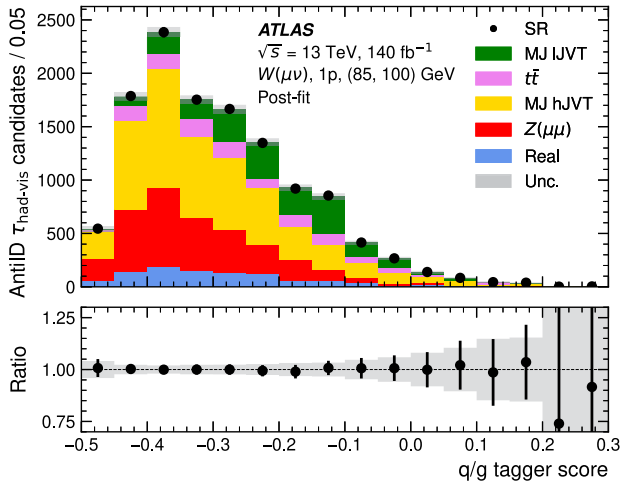

(a)

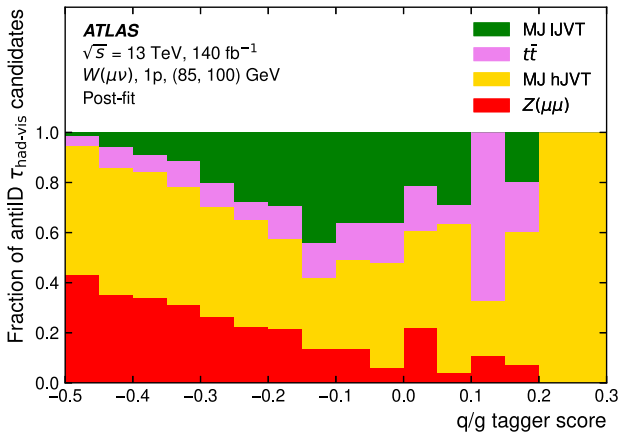

(b)

Fig. 4 **a** Results of the template fit in the 1-prong and $p_{\text{T}} \in (85, 100)$ GeV bin of the $W(\mu\nu)$ region. The black points represent the q/g tagger score distribution from the $W(\mu\nu)$ antiID subregion. The coloured histogram areas show the templates of the $Z(\mu\mu)$, $t\bar{t}$, MJ hJVT and MJ lJVT antiID subregions and the real-τ-lepton background in the antiID subregion of the SR. The four normalized templates are scaled by their corresponding post-fit normalization factors. The grey band displays the statistical uncertainty of the sum of the four templates and the real-τ-lepton background. The post-fit normalization factors are $\mu_{Z(\mu\mu)} = 0.28 \pm 0.16$, $\mu_{t\bar{t}} = 0.10 \pm 0.09$, $\mu_{\text{MJ hJVT}} = 0.45 \pm 0.19$, $\mu_{\text{MJ lJVT}} = 0.18 \pm 0.06$. **b** Breakdown plot of the post-fit $Z(\mu\mu)$, $t\bar{t}$, MJ hJVT, and MJ lJVT templates. Their sum is normalized to unity in each q/g tagger score bin so that each template contribution had the meaning of a fraction of the antiID $\tau_{\text{had-vis}}$ candidates in the bin

Z + jets MC is used for the $Z(\mu\mu)$ region, $t\bar{t}$ MC for the $t\bar{t}$ region, etc. Figure 5 shows the FFs for the q fakes in the five regions. They are rebinned and smoothed as a function of p_{T} to reduce the statistical fluctuations. Bins are combined iteratively from the highest p_{T} bin with non-zero content until the FF is non-zero with a statistical significance of 1.5σ, or the lowest p_{T} bin is reached. As the next step, FF values in the wide bins are copied to finer bins in which the nominal UFF prediction is evaluated. For the smoothing, each FF set is further copied to an equidistant binning with a bin width of 1. Then, it is smoothed using a Gaussian kernel with a width of 2. A systematic uncertainty is assigned to the $Z(\mu\mu)$ FFs shown in Fig. 2 by using the differences between the $Z(\mu\mu)$ MC FFs and the others to form the symmetrized uncertainty envelope shown in Fig. 5. In each p_{T} and prongness bin, the largest deviation of a FF from the $Z(\mu\mu)$ MC FF defines the envelope. Subsequently, this is divided by the $Z(\mu\mu)$ MC FF to get the relative systematic uncertainty. A similar procedure assesses the uncertainty of the $t\bar{t}$ and MJ hJVT FFs. The envelope around the $t\bar{t}$ (MJ hJVT) MC FFs in Fig. 6 (Fig. 7) divided by the $t\bar{t}$ MC b FFs (MJ hJVT MC g FFs) is used as the relative symmetric systematic uncertainty of the $t\bar{t}$ (MJ hJVT) FFs. When estimating the uncertainty of the $t\bar{t}$ FFs, the $W(\mu\nu)$ FFs are removed from the envelope because the $W(\mu\nu)$ sample is very small, implying no need to include it.

The systematic uncertainty of the MJ lJVT FFs is estimated in a similar way. The main difference is that data is used instead of MC simulation. The JVT score of the jets seeding the $\tau_{\text{had-vis}}$ candidate is used to select suitable p fake samples from data. Five regions are defined, including the MJ lJVT and γ lJVT regions, and the systematic uncertainty is determined as the largest difference between the MJ lJVT FF and the other FFs within each p_{T} and prongness bin. The uncertainty is symmetrized. Three regions, $Z(\mu\mu)$ lJVT, $t\bar{t}$ lJVT, and $W(\mu\nu)$ lJVT are defined as the $Z(\mu\mu)$, $t\bar{t}$, and $W(\mu\nu)$ regions in which just the JVT requirement on the $\tau_{\text{had-vis}}$ candidate's seed jet is inverted: JVT < 0.8 is required. Figure 8 shows the FFs for the p fakes in the five regions and the uncertainty of the MJ lJVT FFs.

The systematic uncertainty is propagated to FF_{UFF} separately for each uncertainty source (i.e. the q, g, b or p FF uncertainty). One FF from Eq. (4) is varied at a time, both upwards and downwards, and in each case the FF_{UFF} value is recalculated, giving rise to the $\pm 1\sigma$ FF_{UFF} uncertainty estimate. For each source, the resulting FF_{UFF} uncertainty is smoothed as a function of p_{T} to reduce the impact of statistical fluctuations. For the smoothing, the relative uncertainty is evaluated, copied to a uniform binning with a bin width of 1 and smoothed using a Gaussian kernel with a width of 1. Finally, it is copied back to the original p_{T} bins. These uncertainty sources should be treated as being uncorrelated and introduced as four separate nuisance parameters for each prongness in statistical models, assuming a correlation between p_{T} bins and no correlation between prongness bins. If an analysis is susceptible to the p_{T} and prongness cor-

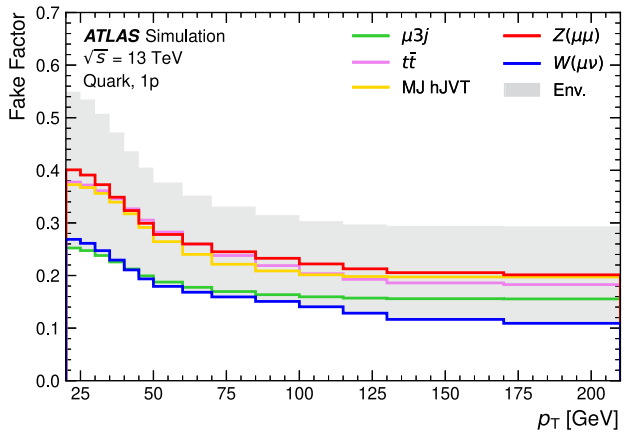

(a)

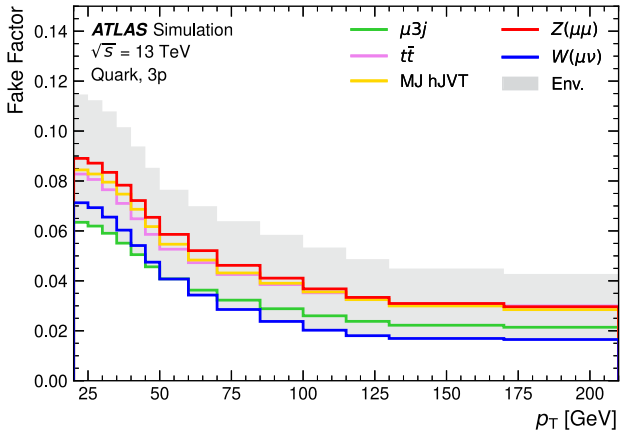

(b)

Fig. 5 FFs for the **a** 1-prong (1p) q fakes and **b** 3-prong (3p) q fakes as a function of the fake-$\tau_{\text{had-vis}}$ p_{T} in five regions of phase space, evaluated using the MC simulation and smoothed. The grey band displays the symmetrized envelope around the $Z(\mu\mu)$ FFs. The envelope is used to estimate the systematic uncertainty of the $Z(\mu\mu)$ FFs. The highest p_{T} bin contains events with fake-$\tau_{\text{had-vis}}$ with p_{T} of up to 300 GeV

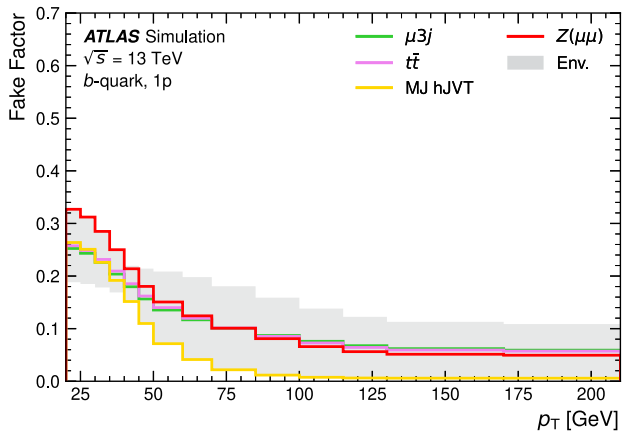

(a)

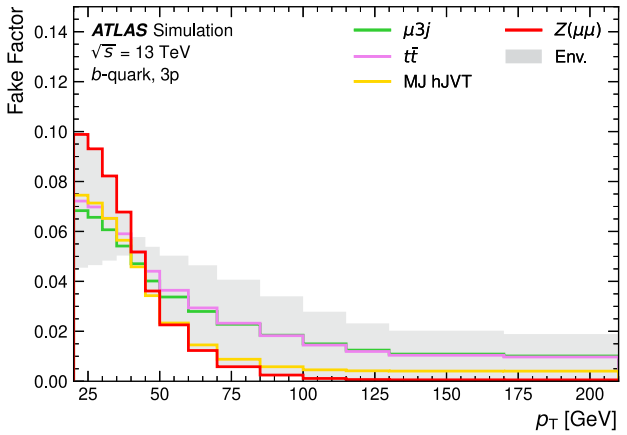

(b)

Fig. 6 FFs for the **a** 1-prong (1p) b fakes and **b** 3-prong (3p) b fakes as a function of the fake-$\tau_{\text{had-vis}}$ p_{T} in five regions of phase space, evaluated using the MC simulation and smoothed. The grey band displays the symmetrized envelope around the $t\bar{t}$ FFs. The envelope is used to estimate the systematic uncertainty of the $t\bar{t}$ FFs. The highest p_{T} bin contains events with fake-$\tau_{\text{had-vis}}$ with p_{T} of up to 300 GeV

relation scenario, it can determine whether a specific decorrelation in p_{T} and/or correlation in prongness results in a more realistic model. Decorrelation in other variables can also be considered. All uncertainty components are summed in quadrature for display purposes.

Additional systematic effects would arise if the q/g score spectra of $q/g/b/p$ fakes were different in different regions of phase space. The spectra were studied using MC (data) for $q/g/b$ (p) fakes, exploiting the same regions as in the FFs comparison. Some differences larger than the statistical uncertainty were observed among the q fake templates; see Fig. 9 as an example. The figure compares the distributions of 1p q fakes with $p_{\text{T}} \in (20, 35)$ GeV determined in the $Z(\mu\mu)$, $t\bar{t}$, MJ hJVT, $W(\mu\nu)$, and $\mu 3j$ antiID subregions using the same MC samples as for the systematic uncertainty determination described above. A MC study was performed to estimate the impact of this effect on the FF_{UFF} value. MC templates for the g, b, and p fakes are built in the $Z(\mu\mu)$ antiID subregion, using the $Z(\mu\mu)$ MC sample from the Powheg set. Similarly, MC templates for the q fakes are built in the $W(\mu\nu)$ antiID subregion, using the $W(\mu\nu)$ MC sample from the Powheg set. Each template is normalized to the total fake yield in the corresponding p_{T} and prongness bin of the $Z(\mu\mu)$ antiID subregion. FFs for the $q/g/b/p$ fakes are determined in the $Z(\mu\mu)$ region using the $Z(\mu\mu)$ MC sample from the Powheg set. In each p_{T} and prong-

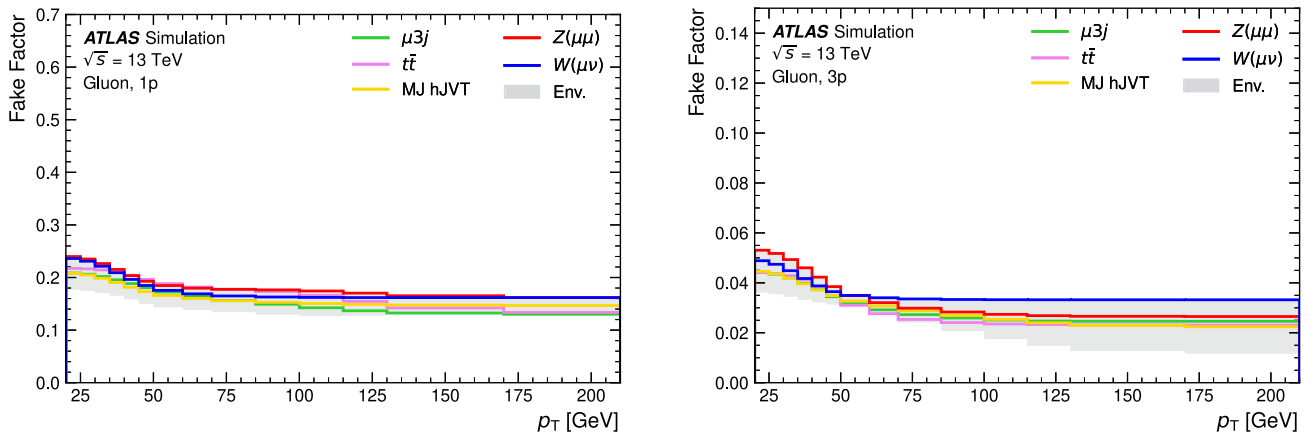

(a) (b)

Fig. 7 FFs for the **a** 1-prong (1p) g fakes and **b** 3-prong (3p) g fakes as a function of the fake-$\tau_{\text{had-vis}}$ p_{T} in five regions of phase space, evaluated using the MC simulation and smoothed. The grey band displays the symmetrized envelope around the MJ hJVT FFs. The envelope is used to estimate the systematic uncertainty of the MJ hJVT FFs. The highest p_{T} bin contains events with fake-$\tau_{\text{had-vis}}$ with p_{T} of up to 300 GeV

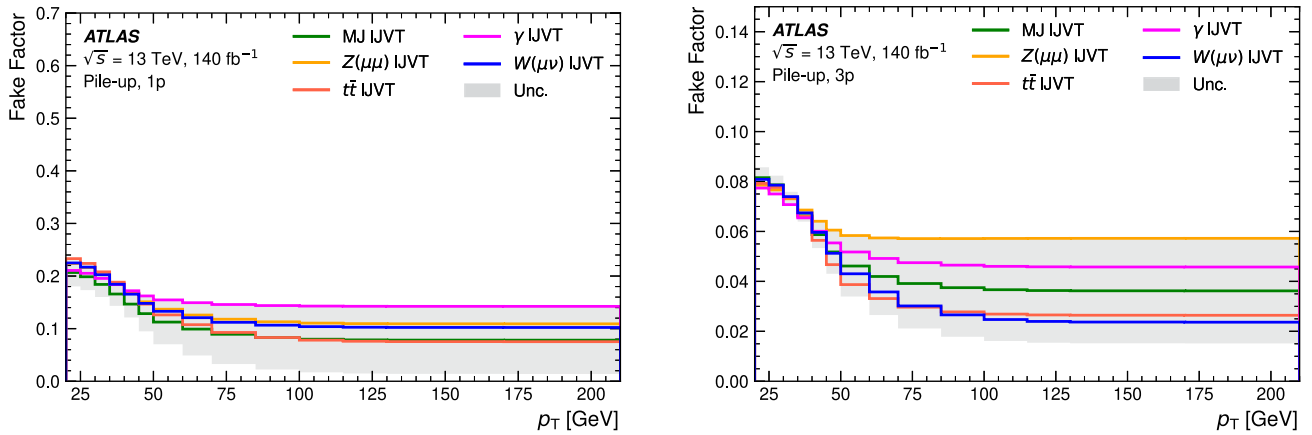

(a) (b)

Fig. 8 FFs for the **a** 1-prong (1p) p fakes and **b** 3-prong (3p) p fakes as a function of the fake-$\tau_{\text{had-vis}}$ p_{T} in five regions of phase space and smoothed. The grey band displays the assigned systematic uncertainty of the MJ lJVT FFs. The highest p_{T} bin contains events with fake-$\tau_{\text{had-vis}}$ with p_{T} of up to 300 GeV

ness bin, the $q/g/b/p$ templates are fitted to the total fake yield in the $Z(\mu\mu)$ antiID subregion, similarly to the procedure described in Sect. 6.3. The FFs are then combined in a similar way as described in Sect. 6.2. The resulting FF is compared to a reference FF directly calculated using $Z(\mu\mu)$ fakes predicted by the $Z(\mu\mu)$ MC sample from the Powheg set. In most p_{T} and prongness bins, the difference between the resulting FF and the $Z(\mu\mu)$ one is within their statistical uncertainty. In the minority of the bins, the difference is larger than the statistical uncertainty but within the systematic uncertainty of the q FFs, see Fig. 5. Therefore, no additional systematic uncertainty is assigned to the FF_{UFF} value due to the differences in the q/g score spectra of $q/g/b/p$ fakes in different regions of phase space.

It was also found that varying the JVT cut value from 0.8 to 0.5 or 0.9 in the $Z(\mu\mu)$, $t\bar{t}$, MJ hJVT and MJ lJVT region definitions does not affect the results significantly.

7 Tests of the Universal Fake Factor method

The UFF method is tested in several regions, and the test in the $W(\mu\nu)$ region is discussed here in depth as an example. Given that the region is highly enriched in fakes, it is possible to determine the FFs directly – as the ratio of the ID to antiID event yields. This gives a reference value for the FF_{UFF} that are evaluated using the q/g tagger score in the antiID subregion in order to predict the ID subregion yields. The FFs

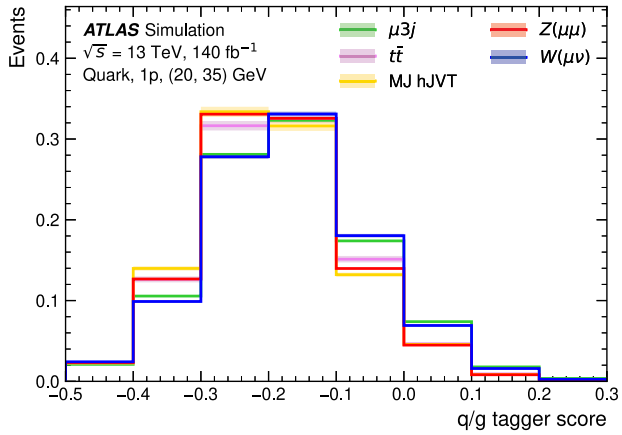

Fig. 9 Spectra of the q/g tagger score determined for q fakes in the $Z(\mu\mu)$, $t\bar{t}$, MJ hJVT, $W(\mu\nu)$, and $\mu 3j$ antiID subregions using MC. They are normalized to unity. The bands correspond to the statistical uncertainty of each spectrum

are compared in Fig. 10. The systematic uncertainty of the estimated $\mathrm{FF_{UFF}}$ ranges between 15% and 35%, depending on p_{T} and prongness. The UFF predictions agree with the reference FFs within the uncertainties. However, the $\mathrm{FF_{UFF}}$ are shifted systematically upwards relative the reference FFs. This is due to the q FFs being lower in the $W(\mu\nu)$ region than in the $Z(\mu\mu)$ and MJ hJVT regions that are used in the combination formula of Eq. (4). Figure 5 shows the various FFs estimated with the MC simulation.

To test the UFF method further, the fake-background prediction is compared with the data in the $W(\mu\nu)$ ID subregion. Figure 11 (Fig. 12) shows the comparison for events containing a 1-prong (3-prong) $\tau_{\text{had-vis}}$ candidate, and for several variables, namely the $\tau_{\text{had-vis}}$ transverse momentum and η, the muon transverse momentum p_{T}^{μ}, the $E_{\mathrm{T}}^{\mathrm{miss}}$, the transverse mass $m_{\mathrm{T}}(\mu, E_{\mathrm{T}}^{\mathrm{miss}})$ of the muon and $E_{\mathrm{T}}^{\mathrm{miss}}$ system, and the angular separation $\Delta R(\mu, \tau)$ of the $\tau_{\text{had-vis}}$ and muon. The real-τ-lepton background is also shown. It is estimated using the Default set of MC samples. The fake-background prediction agrees with the data, within the uncertainties, in all the variables. The systematic shift of the $\mathrm{FF_{UFF}}$ discussed above is also visible in this comparison.

The UFF method was also tested in $\mu 3j$ region, where the fake composition is different from that in the $W(\mu\nu)$ region, as shown in Fig. 1. The testing procedure in the $\mu 3j$ region is similar to that in $W(\mu\nu)$. The $\mathrm{FF_{UFF}}$ are compared with the reference FFs in Fig. 13. Figures 14 and 15 compare the fake-background predictions with the data. The UFF predictions agree with the data within the uncertainties. Here, the $\mathrm{FF_{UFF}}$ are shifted systematically downwards relative to the reference FFs, and this is also visible in the comparison of the fake-background prediction with the data. The reason is the same as discussed for the $W(\mu\nu)$ region. The different direction of the shift is a consequence of negative $Z(\mu\mu)$ normalization factors in the $\mu 3j$ region and the fact that the $Z(\mu\mu)$ FFs are the highest ones, as shown in Fig. 2.

Preliminary versions of the UFF method, using a lower number of DRs, a different discriminating variable and/or different systematic uncertainty estimates, were successfully used for fake-background estimation in three published ATLAS analyses. Final states $\tau_{\text{had-vis}}$ + jets, $\tau_{\text{had-vis}} + e/\mu$,

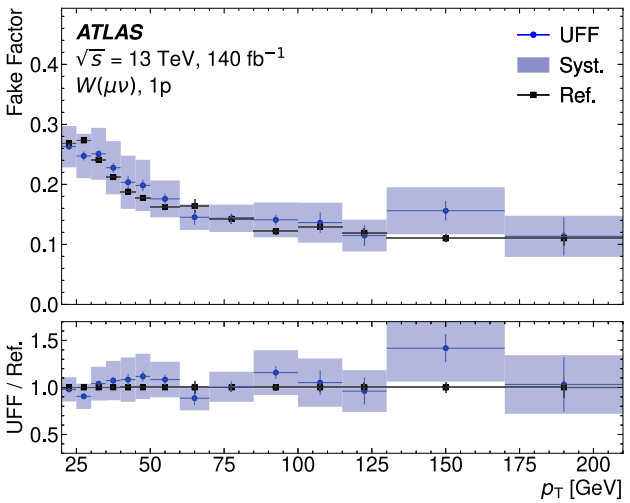

(a)

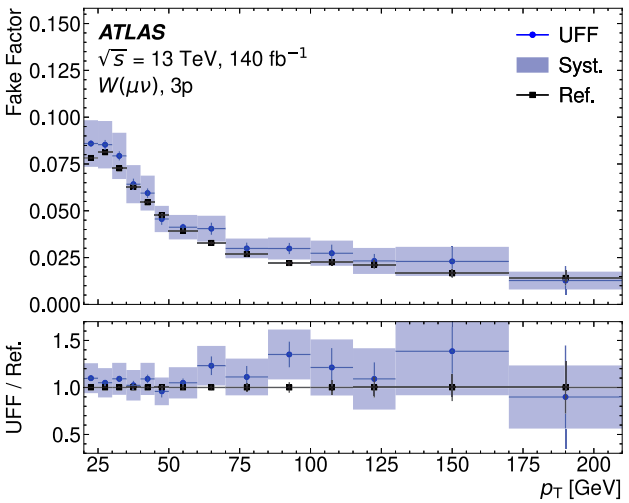

(b)

Fig. 10 FFs for the **a** 1-prong (1p) and **b** 3-prong (3p) fakes as a function of the fake-$\tau_{\text{had-vis}}$ p_{T} in the $W(\mu\nu)$ region. Blue-circle points display FFs estimated using the UFF method. The statistical (systematic) uncertainty is displayed as the blue error bars (band). The reference FFs, which are measured directly in the region, are shown as the black-square points, and their statistical uncertainty is displayed as the black error bars. The highest p_{T} bin contains events with fake-$\tau_{\text{had-vis}}$ with p_{T} of up to 300 GeV

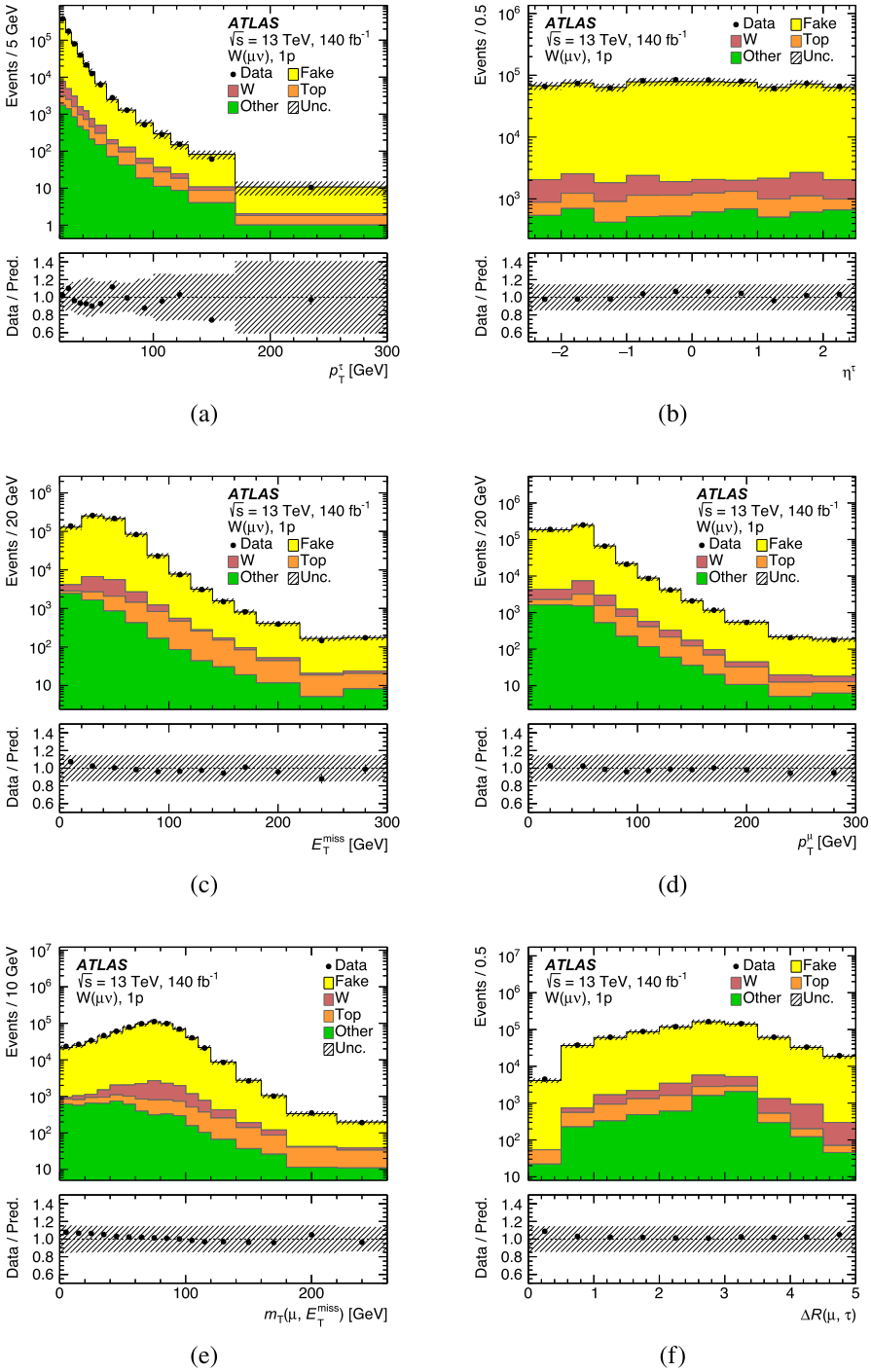

Fig. 11 Comparison of the 1-prong (1p) fake-background prediction (yellow area) with the data (black points) in the $W(\mu\nu)$ region. The real-τ-lepton backgrounds are also shown. The shaded band displays the total uncertainty of the prediction. It includes the fake-related systematic uncertainty, the statistical uncertainty of the $\mathrm{FF_{UFF}}$, and the uncertainty due to the limited number of events in the antiID subregion of the SR and the MC samples. The comparison is shown for several variables: **a** $\tau_{\text{had-vis}}$ transverse momentum, **b** $\tau_{\text{had-vis}}$ η, **c** $E_{\mathrm{T}}^{\mathrm{miss}}$, **d** p_{T}^{μ}, **e** $m_{\mathrm{T}}(\mu, E_{\mathrm{T}}^{\mathrm{miss}})$, and **f** $\Delta R(\mu, \tau)$. The compact notation p_{T}^{τ} and η^{τ} is used in the x-axis labels of figures **a** and **b** to denote the transverse momentum and η of $\tau_{\text{had-vis}}$

$\tau_{\text{had-vis}} + E_{\mathrm{T}}^{\mathrm{miss}}$, $2\tau_{\text{had-vis}} + E_{\mathrm{T}}^{\mathrm{miss}}/b$-jets, and $2\tau_{\text{had-vis}}$ inclusive have been probed.

8 Applicability and limitations of the Universal Fake Factor method

The UFF method offers a valuable approach for estimating fake-$\tau_{\text{had-vis}}$ background. However, it is crucial to acknowledge its advantages and limitations to delineate the types of analyses for which it is best suited. The UFF method resolves the problem related to the a priori unknown fake-$\tau_{\text{had-vis}}$ composition of a SR. The FFs suitable for a SR are evaluated as a linear combination of FFs determined in four predefined DRs, $Z(\mu\mu)$, $t\bar{t}$, MJ hJVT, and MJ lJVT. The related systematic uncertainty is physically motivated and simple to evaluate. The only input required to use the UFF method in an analysis are the q/g tagger score distributions (data and

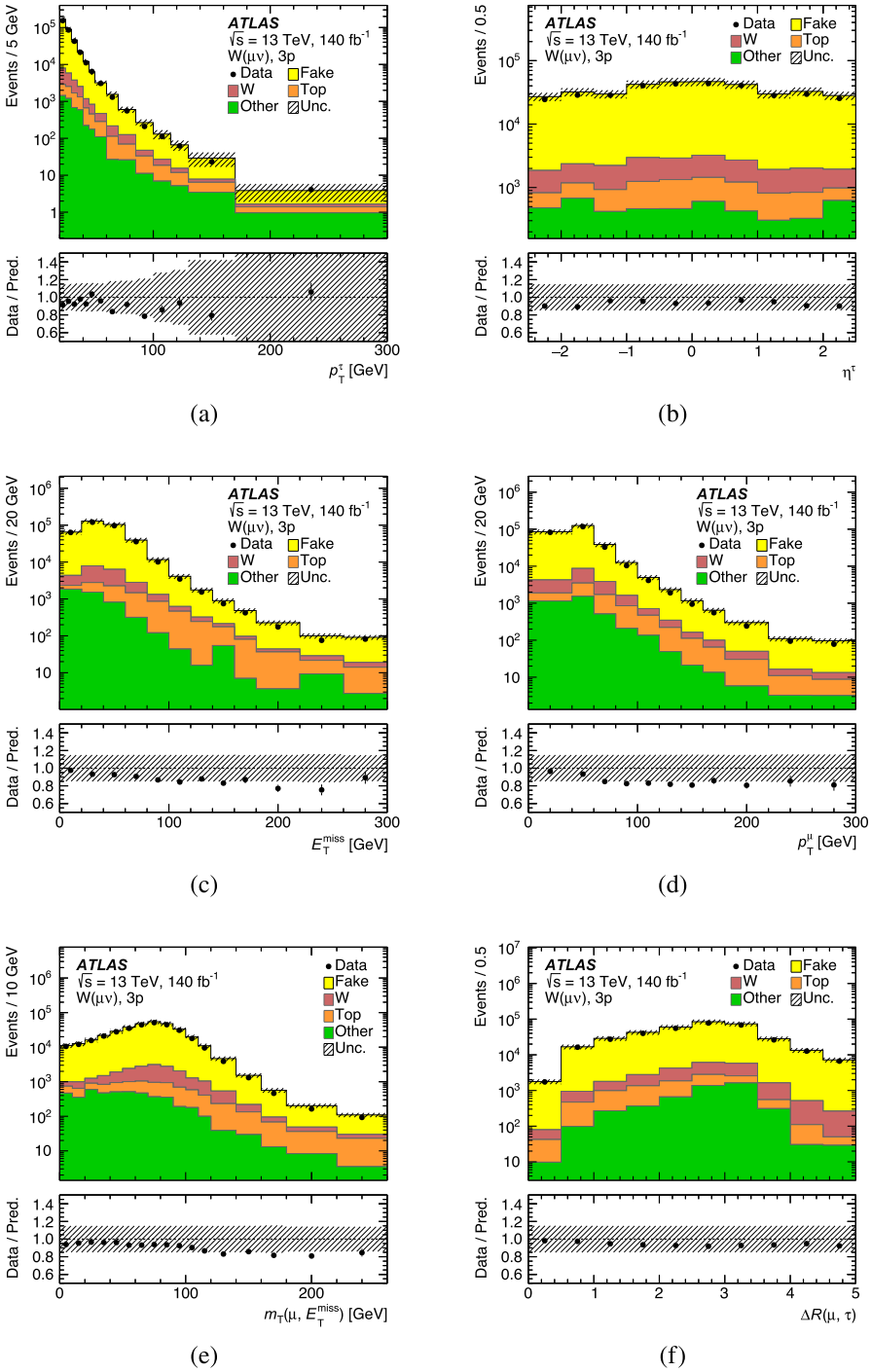

Fig. 12 Comparison of the 3-prong (3p) fake-background prediction (yellow area) with the data (black points) in the $W(\mu\nu)$ region. The real-τ-lepton backgrounds are also shown. The shaded band displays the total uncertainty of the prediction. It includes the fake-related systematic uncertainty, the statistical uncertainty of the $\mathrm{FF_{UFF}}$, and the uncertainty due to the limited number of events in the antiID subregion of the SR and the MC samples. The comparison is shown for several variables: **a** $\tau_{\text{had-vis}}$ transverse momentum, **b** $\tau_{\text{had-vis}}$ η, **c** $E_{\mathrm{T}}^{\mathrm{miss}}$, **d** p_{T}^{μ}, **e** $m_{\mathrm{T}}(\mu, E_{\mathrm{T}}^{\mathrm{miss}})$, and **f** $\Delta R(\mu, \tau)$. The compact notation p_{T}^{τ} and η^{τ} is used in the x-axis labels of figures **a** and **b** to denote the transverse momentum and η of $\tau_{\text{had-vis}}$

the MC-based real-τ-lepton contamination estimate) in the different phase space bins of the antiID subregion of the SR. The analysis using the UFF method does not need to exploit regions of phase space similar to the SR (in terms of the selection criteria) to determine FFs suitable for the analysis' SR. These regions can be employed for a detailed validation of the UFF-method-based prediction.

The UFF method is best suited for analyses with fake-$\tau_{\text{had-vis}}$ with p_{T} below $\sim$ 150 GeV and a statistical uncertainty of the background prediction larger than the UFF-related systematic uncertainty. Such analyses can highly benefit from the predefined UFF methodology and the ready-to-use DR FFs and templates, resulting in faster analysis development.

The applicability of the UFF method to analyses involving very high-p_{T} $\tau_{\text{had-vis}}$ warrants examination. In the present paper, the method is tested for $\tau_{\text{had-vis}}$ p_{T} of up to $\sim$ 200$-$300 GeV, see Figs. 11a, 12a, 14a, and 15a. The p_{T}

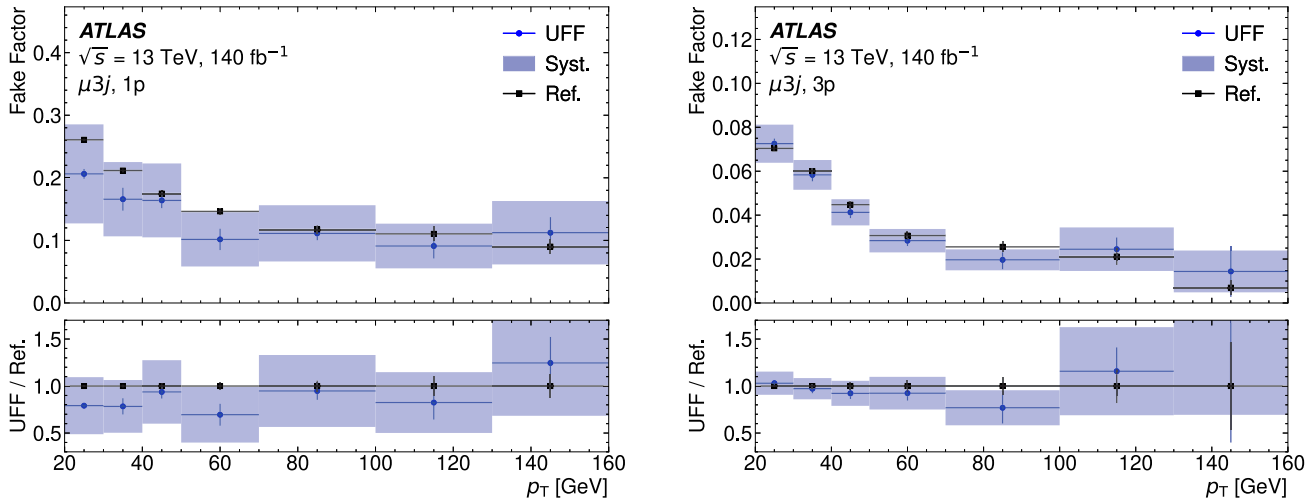

Fig. 13 FFs for the **a** 1-prong (1p) and **b** 3-prong (3p) fakes as a function of the fake-$\tau_{\text{had-vis}}$ p_T in the $\mu 3j$ region. Blue-circle points display FFs estimated using the UFF method. The statistical (systematic) uncertainty is displayed as the blue error bars (band). The reference FFs, which are measured directly in the region, are shown as the black-square points, and their statistical uncertainty is displayed as the black error bars. The highest p_T bin contains events with fake-$\tau_{\text{had-vis}}$ with p_T of up to 300 GeV

reach is mainly limited by the available statistics in the DRs. In Fig. 2, the highest-p_T bin takes into account the overflow events containing $\tau_{\text{had-vis}}$ candidates with p_T up to 300 GeV, but the p_T binning can be adjusted to accommodate the analysis needs. When deciding to use fine binning in the high-p_T region, the analysis using the UFF method should consider assigning a related systematic uncertainty.

A second question the analysis using the UFF method should address is the size of the total systematic uncertainty. Precision measurements and systematics-dominated searches might prefer to use the original FF method and a set of dedicated DRs defined by selection criteria similar to those in the SR if the DRs have high enough statistics and the extrapolation of the FFs to the SR has lower systematic uncertainty. The decision has to be made on a case-by-case basis, and no general rule can be given.

A problem arises if the SR largely overlaps with the DRs. In this case, the UFF method is not applicable, as the FFs in the DRs are not independent of the SR. The fraction of overlapping events must be checked before making the decision to use the UFF method.

Analyses dominated by q fakes and sensitive to the amplitude of the uncertainty band can mitigate potential bias by deriving the UFF templates and FFs from $W(\mu\nu)$ events instead of $Z(\mu\mu)$. This substitution can shift the nominal prediction by about 1σ of the quoted systematic uncertainty and provide an alternative modelling with different kinematic composition. The analysis can take the envelope of the Z- and W-based implementations as an additional shape uncertainty, validate with closure tests in 3-prong-enhanced control regions, and profile the corresponding nuisance parameters independently in the fit to reduce fit-induced artifacts in high-mass searches.

Analyses dominated by rare fake-$\tau_{\text{had-vis}}$ sources, where the physics origin of the fakes induces correlations not fully captured by the envelope method, might require a refinement of the systematic uncertainty estimation described in Sect. 6.4. For example, a hypothetical analysis dominated by b fakes from $Z(\mu\mu) + b$-jet events would be sensitive to the sign of the difference between the FFs derived from $t\bar{t}$ and $Z(\mu\mu) + b$ samples. In such a case, it would be more appropriate to use the relative difference between the two FF sets as the $t\bar{t}$ systematic uncertainty, taking the sign of the difference into account. For analyses where the MC-based prediction may lie outside the envelope defined by the reference regions, making the symmetrization both impactful and potentially inappropriate, a more tailored treatment should be adopted – for example, by retaining the sign of the difference or by constructing an analysis-specific uncertainty model that preserves genuine shape dependencies.

This paper presents the UFF method using the *Loose* $\tau_{\text{had-vis}}$ ID working point, but the method can be adapted to other $\tau_{\text{had-vis}}$ ID selections. Different inputs to the UFF method are required for each $\tau_{\text{had-vis}}$ ID efficiency working point. Similarly, recalculations are required for analyses utilizing $\tau_{\text{had-vis}}$ triggers that include specific $\tau_{\text{had-vis}}$ ID criteria. Finally, if the q/g tagger is updated, its templates will also need to be recalculated in the antiID $Z(\mu\mu)$, $t\bar{t}$, MJ hJVT and MJ lJVT subregions.

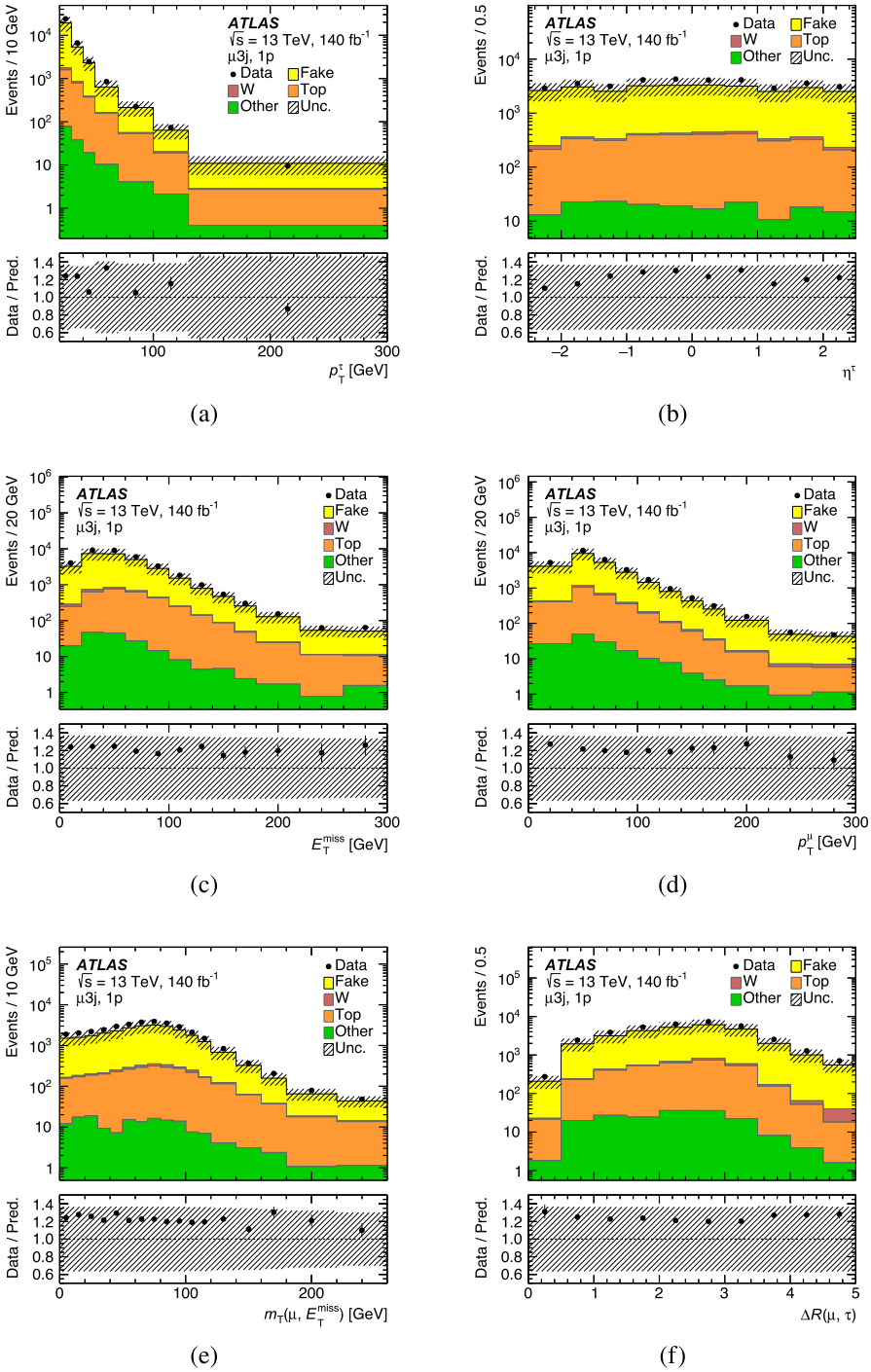

Fig. 14 Comparison of the 1-prong (1p) fake-background prediction (yellow area) with the data (black points) in the $\mu 3j$ region. The real-τ-lepton backgrounds are also shown. The shaded band displays the total uncertainty of the prediction. It includes the fake-related systematic uncertainty, the statistical uncertainty of the $\mathrm{FF_{UFF}}$, and the uncertainty due to the limited number of events in the antiID subregion of the SR and the MC samples. The comparison is shown for several variables: **a** $\tau_{\text{had-vis}}$ transverse momentum, **b** $\tau_{\text{had-vis}}$ η, **c** $E_{\mathrm{T}}^{\mathrm{miss}}$, **d** p_{T}^{μ}, **e** $m_{\mathrm{T}}(\mu, E_{\mathrm{T}}^{\mathrm{miss}})$, and **f** $\Delta R(\mu, \tau)$. The compact notation p_{T}^{τ} and η^{τ} is used in the x-axis labels of figures **a** and **b** to denote the transverse momentum and η of $\tau_{\text{had-vis}}$

9 Conclusions

This paper presents the UFF method, a generalization of the FF method, commonly used by the ATLAS experiment at the LHC to estimate the fake-$\tau_{\text{had-vis}}$ background. The UFF method provides a prescription for estimating the FFs suitable for the SR of an analysis. The method does not require to define one or more dedicated DRs for the FFs measurement; instead, it is based on the usage of four predefined regions enriched in different types of fakes. The $Z(\mu\mu)$, $t\bar{t}$, MJ hJVT and MJ lJVT regions target q fakes (from light-quark jets), b fakes (from b-jets), g fakes (from gluon-initiated jets), and p fakes (from pile-up jets), respectively. The analysis is provided with the FFs and q/g tagger score spectra determined in the corresponding antiID subregions. The only input the analysis has to prepare is the set of q/g tagger score spectra corresponding to the various p_{T} and prongness bins of its antiID subregion of the SR. The UFF method then estimates

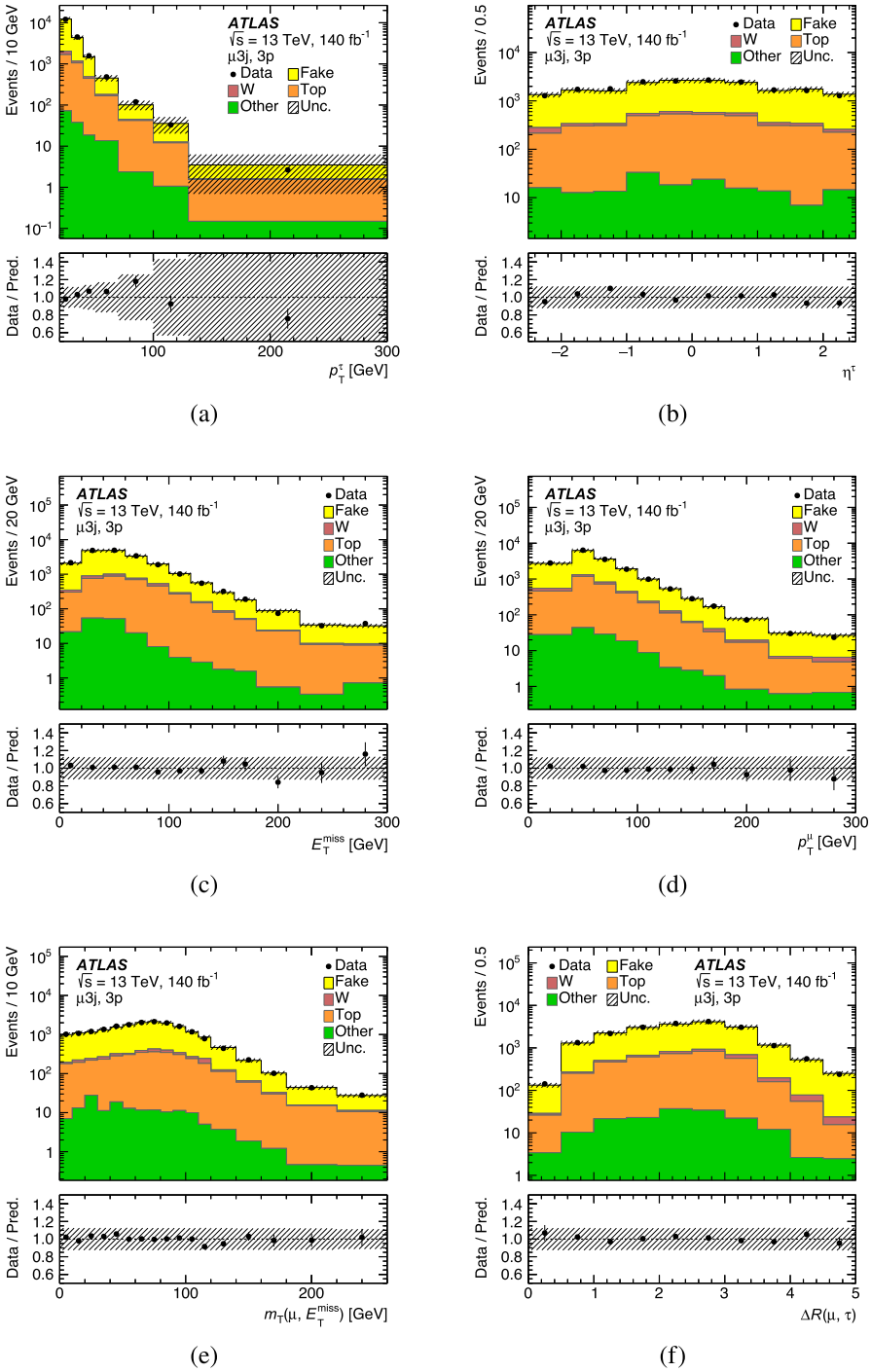

Fig. 15 Comparison of the 3-prong (3p) fake-background prediction (yellow area) with the data (black points) in the $\mu 3j$ region. The real-τ-lepton backgrounds are also shown. The shaded band displays the total uncertainty of the prediction. It includes the fake-related systematic uncertainty, the statistical uncertainty on the $\mathrm{FF_{UFF}}$, and the uncertainty due to the limited number of events in the antiID subregion of the SR and the MC samples. The comparison is shown for several variables: **a** $\tau_{\text{had-vis}}$ transverse momentum, **b** $\tau_{\text{had-vis}}$ η, **c** $E_{\mathrm{T}}^{\mathrm{miss}}$, **d** p_{T}^{μ}, (e) $m_{\mathrm{T}}(\mu, E_{\mathrm{T}}^{\mathrm{miss}})$, and (f) $\Delta R(\mu, \tau)$. The compact notation p_{T}^{τ} and η^{τ} is used in the x-axis labels of Figures **a** and **b** to denote the transverse momentum and η of $\tau_{\text{had-vis}}$

the suitable FFs using a template fit in each p_{T} and prongness bin and a simple formula for the combination of the four provided FFs. The method was successfully applied in several phase-space regions. In particular, the $W(\mu\nu)$ region shows that the UFF method can predict the FFs and the fake-$\tau_{\text{had-vis}}$ background within the associated systematic uncertainty. The present study used the full Run 2 pp collision data set, and the systematic uncertainty of the FFs for the $W(\mu\nu)$ region was estimated to be between 15% and 35%, depending on the fake-$\tau_{\text{had-vis}}$ p_{T} and prongness. A testing procedure applied to the $\mu 3j$ region demonstrated that the UFF method also works well in a region enriched in b fakes.

Besides providing a simple generic algorithm and the necessary inputs, the UFF method has one more advantage. The fake-background prediction obtained with the UFF method can be validated in the DRs that the original FF method would use for the FFs measurement and the estimation of systematic uncertainties. This resolves a serious drawback of the

original FF method, that it is very demanding in terms of the number of required DRs, and an exhaustive validation of the predictions often is not possible. It is also important to emphasize that the UFF method is data-driven to a large extent. MC simulation is used only for the subtraction of the real-τ-lepton contamination and the systematic uncertainty estimation. The UFF method is thus a powerful tool that can be used in a wide range of analyses.

Funding We thank CERN for the very successful operation of the LHC and its injectors, as well as the support staff at CERN and at our institutions worldwide without whom ATLAS could not be operated efficiently. The crucial computing support from all WLCG partners is acknowledged gratefully, in particular from CERN, the ATLAS Tier-1 facilities at TRIUMF/SFU (Canada), NDGF (Denmark, Norway, Sweden), CC-IN2P3 (France), KIT/GridKA (Germany), INFN-CNAF (Italy), NL-T1 (Netherlands), PIC (Spain), RAL (UK) and BNL (USA), the Tier-2 facilities worldwide and large non-WLCG resource providers. Major contributors of computing resources are listed in Ref. [84]. We gratefully acknowledge the support of ANPCyT, Argentina; YerPhI, Armenia; ARC, Australia; BMWFW and FWF, Austria; ANAS, Azerbaijan; CNPq and FAPESP, Brazil; NSERC, NRC and CFI, Canada; CERN; ANID, Chile; CAS, MOST and NSFC, China; Minciencias, Colombia; MEYS CR, Czech Republic; DNRF and DNSRC, Denmark; IN2P3-CNRS and CEA-DRF/IRFU, France; SRNSFG, Georgia; BMFTR, HGF and MPG, Germany; GSRI, Greece; RGC and Hong Kong SAR, China; ICHEP and Academy of Sciences and Humanities, Israel; INFN, Italy; MEXT and JSPS, Japan; CNRST, Morocco; NWO, Netherlands; RCN, Norway; MNiSW, Poland; FCT, Portugal; MNE/IFA, Romania; MSTDI, Serbia; MSSR, Slovakia; ARIS and MVZI, Slovenia; DSI/NRF, South Africa; MICIU/AEI, Spain; SRC and Wallenberg Foundation, Sweden; SERI, SNSF and Cantons of Bern and Geneva, Switzerland; NSTC, Taipei; TENMAK, Türkiye; STFC/UKRI, United Kingdom; DOE and NSF, United States of America.
Individual groups and members have received support from BCKDF, CANARIE, CRC and DRAC, Canada; CERN-CZ, FORTE and PRIMUS, Czech Republic; COST, ERC, ERDF, Horizon 2020, ICSC-NextGenerationEU and Marie Skłodowska-Curie Actions, European Union; Investissements d'Avenir Labex, Investissements d'Avenir Idex and ANR, France; DFG and AvH Foundation, Germany; Herakleitos, Thales and Aristeia programmes co-financed by EU-ESF and the Greek NSRF, Greece; BSF-NSF and MINERVA, Israel; NCN and NAWA, Poland; La Caixa Banking Foundation, CERCA Programme Generalitat de Catalunya and PROMETEO and GenT Programmes Generalitat Valenciana, Spain; Göran Gustafssons Stiftelse, Sweden; The Royal Society and Leverhulme Trust, United Kingdom. In addition, individual members wish to acknowledge support from Armenia: Yerevan Physics Institute (FAPERJ); CERN: European Organization for Nuclear Research (CERN DOCT); Chile: Agencia Nacional de Investigación y Desarrollo (FONDECYT 1230812, FONDECYT 1240864, Fondecyt 3240661); China: Chinese Ministry of Science and Technology (MOST-2023YFA1605700, MOST-2023YFA1609300), National Natural Science Foundation of China (NSFC - 12175119, NSFC 12275265, NSFC-12075060); Czech Republic: Czech Science Foundation (GACR - 24-11373S), Ministry of Education Youth and Sports (ERC-CZ-LL2327, FORTE CZ.02.01.01/00/22_008/0004632), PRIMUS Research Programme (PRIMUS/21/SCI/017); EU: H2020 European Research Council (ERC - 101002463); European Union: European Research Council (BARD No. 101116429, ERC - 948254, ERC 101089007), Horizon 2020 Framework Programme (MUCCA - CHIST-ERA-19-XAI-00), European Union, Future Artificial Intelligence Research (FAIR-NextGenerationEU PE00000013), Italian Center for High Performance Computing, Big Data and Quantum Computing (ICSC, NextGenerationEU); France: Agence Nationale de la Recherche (ANR-20-CE31-0013, ANR-21-CE31-0013, ANR-21-CE31-0022, ANR-22-EDIR-0002); Germany: Baden-Württemberg Stiftung (BW Stiftung-Postdoc Eliteprogramme), Deutsche Forschungsgemeinschaft (DFG - 469666862, DFG - CR 312/5-2); Italy: Istituto Nazionale di Fisica Nucleare (ICSC, NextGenerationEU), Ministero dell'Università e della Ricerca (NextGenEU 153D23001490006 M4C2.1.1, NextGenEU I53D23000820006 M4C2.1.1, NextGenEU I53D23001490006 M4C2.1.1); Japan: Japan Society for the Promotion of Science (JSPS KAKENHI JP22H01227, JSPS KAKENHI JP22H04944, JSPS KAKENHI JP22KK0227, JSPS KAKENHI JP23KK0245); Norway: Research Council of Norway (RCN-314472); Poland: Ministry of Science and Higher Education (IDUB AGH, POB8, D4 no 9722), Polish National Agency for Academic Exchange (PPN/PPO/2020/1/00002/U/00001), Polish National Science Centre (NCN 2021/42/E/ST2/00350, NCN OPUS 2023/51/B/ST2/02507, NCN OPUS nr 2022/47/B/ST2/03059, NCN UMO-2019/34/E/ST2/00393, UMO-2020/37/B/ST2/01043, UMO-2021/40/C/ST2/00187, UMO-2022/47/O/ST2/00148, UMO-2023/49/B/ST2/04085, UMO-2023/51/B/ST2/00920); Portugal: Foundation for Science and Technology (FCT); Spain: Generalitat Valenciana (Artemisa, FEDER, IDIFEDER/2018/048), Ministry of Science and Innovation (MCIN and NextGenEU PCI2022-135018-2, MICIN and FEDER PID2021-125273NB, RYC2019-028510-I, RYC2020-030254-I, RYC2021-031273-I, RYC2022-038164-I); Sweden: Carl Trygger Foundation (Carl Trygger Foundation CTS 22:2312), Swedish Research Council (Swedish Research Council 2023-04654, VR 2018-00482, VR 2021-03651, VR 2022-03845, VR 2022-04683, VR 2023-03403), Knut and Alice Wallenberg Foundation (KAW 2018.0458, KAW 2019.0447, KAW 2022.0358); Switzerland: Swiss National Science Foundation (SNSF - PCEFP2_194658); United Kingdom: Leverhulme Trust (Leverhulme Trust RPG-2020-004), Royal Society (NIF-R1-231091); United States of America: U.S. Department of Energy (ECA DE-AC02-76SF00515), Neubauer Family Foundation.

Data Availability Statement This manuscript has associated data in a data repository. [Author's comment: The public release of data supporting the findings of this article will follow the CERN Open Data Policy [85]. Inquiries about plots and tables associated with this article can be addressed to atlas.publications@cern.ch.]

Code Availability Statement This manuscript has associated code/software in a data repository. [Author's comment: The ATLAS Collaboration's Athena software, including the configuration of the event generators, is open source (http://gitlab.cern.ch/atlas/athena).]

Funded by SCOAP[3].

References

1. K. Lehmann, B. Stelzer, The Fake Factor Method and its relation to the Matrix Method. Nucl. Instrum. Methods A **1054**, 168376 (2023). https://doi.org/10.1016/j.nima.2023.168376
2. ATLAS Collaboration, Differential cross-section measurements of Higgs boson production in the $H \to \tau^+\tau^-$ decay channel in pp collisions at $\sqrt{s} = 13\,\text{TeV}$ with the ATLAS detector. JHEP **03**, 010 (2025). https://doi.org/10.1007/JHEP03(2025)010. arXiv:2407.16320 [hep-ex]
3. ATLAS Collaboration, Measurements of Higgs boson production cross-sections in the $H \to \tau^+\tau^-$ decay channel in pp collisions at $\sqrt{s} = 13\,\text{TeV}$ with the ATLAS detector. JHEP **08**, 175 (2022). https://doi.org/10.1007/JHEP08(2022)175. arxiv:2201.08269 [hep-ex]
4. ATLAS Collaboration, Search for the non-resonant production of Higgs boson pairs via gluon fusion and vector-boson fusion in the $b\bar{b}\tau^+\tau^-$ final state in proton–proton collisions at $\sqrt{s} = 13\,\text{TeV}$ with the ATLAS detector. Phys. Rev. D **110**, 032012 (2024). https://doi.org/10.1103/PhysRevD.110.032012. arXiv:2404.12660 [hep-ex]
5. ATLAS Collaboration, Measurement of the $VH, H \to \tau\tau$ process with the ATLAS detector at 13 TeV. Phys. Lett. B **855**, 138817 (2024). https://doi.org/10.1016/j.physletb.2024.138817. arXiv:2312.02394 [hep-ex]
6. ATLAS Collaboration, Measurement of the (CP) properties of Higgs boson interactions with τ-leptons with the ATLAS detector. Eur. Phys. J. C **83**, 563 (2023). https://doi.org/10.1140/epjc/s10052-023-11583-y. arXiv:2212.05833 [hep-ex]
7. ATLAS Collaboration, Search for additional heavy neutral Higgs and gauge bosons in the ditau final state produced in 36, fb^{-1} of pp collisions at $\sqrt{s} = 13\,\text{TeV}$ with the ATLAS detector. JHEP **01**, 055 (2018). https://doi.org/10.1007/JHEP01(2018)055. arXiv:1709.07242 [hep-ex]
8. ATLAS Collaboration, Searches for lepton-flavour-violating decays of the Higgs boson in $\sqrt{s} = 13\,\text{TeV}$ pp collisions with the ATLAS detector. Phys. Lett. B **800**, 135069 (2020). https://doi.org/10.1016/j.physletb.2019.135069. arXiv:1907.06131 [hep-ex]
9. ATLAS Collaboration, Search for excited τ-leptons and leptoquarks in the final state with τ-leptons and jets in pp collisions at $\sqrt{s} = 13\,\text{TeV}$ with the ATLAS detector. JHEP **06**, 199 (2023). https://doi.org/10.1007/JHEP06(2023)199. arXiv:2303.09444 [hep-ex]
10. ATLAS Collaboration, Search for leptoquarks decaying into the $b\tau$ final state in pp collisions at $\sqrt{s} = 13\,\text{TeV}$ with the ATLAS detector. JHEP **10**, 001 (2023). https://doi.org/10.1007/JHEP10(2023)001. arXiv:2305.15962 [hep-ex]
11. ATLAS Collaboration, Search for pair production of third-generation leptoquarks decaying into a bottom quark and a τ-lepton with the ATLAS detector. Eur. Phys. J. C **83**, 1075 (2023). https://doi.org/10.1140/epjc/s10052-023-12104-7. arXiv:2303.01294 [hep-ex]
12. ATLAS Collaboration, Search for third-generation vector-like leptons in pp collisions at $\sqrt{s} = 13\,\text{TeV}$ with the ATLAS detector. JHEP **07**, 118 (2023). https://doi.org/10.1007/JHEP07(2023)118. arXiv:2303.05441 [hep-ex]
13. CMS Collaboration, Measurement of the production cross section of a Higgs boson with large transverse momentum in its decays to a pair of τ leptons in proton–proton collisions at $\sqrt{s} = 13\,\text{TeV}$. Phys. Lett. B **857**, 138964 (2024). https://doi.org/10.1016/j.physletb.2024.138964. arXiv:2403.20201 [hep-ex]
14. CMS Collaboration, Search for excited tau leptons in the $\tau\tau\gamma$ final state in proton–proton collisions at $\sqrt{s} = 13\,\text{TeV}$. JHEP **06**, 006 (2024). https://doi.org/10.1007/JHEP06(2025)006. arXiv:2410.21137 [hep-ex]
15. CMS Collaboration, Search for new physics in the lepton plus missing transverse momentum final state in proton–proton collisions at $\sqrt{s} = 13\,\text{TeV}$. JHEP **07**, 067 (2022). https://doi.org/10.1007/JHEP07(2022)067. arXiv:2202.06075 [hep-ex]
16. ATLAS Collaboration, Tools for estimating fake/non-prompt lepton backgrounds with the ATLAS detector at the LHC. JINST **18**, T11004 (2023). https://doi.org/10.1088/1748-0221/18/11/T11004. arXiv:2211.16178 [hep-ex]
17. ATLAS Collaboration, Search for charged Higgs bosons decaying via $H^\pm \to \tau^\pm \nu_\tau$ in the τ+jets and τ+lepton final states with 36, fb^{-1} of pp collision data recorded at $\sqrt{s} = 13\,\text{TeV}$ with the ATLAS experiment. JHEP **09**, 139 (2018). https://doi.org/10.1007/JHEP09(2018)139. arXiv:1807.07915 [hep-ex]
18. ATLAS Collaboration, Search for dark matter produced in association with a Higgs boson decaying to tau leptons at $\sqrt{s} = 13\,\text{TeV}$ with the ATLAS detector. JHEP **09**, 189 (2023). https://doi.org/10.1007/JHEP09(2023)189. arXiv:2305.12938 [hep-ex]
19. ATLAS Collaboration, A measurement of the high-mass $\tau\bar{\tau}$ production cross-section at $\sqrt{s} = 13\,\text{TeV}$ with the ATLAS detector and constraints on new particles and couplings. JHEP **10**, 054 (2025). https://doi.org/10.1007/JHEP10(2025)054. arXiv:2503.19836 [hep-ex]
20. CMS Collaboration, Measurement of the $Z/\gamma^* \to \tau\tau$ cross section in pp collisions at $\sqrt{s} = 13\,\text{TeV}$ and validation of τ lepton analysis techniques. Eur. Phys. J. C **78**, 708 (2018). https://doi.org/10.1140/epjc/s10052-018-6146-9. arXiv:1801.03535 [hep-ex]
21. CMS Collaboration, Search for bottom quark associated production of the standard model Higgs boson in final states with leptons in proton-proton collisions at $\sqrt{s} = 13\,\text{TeV}$. Phys. Lett. B **860**, 139173 (2025). https://doi.org/10.1016/j.physletb.2024.139173. arXiv:2408.01344 [hep-ex]
22. CMS Collaboration, Searches for additional Higgs bosons and for vector leptoquarks in $\tau\tau$ final states in proton–proton collisions at $\sqrt{s} = 13\,\text{TeV}$. JHEP **07**, 073 (2023). https://doi.org/10.1007/JHEP07(2023)073. arXiv:2208.02717 [hep-ex]
23. CMS Collaboration, Search for additional neutral MSSM Higgs bosons in the $\tau\tau$ final state in proton–proton collisions at $\sqrt{s} = 13\,\text{TeV}$. JHEP **09**, 007 (2018). https://doi.org/10.1007/JHEP09(2018)007. arXiv:1803.06553 [hep-ex]
24. CMS Collaboration, Search for a third-generation leptoquark coupled to a τ lepton and a (b) quark through single, pair, and non-resonant production in proton–proton collisions at $\sqrt{s} = 13\,\text{TeV}$. JHEP **05**, 311 (2024). https://doi.org/10.1007/JHEP05(2024)311. arXiv:2308.07826 [hep-ex]
25. ATLAS Collaboration, The ATLAS experiment at the CERN large hadron collider. JINST **3**, S08003 (2008). https://doi.org/10.1088/1748-0221/3/08/S08003
26. ATLAS Collaboration, ATLAS Insertable B-Layer: Technical Design Report, ATLAS-TDR-19; CERN-LHCC-2010-013 (2010). https://cds.cern.ch/record/1291633. [Addendum: ATLAS-TDR-19-ADD-1; CERN-LHCC-2012-009 (2012). https://cds.cern.ch/record/1451888]
27. B. Abbott et al., Production and integration of the ATLAS Insertable B-Layer. JINST **13**, T05008 (2018). https://doi.org/10.1088/1748-0221/3/08/S08003. arXiv:1803.00844 [physics.ins-det]
28. G. Avoni et al., The new LUCID-2 detector for luminosity measurement and monitoring in ATLAS. JINST **13**, P07017 (2018). https://doi.org/10.1088/1748-0221/13/07/P07017
29. ATLAS Collaboration, Performance of the ATLAS trigger system in 2015. Eur. Phys. J. C **77**, 317 (2017). https://doi.org/10.1140/epjc/s10052-017-4852-3. arXiv:1611.09661 [hep-ex]
30. ATLAS Collaboration, Software and computing for Run 3 of the ATLAS experiment at the LHC. Eur. Phys. J. C **85**, 234 (2025). https://doi.org/10.1140/epjc/s10052-024-13701-w. arXiv:2404.06335 [hep-ex]

31. ATLAS Collaboration, ATLAS data quality operations and performance for 2015–2018 data-taking. JINST **15**, P04003 (2020). https://doi.org/10.1088/1748-0221/15/04/P04003. arXiv:1911.04632 [physics.ins-det]
32. ATLAS Collaboration, Luminosity determination in pp collisions at $\sqrt{s} = 13$ TeV using the ATLAS detector at the LHC. Eur. Phys. J. C **83**, 982 (2023). https://doi.org/10.1140/epjc/s10052-023-11747-w. arXiv:2212.09379 [hep-ex]
33. E. Bothmann et al., Event generation with Sherpa 2.2. SciPost Phys. **7**, 034 (2019). https://doi.org/10.21468/SciPostPhys.7.3.034. arXiv:1905.09127 [hep-ph]
34. S. Frixione, G. Ridolfi, P. Nason, A positive-weight next-to-leading-order Monte Carlo for heavy flavour hadroproduction. JHEP **09**, 126 (2007). https://doi.org/10.1088/1126-6708/2007/09/126. arXiv:0707.3088 [hep-ph]
35. P. Nason, A new method for combining NLO QCD with shower Monte Carlo algorithms. JHEP **11**, 040 (2004). https://doi.org/10.1088/1126-6708/2004/11/040. arXiv:hep-ph/0409146
36. S. Frixione, P. Nason, C. Oleari, Matching NLO QCD computations with parton shower simulations: the POWHEG method. JHEP **11**, 070 (2007). https://doi.org/10.1088/1126-6708/2007/11/070. arXiv:0709.2092 [hep-ph]
37. S. Alioli, P. Nason, C. Oleari, E. Re, A general framework for implementing NLO calculations in shower Monte Carlo programs: the POWHEG BOX. JHEP **06**, 043 (2010). https://doi.org/10.1007/JHEP06(2010)043. arXiv:1002.2581 [hep-ph]
38. T. Sjöstrand et al, An introduction to PYTHIA 8.2. Comput. Phys. Commun. **191**, 159 (2015). https://doi.org/10.1016/j.cpc.2015.01.024. arXiv:1410.3012 [hep-ph]
39. J. Alwall et al., The automated computation of tree-level and next-to-leading order differential cross sections, and their matching to parton shower simulations. JHEP **07**, 079 (2014). https://doi.org/10.1007/JHEP07(2014)079. arXiv:1405.0301 [hep-ph]
40. S. Alioli, P. Nason, C. Oleari, E. Re, NLO vector-boson production matched with shower in POWHEG. JHEP **07**, 060 (2008). https://doi.org/10.1088/1126-6708/2008/07/060. arXiv:0805.4802 [hep-ph]
41. ATLAS Collaboration, ATLAS Pythia 8 tunes to 7 TeV data. ATL-PHYS-PUB-2014-021 (2014). https://cds.cern.ch/record/1966419
42. ATLAS Collaboration, Measurement of the Z/γ^* boson transverse momentum distribution in pp collisions at ($\sqrt{s} = 7$ TeV) with the ATLAS detector. JHEP **09**, 145 (2014). https://doi.org/10.1007/JHEP09(2014)145. arXiv:1406.3660 [hep-ex]
43. ATLAS Collaboration, The ATLAS simulation infrastructure. Eur. Phys. J. C **70**, 823 (2010). https://doi.org/10.1140/epjc/s10052-010-1429-9. arXiv:1005.4568 [physics.ins-det]
44. S. Agostinelli et al., Geant4—a simulation toolkit. Nucl. Instrum. Methods A **506**, 250 (2003). https://doi.org/10.1016/S0168-9002(03)01368-8
45. T. Sjöstrand, S. Mrenna, P. Skands, A brief introduction to PYTHIA 8.1. Comput. Phys. Commun. **178**, 852 (2008). https://doi.org/10.1016/j.cpc.2008.01.036. arXiv:0710.3820 [hep-ph]
46. NNPDF Collaboration, R.D. Ball et al., Parton distributions with LHC data. Nucl. Phys. B **867**, 244 (2013). https://doi.org/10.1016/j.nuclphysb.2012.10.003. arXiv:1207.1303 [hep-ph]
47. ATLAS Collaboration, The Pythia 8 A3 tune description of ATLAS minimum bias and inelastic measurements incorporating the Donnachie–Landshoff diffractive model. ATL-PHYS-PUB-2016-017 (2016). https://cds.cern.ch/record/2206965
48. ATLAS Collaboration, Vertex reconstruction performance of the ATLAS detector at $\sqrt{s} = 13$ TeV. ATL-PHYS-PUB-2015-026 (2015). https://cds.cern.ch/record/2037717
49. ATLAS Collaboration, Electron and photon efficiencies in LHC Run 2 with the ATLAS experiment. JHEP **05**, 162 (2024). https://doi.org/10.1007/JHEP05(2024)162. arXiv:2308.13362 [hep-ex]
50. ATLAS Collaboration, Electron and photon energy calibration with the ATLAS detector using LHC Run 2 data. JINST **19**, P02009 (2024). https://doi.org/10.1088/1748-0221/19/02/P02009. arXiv:2309.05471 [hep-ex]
51. ATLAS Collaboration, Electron and photon performance measurements with the ATLAS detector using the 2015–2017 LHC proton–proton collision data. JINST **14**, P12006 (2019). https://doi.org/10.1088/1748-0221/14/12/P12006. arXiv:1908.00005 [hep-ex]
52. ATLAS Collaboration, Evidence for the associated production of the Higgs boson and a top quark pair with the ATLAS detector. Phys. Rev. D **97**, 072003 (2018). https://doi.org/10.1103/PhysRevD.97.072003. arXiv:1712.08891 [hep-ex]
53. ATLAS Collaboration, Measurement of the photon identification efficiencies with the ATLAS detector using LHC Run 2 data collected in 2015 and 2016. Eur. Phys. J. C **79**, 205 (2019). https://doi.org/10.1140/epjc/s10052-019-6650-6. arXiv:1810.05087 [hep-ex]
54. ATLAS Collaboration, Muon reconstruction performance of the ATLAS detector in proton–proton collision data at $\sqrt{s} = 13$ TeV. Eur. Phys. J. C **76**, 292 (2016). https://doi.org/10.1140/epjc/s10052-016-4120-y. arXiv:1603.05598 [hep-ex]
55. ATLAS Collaboration, Muon reconstruction and identification efficiency in ATLAS using the full Run 2 pp collision data set at $\sqrt{s} = 13$ TeV. Eur. Phys. J. C **81**, 578 (2021). https://doi.org/10.1140/epjc/s10052-021-09233-2. arXiv:2012.00578 [hep-ex]
56. ATLAS Collaboration, Jet reconstruction and performance using particle flow with the ATLAS detector. Eur. Phys. J. C **77**, 466 (2017). https://doi.org/10.1140/epjc/s10052-017-5031-2. arXiv:1703.10485 [hep-ex]
57. M. Cacciari, G.P. Salam, G. Soyez, The anti-k_t jet clustering algorithm. JHEP **04**, 063 (2008). https://doi.org/10.1088/1126-6708/2008/04/063. arXiv:0802.1189 [hep-ph]
58. M. Cacciari, G.P. Salam, G. Soyez, FastJet user manual. Eur. Phys. J. C **72**, 1896 (2012). https://doi.org/10.1140/epjc/s10052-012-1896-2. arXiv:1111.6097 [hep-ph]
59. ATLAS Collaboration, Jet energy scale and resolution measured in proton–proton collisions at $\sqrt{s} = 13$ TeV with the ATLAS detector. Eur. Phys. J. C **81**, 689 (2021). https://doi.org/10.1140/epjc/s10052-021-09402-3. arXiv:2007.02645 [hep-ex]
60. ATLAS Collaboration, ATLAS flavour-tagging algorithms for the LHC Run 2 pp collision dataset. Eur. Phys. J. C **83**, 681 (2023). https://doi.org/10.1140/epjc/s10052-023-11699-1. arXiv:2211.16345 [physics.data-an]
61. ATLAS Collaboration, ATLAS (b)-jet identification performance and efficiency measurement with $t\bar{t}$ events in pp collisions at $\sqrt{s} = 13$ TeV. Eur. Phys. J. C **79**, 970 (2019). https://doi.org/10.1140/epjc/s10052-019-7450-8. arXiv:1907.05120 [hep-ex]
62. ATLAS Collaboration, Calibration of the light-flavour jet mistagging efficiency of the b-tagging algorithms with Z+jets events using 139fb^{-1} of ATLAS proton–proton collision data at $\sqrt{s} = 13$ TeV. Eur. Phys. J. C **83**, 728 (2023). https://doi.org/10.1140/epjc/s10052-023-11736-z. arXiv:2301.06319 [hep-ex]
63. ATLAS Collaboration, Measurement of the c-jet mistagging efficiency in $t\bar{t}$ events using pp collision data at $\sqrt{s} = 13$ TeV collected with the ATLAS detector. Eur. Phys. J. C **82**, 95 (2022). https://doi.org/10.1140/epjc/s10052-021-09843-w. arXiv:2109.10627 [hep-ex]
64. ATLAS Collaboration, Performance of pile-up mitigation techniques for jets in pp collisions at $\sqrt{s} = 8$ TeV using the ATLAS detector. Eur. Phys. J. C **76**, 581 (2016). https://doi.org/10.1140/epjc/s10052-016-4395-z. arXiv:1510.03823 [hep-ex]
65. ATLAS Collaboration, Identification and rejection of pile-up jets at high pseudorapidity with the ATLAS detector. Eur. Phys. J. C **77**, 580 (2017). https://doi.org/10.1140/epjc/s10052-017-5081-5. arXiv:1705.02211 [hep-ex]. [Erratum: Eur. Phys. J. C **77**, 712 (2017). https://doi.org/10.1140/epjc/s10052-017-5245-3]

66. ATLAS Collaboration, Measurement of the tau lepton reconstruction and identification performance in the ATLAS experiment using pp collisions at $\sqrt{s} = 13$ TeV. ATLAS-CONF-2017-029 (2017). https://cds.cern.ch/record/2261772
67. ATLAS Collaboration, Reconstruction, energy calibration, and identification of hadronically decaying tau leptons in the ATLAS experiment for Run-2 of the LHC. ATL-PHYS-PUB-2015-045 (2015). https://cds.cern.ch/record/2064383
68. ATLAS Collaboration, Identification and energy calibration of hadronically decaying tau leptons with the ATLAS experiment in pp collisions at $\sqrt{s} = 8$ TeV. Eur. Phys. J. C **75**, 303 (2015). https://doi.org/10.1140/epjc/s10052-015-3500-z. arXiv:1412.7086 [hep-ex]
69. ATLAS Collaboration, Topological cell clustering in the ATLAS calorimeters and its performance in LHC Run 1. Eur. Phys. J. C **77**, 490 (2017). https://doi.org/10.1140/epjc/s10052-017-5004-5. arXiv:1603.02934 [hep-ex]
70. T. Barillari et al., Local hadronic calibration. ATL-LARG-PUB-2009-001-2 (2008). https://cds.cern.ch/record/1112035
71. ATLAS Collaboration, Reconstruction of hadronic decay products of tau leptons with the ATLAS experiment. Eur. Phys. J. C **76**, 295 (2016). https://doi.org/10.1140/epjc/s10052-016-4110-0. arXiv:1512.05955 [hep-ex]
72. ATLAS Collaboration, Identification of hadronic tau lepton decays using neural networks in the ATLAS experiment. ATL-PHYS-PUB-2019-033 (2019). https://cds.cern.ch/record/2688062
73. ATLAS Collaboration, The performance of missing transverse momentum reconstruction and its significance with the ATLAS detector using 140 fb^{-1} of $\sqrt{s} = 13$ TeV pp collisions. Eur. Phys. J. C **85**, 606 (2025). https://doi.org/10.1140/epjc/s10052-025-14062-8. arXiv:2402.05858 [hep-ex]
74. ATLAS Collaboration, Performance of the ATLAS muon triggers in Run 2. JINST **15**, P09015 (2020). https://doi.org/10.1088/1748-0221/15/09/p09015. arXiv:2004.13447 [physics.ins-det]
75. ATLAS Collaboration, The ATLAS inner detector trigger performance in pp collisions at 13 TeV during LHC Run 2. Eur. Phys. J. C **82**, 206 (2022). https://doi.org/10.1140/epjc/s10052-021-09920-0. arXiv:2107.02485 [hep-ex]
76. ATLAS Collaboration, Performance of electron and photon triggers in ATLAS during LHC Run 2. Eur. Phys. J. C **80**, 47 (2020). https://doi.org/10.1140/epjc/s10052-019-7500-2. arXiv:1909.00761 [hep-ex]
77. ATLAS Collaboration, The performance of the jet trigger for the ATLAS detector during, data taking. Eur. Phys. J. C **76**(2016), 526 (2011). https://doi.org/10.1140/epjc/s10052-016-4325-0. arXiv:1606.07759 [hep-ex]
78. ATLAS Collaboration, Performance and calibration of quark/gluon-jet taggers using 140 fb^{-1} of pp collisions at $\sqrt{s} = 13$ TeV with the ATLAS detector. Chin. Phys. C **48**, 023001 (2024). https://doi.org/10.1088/1674-1137/acf701. arXiv:2308.00716 [hep-ex]
79. M. Baak et al., HistFitter software framework for statistical data analysis. Eur. Phys. J. C **75**, 153 (2015). https://doi.org/10.1140/epjc/s10052-015-3327-7. arXiv:1410.1280 [hep-ex]
80. K. Cranmer, G. Lewis, L. Moneta, A. Shibata, W. Verkerke, HistFactory: a tool for creating statistical models for use with RooFit and RooStats. CERN-OPEN-2012-016 (2012). https://cds.cern.ch/record/1456844
81. L. Moneta, K. Belasco, K.S. Cranmer, S. Kreiss, A. Lazzaro, D. Piparo, G. Schott, W. Verkerke, M. Wolf, The RooStats project. PoS **ACAT2010**, 057 (2010). https://doi.org/10.22323/1.093.0057. arXiv:1009.1003 [physics.data-an]
82. W. Verkerke, D.P. Kirkby, The RooFit toolkit for data modeling. eConf **C0303241**, MOLT007 (2003)
83. F. James, MINUIT function minimization and error analysis: reference manual version 94.1. CERN-D506 (1994). https://cds.cern.ch/record/2296388
84. ATLAS Collaboration, ATLAS computing acknowledgements. ATL-SOFT-PUB-2025-001 (2025). https://cds.cern.ch/record/2922210
85. CERN, CERN Open Data Policy for the LHC Experiments, CERN-OPEN-2020-013 (2020). https://cds.cern.ch/record/2745133

ATLAS Collaboration[★]

G. Aad[105], E. Aakvaag[17], B. Abbott[124], S. Abdelhameed[120a], K. Abeling[56], N. J. Abicht[50], S. H. Abidi[30], M. Aboelela[46], A. Aboulhorma[36e], H. Abramowicz[158], Y. Abulaiti[121], B. S. Acharya[70a,70b,o], A. Ackermann[64a], C. Adam Bourdarios[4], L. Adamczyk[88a], S. V. Addepalli[150], M. J. Addison[104], J. Adelman[119], A. Adiguzel[22c], T. Adye[138], A. A. Affolder[140], Y. Afik[41], M. N. Agaras[13], A. Aggarwal[103], C. Agheorghiesei[28c], F. Ahmadov[40,ae], S. Ahuja[98], X. Ai[144b], G. Aielli[77a,77b], A. Aikot[170], M. Ait Tamlihat[36e], B. Aitbenchikh[36a], M. Akbiyik[103], T. P. A. Åkesson[101], A. V. Akimov[152], D. Akiyama[175], N. N. Akolkar[25], S. Aktas[22a], G. L. Alberghi[24b], J. Albert[172], P. Albicocco[54], G. L. Albouy[61], S. Alderweireldt[53], Z. L. Alegria[125], M. Aleksa[37], I. N. Aleksandrov[40], C. Alexa[28b], T. Alexopoulos[10], F. Alfonsi[24b], M. Algren[57], M. Alhroob[174], B. Ali[136], H. M. J. Ali[94,x], S. Ali[32], S. W. Alibocus[95], M. Aliev[34c], G. Alimonti[72a], W. Alkakhi[56], C. Allaire[67], B. M. M. Allbrooke[153], J. S. Allen[104], J. F. Allen[53], P. P. Allport[21], A. Aloisio[73a,73b], F. Alonso[93], C. Alpigiani[143], Z. M. K. Alsolami[94], A. Alvarez Fernandez[103], M. Alves Cardoso[57], M. G. Alviggi[73a,73b], M. Aly[104], Y. Amaral Coutinho[84b], A. Ambler[107], C. Amelung[37], M. Amerl[104], C. G. Ames[112], D. Amidei[109], B. Amini[55], K. Amirie[162], A. Amirkhanov[40], S. P. Amor Dos Santos[134a], K. R. Amos[170], D. Amperiadou[159], S. An[85], V. Ananiev[129], C. Anastopoulos[146], T. Andeen[11], J. K. Anders[95], A. C. Anderson[60], A. Andreazza[72a,72b], S. Angelidakis[9], A. Angerami[43], A. V. Anisenkov[40], A. Annovi[75a], C. Antel[57], E. Antipov[152], M. Antonelli[54], F. Anulli[76a], M. Aoki[85], T. Aoki[160], M. A. Aparo[153], L. Aperio Bella[49], C. Appelt[158], A. Apyan[27], S. J. Arbiol Val[89], C. Arcangeletti[54], A. T. H. Arce[52], J.-F. Arguin[111], S. Argyropoulos[159], J.-H. Arling[49], O. Arnaez[4], H. Arnold[152], G. Artoni[76a,76b], H. Asada[114], K. Asai[122], S. Asai[160], N. A. Asbah[37], R. A. Ashby Pickering[174], A. M. Aslam[98], K. Assamagan[30], R. Astalos[29a], K. S. V. Astrand[101], S. Atashi[166], R. J. Atkin[34a], H. Atmani[36f], P. A. Atmasiddha[132], K. Augsten[136], A. D. Auriol[42], V. A. Austrup[104], G. Avolio[37], K. Axiotis[57], G. Azuelos[111,aj], D. Babal[29b], H. Bachacou[139], K. Bachas[159,s], A. Bachiu[35], E. Bachmann[51], M. J. Backes[64a], A. Badea[41], T. M. Baer[109], P. Bagnaia[76a,76b], M. Bahmani[19], D. Bahner[55], K. Bai[127], J. T. Baines[138], L. Baines[97], O. K. Baker[179], E. Bakos[16], D. Bakshi Gupta[8], L. E. Balabram Filho[84b], V. Balakrishnan[124], R. Balasubramanian[4], E. M. Baldin[39], P. Balek[88a], E. Ballabene[24a,24b], F. Balli[139], L. M. Baltes[64a], W. K. Balunas[33], J. Balz[103], I. Bamwidhi[120b], E. Banas[89], M. Bandieramonte[133], A. Bandyopadhyay[25], S. Bansal[25], L. Barak[158], M. Barakat[49], E. L. Barberio[108], D. Barberis[18b], M. Barbero[105], M. Z. Barel[118], T. Barillari[113], M.-S. Barisits[37], T. Barklow[150], P. Baron[126], D. A. Baron Moreno[104], A. Baroncelli[63], A. J. Barr[130], J. D. Barr[99], F. Barreiro[102], J. Barreiro Guimarães da Costa[14], M. G. Barros Teixeira[134a], S. Barsov[39], F. Bartels[64a], R. Bartoldus[150], A. E. Barton[94], P. Bartos[29a], A. Basan[103], M. Baselga[50], S. Bashiri[89], A. Bassalat[67,b], M. J. Basso[163a], S. Bataju[46], R. Bate[171], R. L. Bates[60], S. Batlamous[102], M. Battaglia[140], D. Battulga[19], M. Bauce[76a,76b], M. Bauer[80], P. Bauer[25], L. T. Bayer[49], L. T. Bazzano Hurrell[31], J. B. Beacham[113], T. Beau[131], J. Y. Beaucamp[93], P. H. Beauchemin[165], P. Bechtle[25], H. P. Beck[20,r], K. Becker[174], A. J. Beddall[83], V. A. Bednyakov[40], C. P. Bee[152], L. J. Beemster[16], M. Begalli[84d], M. Begel[30], J. K. Behr[49], J. F. Beirer[37], F. Beisiegel[25], M. Belfkir[120b], G. Bella[158], L. Bellagamba[24b], A. Bellerive[35], P. Bellos[21], K. Beloborodov[39], D. Benchekroun[36a], F. Bendebba[36a], Y. Benhammou[158], K. C. Benkendorfer[62], L. Beresford[49], M. Beretta[54], E. Bergeaas Kuutmann[168], N. Berger[4], B. Bergmann[136], J. Beringer[18a], G. Bernardi[5], C. Bernius[150], F. U. Bernlochner[25], F. Bernon[37], A. Berrocal Guardia[13], T. Berry[98], P. Berta[137], A. Berthold[51], R. Bertrand[105], S. Bethke[113], A. Betti[76a,76b], A. J. Bevan[97], L. Bezio[57], N. K. Bhalla[55], S. Bharthuar[113], S. Bhatta[152], D. S. Bhattacharya[173], P. Bhattarai[150], Z. M. Bhatti[121], K. D. Bhide[55], V. S. Bhopatkar[125], R. M. Bianchi[133], G. Bianco[24a,24b], O. Biebel[112], M. Biglietti[78a], C. S. Billingsley[46], Y. Bimgdi[36f], M. Bindi[56], A. Bingham[178], A. Bingul[22b], C. Bini[76a,76b], G. A. Bird[33], M. Birman[176], M. Biros[137], S. Biryukov[153], T. Bisanz[50], E. Bisceglie[24a,24b], J. P. Biswal[138], D. Biswas[148], I. Bloch[49], A. Blue[60], U. Blumenschein[97], J. Blumenthal[103], V. S. Bobrovnikov[40], M. Boehler[55], B. Boehm[173], D. Bogavac[37], A. G. Bogdanchikov[39], L. S. Boggia[131], V. Boisvert[98], P. Bokan[37], T. Bold[88a], M. Bomben[5], M. Bona[97], M. Boonekamp[139], A. G. Borbély[60], I. S. Bordulev[39], G. Borissov[94], D. Bortoletto[130], D. Boscherini[24b], M. Bosman[13], K. Bouaouda[36a], N. Bouchhar[170], L. Boudet[4], J. Boudreau[133], E. V. Bouhova-Thacker[94], D. Boumediene[42], R. Bouquet[58a,58b], A. Boveia[123], J. Boyd[37], D. Boye[30], I. R. Boyko[40], L. Bozianu[57], J. Bracinik[21], N. Brahimi[4], G. Brandt[178], O. Brandt[33], B. Brau[106], J. E. Brau[127], R. Brener[176], L. Brenner[118], R. Brenner[168], S. Bressler[176], G. Brianti[79a,79b], D. Britton[60], D. Britzger[113], I. Brock[25],

R. Brock[110], G. Brooijmans[43], A. J. Brooks[69], E. M. Brooks[163b], E. Brost[30], L. M. Brown[163a,172], L. E. Bruce[62], T. L. Bruckler[130], P. A. Bruckman de Renstrom[89], B. Brüers[49], A. Bruni[24b], G. Bruni[24b], D. Brunner[48a,48b], M. Bruschi[24b], N. Bruscino[76a,76b], T. Buanes[17], Q. Buat[143], D. Buchin[113], A. G. Buckley[60], O. Bulekov[39], B. A. Bullard[150], S. Burdin[95], C. D. Burgard[50], A. M. Burger[37], B. Burghgrave[8], O. Burlayenko[55], J. Burleson[169], J. T. P. Burr[33], J. C. Burzynski[149], E. L. Busch[43], V. Büscher[103], P. J. Bussey[60], J. M. Butler[26], C. M. Buttar[60], J. M. Butterworth[99], W. Buttinger[138], C. J. Buxo Vazquez[110], A. R. Buzykaev[40], S. Cabrera Urbán[170], L. Cadamuro[67], D. Caforio[59], H. Cai[133], Y. Cai[24a,24b,115c], Y. Cai[115a], V. M. M. Cairo[37], O. Cakir[3a], N. Calace[37], P. Calafiura[18a], G. Calderini[131], P. Calfayan[35], G. Callea[60], L. P. Caloba[84b], D. Calvet[42], S. Calvet[42], R. Camacho Toro[131], S. Camarda[37], D. Camarero Munoz[27], P. Camarri[77a,77b], M. T. Camerlingo[73a,73b], C. Camincher[172], M. Campanelli[99], A. Camplani[44], V. Canale[73a,73b], A. C. Canbay[3a], E. Canonero[98], J. Cantero[170], Y. Cao[169], F. Capocasa[27], M. Capua[45a,45b], A. Carbone[72a,72b], R. Cardarelli[77a], J. C. J. Cardenas[8], M. P. Cardiff[27], G. Carducci[45a,45b], T. Carli[37], G. Carlino[73a], J. I. Carlotto[13], B. T. Carlson[133,t], E. M. Carlson[172], J. Carmignani[95], L. Carminati[72a,72b], A. Carnelli[4], M. Carnesale[37], S. Caron[117], E. Carquin[141f], I. B. Carr[108], S. Carrá[72a], G. Carratta[24a,24b], A. M. Carroll[127], M. P. Casado[13,i], M. Caspar[49], F. L. Castillo[4], L. Castillo Garcia[13], V. Castillo Gimenez[170], N. F. Castro[134a,134e], A. Catinaccio[37], J. R. Catmore[129], T. Cavaliere[4], V. Cavaliere[30], L. J. Caviedes Betancourt[23b], Y. C. Cekmecelioglu[49], E. Celebi[83], S. Cella[37], V. Cepaitis[57], K. Cerny[126], A. S. Cerqueira[84a], A. Cerri[75a,75b], L. Cerrito[77a,77b], F. Cerutti[18a], B. Cervato[72a,72b], A. Cervelli[24b], G. Cesarini[54], S. A. Cetin[83], P. M. Chabrillat[131], J. Chan[18a], W. Y. Chan[160], J. D. Chapman[33], E. Chapon[139], B. Chargeishvili[156b], D. G. Charlton[21], C. Chauhan[137], Y. Che[115a], S. Chekanov[6], S. V. Chekulaev[163a], G. A. Chelkov[40,a], B. Chen[158], B. Chen[172], H. Chen[115a], H. Chen[30], J. Chen[145a], J. Chen[149], M. Chen[130], S. Chen[90], S. J. Chen[115a], X. Chen[145a], X. Chen[15,ai], Z. Chen[63], C. L. Cheng[177], H. C. Cheng[65a], S. Cheong[150], A. Cheplakov[40], E. Cheremushkina[49], E. Cherepanova[118], R. Cherkaoui El Moursli[36e], E. Cheu[7], K. Cheung[66], L. Chevalier[139], V. Chiarella[54], G. Chiarelli[75a], N. Chiedde[105], G. Chiodini[71a], A. S. Chisholm[21], A. Chitan[28b], M. Chitishvili[170], M. V. Chizhov[40,u], K. Choi[11], Y. Chou[143], E. Y. S. Chow[117], K. L. Chu[176], M. C. Chu[65a], X. Chu[14,115c], Z. Chubinidze[54], J. Chudoba[135], J. J. Chwastowski[89], D. Cieri[113], K. M. Ciesla[88a], V. Cindro[96], A. Ciocio[18a], F. Cirotto[73a,73b], Z. H. Citron[176], M. Citterio[72a], D. A. Ciubotaru[28b], A. Clark[57], P. J. Clark[53], N. Clarke Hall[99], C. Clarry[162], S. E. Clawson[49], C. Clement[48a,48b], Y. Coadou[105], M. Cobal[70a,70c], A. Coccaro[58b], R. F. Coelho Barrue[134a], R. Coelho Lopes De Sa[106], S. Coelli[72a], L. S. Colangeli[162], B. Cole[43], P. Collado Soto[102], J. Collot[61], P. Conde Muiño[134a,134g], M. P. Connell[34c], S. H. Connell[34c], E. I. Conroy[130], M. Contreras Cossio[11], F. Conventi[73a,ak], H. G. Cooke[21], A. M. Cooper-Sarkar[130], F. A. Corchia[24a,24b], A. Cordeiro Oudot Choi[131], L. D. Corpe[42], M. Corradi[76a,76b], F. Corriveau[107,ac], A. Cortes-Gonzalez[19], M. J. Costa[170], F. Costanza[4], D. Costanzo[146], B. M. Cote[123], J. Couthures[4], G. Cowan[98], K. Cranmer[177], L. Cremer[50], D. Cremonini[24a,24b], S. Crépé-Renaudin[61], F. Crescioli[131], T. Cresta[74a,74b], M. Cristinziani[148], M. Cristoforetti[79a,79b], V. Croft[118], J. E. Crosby[125], G. Crosetti[45a,45b], A. Cueto[102], H. Cui[99], Z. Cui[7], W. R. Cunningham[60], F. Curcio[170], J. R. Curran[53], P. Czodrowski[37], M. J. Da Cunha Sargedas De Sousa[58a,58b], J. V. Da Fonseca Pinto[84b], C. Da Via[104], W. Dabrowski[88a], T. Dado[37], S. Dahbi[155], T. Dai[109], D. Dal Santo[20], C. Dallapiccola[106], M. Dam[44], G. D'amen[30], V. D'Amico[112], J. Damp[103], J. R. Dandoy[35], D. Dannheim[37], M. Danninger[149], V. Dao[152], G. Darbo[58b], S. J. Das[30], F. Dattola[49], S. D'Auria[72a,72b], A. D'Avanzo[73a,73b], T. Davidek[137], I. Dawson[97], H. A. Day-hall[136], K. De[8], C. De Almeida Rossi[162], R. De Asmundis[73a], N. De Biase[49], S. De Castro[24a,24b], N. De Groot[117], P. de Jong[118], H. De la Torre[119], A. De Maria[115a], A. De Salvo[76a], U. De Sanctis[77a,77b], F. De Santis[71a,71b], A. De Santo[153], J. B. De Vivie De Regie[61], J. Debevc[96], D. V. Dedovich[40], J. Degens[95], A. M. Deiana[46], J. Del Peso[102], L. Delagrange[131], F. Deliot[139], C. M. Delitzsch[50], M. Della Pietra[73a,73b], D. Della Volpe[57], A. Dell'Acqua[37], L. Dell'Asta[72a,72b], M. Delmastro[4], C. C. Delogu[103], P. A. Delsart[61], S. Demers[179], M. Demichev[40], S. P. Denisov[39], H. Denizli[22a,m], L. D'Eramo[42], D. Derendarz[89], F. Derue[131], P. Dervan[95,*], K. Desch[25], C. Deutsch[25], F. A. Di Bello[58a,58b], A. Di Ciaccio[77a,77b], L. Di Ciaccio[4], A. Di Domenico[76a,76b], C. Di Donato[73a,73b], A. Di Girolamo[37], G. Di Gregorio[37], A. Di Luca[79a,79b], B. Di Micco[78a,78b], R. Di Nardo[78a,78b], K. F. Di Petrillo[41], M. Diamantopoulou[35], F. A. Dias[118], T. Dias Do Vale[149], M. A. Diaz[141a,141b], A. R. Didenko[40], M. Didenko[170], E. B. Diehl[109], S. Díez Cornell[49], C. Diez Pardos[148], C. Dimitriadi[151], A. Dimitrievska[21], A. Dimri[152], J. Dingfelder[25], T. Dingley[130], I.-M. Dinu[28b], S. J. Dittmeier[64b], F. Dittus[37], M. Divisek[137], B. Dixit[95], F. Djama[105], T. Djobava[156b], C. Doglioni[101,104],

A. Dohnalova[29a], Z. Dolezal[137], K. Domijan[88a], K. M. Dona[41], M. Donadelli[84d], B. Dong[110], J. Donini[42], A. D'Onofrio[73a,73b], M. D'Onofrio[95], J. Dopke[138], A. Doria[73a], N. Dos Santos Fernandes[134a], P. Dougan[104], M. T. Dova[93], A. T. Doyle[60], M. A. Draguet[130], M. P. Drescher[56], E. Dreyer[176], I. Drivas-koulouris[10], M. Drnevich[121], M. Drozdova[57], D. Du[63], T. A. du Pree[118], F. Dubinin[40], M. Dubovsky[29a], E. Duchovni[176], G. Duckeck[112], P. K. Duckett[99], O. A. Ducu[28b], D. Duda[53], A. Dudarev[37], E. R. Duden[27], M. D'uffizi[104], L. Duflot[67], M. Dührssen[37], I. Duminica[28g], A. E. Dumitriu[28b], M. Dunford[64a], S. Dungs[50], K. Dunne[48a,48b], A. Duperrin[105], H. Duran Yildiz[3a], M. Düren[59], A. Durglishvili[156b], D. Duvnjak[35], B. L. Dwyer[119], G. I. Dyckes[18a], M. Dyndal[88a], B. S. Dziedzic[37], Z. O. Earnshaw[153], G. H. Eberwein[130], B. Eckerova[29a], S. Eggebrecht[56], E. Egidio Purcino De Souza[84e], G. Eigen[17], K. Einsweiler[18a], T. Ekelof[168], P. A. Ekman[101], S. El Farkh[36b], Y. El Ghazali[63], H. El Jarrari[37], A. El Moussaouy[36a], V. Ellajosyula[168], M. Ellert[168], F. Ellinghaus[178], N. Ellis[37], J. Elmsheuser[30], M. Elsawy[120a], M. Elsing[37], D. Emeliyanov[138], Y. Enari[85], I. Ene[18a], S. Epari[111], D. Ernani Martins Neto[89], M. Errenst[178], M. Escalier[67], C. Escobar[170], E. Etzion[158], G. Evans[134a,134b], H. Evans[69], L. S. Evans[98], A. Ezhilov[39], S. Ezzarqtouni[36a], F. Fabbri[24a,24b], L. Fabbri[24a,24b], G. Facini[99], V. Fadeyev[140], R. M. Fakhrutdinov[39], D. Fakoudis[103], S. Falciano[76a], L. F. Falda Ulhoa Coelho[134a], F. Fallavollita[113], G. Falsetti[45a,45b], J. Faltova[137], C. Fan[169], K. Y. Fan[65b], Y. Fan[14], Y. Fang[14,115c], M. Fanti[72a,72b], M. Faraj[70a,70b], Z. Farazpay[100], A. Farbin[8], A. Farilla[78a], T. Farooque[110], J. N. Farr[179], S. M. Farrington[53,138], F. Fassi[36e], D. Fassouliotis[9], L. Fayard[67], P. Federic[137], P. Federicova[135], O. L. Fedin[39,a], M. Feickert[177], L. Feligioni[105], D. E. Fellers[18a], C. Feng[144a], Z. Feng[118], M. J. Fenton[166], L. Ferencz[49], B. Fernandez Barbadillo[94], P. Fernandez Martinez[68], M. J. V. Fernoux[105], J. Ferrando[94], A. Ferrari[168], P. Ferrari[117,118], R. Ferrari[74a], D. Ferrere[57], C. Ferretti[109], M. P. Fewell[1], D. Fiacco[76a,76b], F. Fiedler[103], P. Fiedler[136], S. Filimonov[40], A. Filipčič[96], E. K. Filmer[163a], F. Filthaut[117], M. C. N. Fiolhais[134a,134c,c], L. Fiorini[170], W. C. Fisher[110], T. Fitschen[104], P. M. Fitzhugh[139], I. Fleck[148], P. Fleischmann[109], T. Flick[178], M. Flores[34d,ag], L. R. Flores Castillo[65a], L. Flores Sanz De Acedo[37], F. M. Follega[79a,79b], N. Fomin[33], J. H. Foo[162], A. Formica[139], A. C. Forti[104], E. Fortin[37], A. W. Fortman[18a], L. Fountas[9,j], D. Fournier[67], H. Fox[94], P. Francavilla[75a,75b], S. Francescato[62], S. Franchellucci[57], M. Franchini[24a,24b], S. Franchino[64a], D. Francis[37], L. Franco[117], V. Franco Lima[37], L. Franconi[49], M. Franklin[62], G. Frattari[27], Y. Y. Frid[158], J. Friend[60], N. Fritzsche[37], A. Froch[57], D. Froidevaux[37], J. A. Frost[130], Y. Fu[110], S. Fuenzalida Garrido[141f], M. Fujimoto[105], K. Y. Fung[65a], E. Furtado De Simas Filho[84e], M. Furukawa[160], J. Fuster[170], A. Gaa[56], A. Gabrielli[24a,24b], A. Gabrielli[162], P. Gadow[37], G. Gagliardi[58a,58b], L. G. Gagnon[18a], S. Gaid[86b], S. Galantzan[158], J. Gallagher[1], E. J. Gallas[130], A. L. Gallen[168], B. J. Gallop[138], K. K. Gan[123], S. Ganguly[160], Y. Gao[53], A. Garabaglu[143], F. M. Garay Walls[141a,141b], B. Garcia[30], C. García[170], A. Garcia Alonso[118], A. G. Garcia Caffaro[179], J. E. García Navarro[170], M. Garcia-Sciveres[18a], G. L. Gardner[132], R. W. Gardner[41], N. Garelli[165], R. B. Garg[150], J. M. Gargan[53], C. A. Garner[162], C. M. Garvey[34a], V. K. Gassmann[165], G. Gaudio[74a], V. Gautam[13], P. Gauzzi[76a,76b], J. Gavranovic[96], I. L. Gavrilenko[134a], A. Gavrilyuk[39], C. Gay[171], G. Gaycken[127], E. N. Gazis[10], A. Gekow[123], C. Gemme[58b], M. H. Genest[61], A. D. Gentry[116], S. George[98], W. F. George[21], T. Geralis[47], A. A. Gerwin[124], P. Gessinger-Befurt[37], M. E. Geyik[178], M. Ghani[174], K. Ghorbanian[97], A. Ghosal[148], A. Ghosh[166], A. Ghosh[7], B. Giacobbe[24b], S. Giagu[76a,76b], T. Giani[118], A. Giannini[63], S. M. Gibson[98], M. Gignac[140], D. T. Gil[88b], A. K. Gilbert[88a], B. J. Gilbert[43], D. Gillberg[35], G. Gilles[118], L. Ginabat[131], D. M. Gingrich[2,aj], M. P. Giordani[70a,70c], P. F. Giraud[139], G. Giugliarelli[70a,70c], D. Giugni[72a], F. Giuli[77a,77b], I. Gkialas[9,j], L. K. Gladilin[39], C. Glasman[102], G. Glemža[49], M. Glisic[127], I. Gnesi[45b], Y. Go[30], M. Goblirsch-Kolb[37], B. Gocke[50], D. Godin[111], B. Gokturk[22a], S. Goldfarb[108], T. Golling[57], M. G. D. Gololo[34c], D. Golubkov[39], J. P. Gombas[110], A. Gomes[134a,134b], G. Gomes Da Silva[148], A. J. Gomez Delegido[170], R. Gonçalo[134a], L. Gonella[21], A. Gongadze[156c], F. Gonnella[21], J. L. Gonski[150], R. Y. González Andana[53], S. González de la Hoz[170], C. Gonzalez Renteria[18a], M. V. Gonzalez Rodrigues[49], R. Gonzalez Suarez[168], S. Gonzalez-Sevilla[57], L. Goossens[37], B. Gorini[37], E. Gorini[71a,71b], A. Gorišek[96], T. C. Gosart[132], A. T. Goshaw[52], M. I. Gostkin[40], S. Goswami[125], C. A. Gottardo[37], S. A. Gotz[112], M. Gouighri[36b], A. G. Goussiou[143], N. Govender[34c], R. P. Grabarczyk[130], I. Grabowska-Bold[88a], K. Graham[35], E. Gramstad[129], S. Grancagnolo[71a,71b], C. M. Grant[1,139], P. M. Gravila[28f], F. G. Gravili[71a,71b], H. M. Gray[18a], M. Greco[113], M. J. Green[1], C. Grefe[25], A. S. Grefsrud[17], I. M. Gregor[49], K. T. Greif[166], P. Grenier[150], S. G. Grewe[113], A. A. Grillo[140], K. Grimm[32], S. Grinstein[13,y], J.-F. Grivaz[67], E. Gross[176], J. Grosse-Knetter[56], L. Guan[109], G. Guerrieri[37], R. Guevara[129], R. Gugel[103], J. A. M. Guhit[109], A. Guida[19], E. Guilloton[174], S. Guindon[37], F. Guo[14,115c], J. Guo[145a], L. Guo[49], L. Guo[115b,w], Y. Guo[109], A. Gupta[50],

R. Gupta[133], S. Gurbuz[25], S. S. Gurdasani[49], G. Gustavino[76a,76b], P. Gutierrez[124], L. F. Gutierrez Zagazeta[132], M. Gutsche[51], C. Gutschow[99], C. Gwenlan[130], C. B. Gwilliam[95], E. S. Haaland[129], A. Haas[121], M. Habedank[60], C. Haber[18a], H. K. Hadavand[8], A. Haddad[42], A. Hadef[51], A. I. Hagan[94], J. J. Hahn[148], E. H. Haines[99], M. Haleem[173], J. Haley[125], G. D. Hallewell[105], L. Halser[20], K. Hamano[172], M. Hamer[25], S. E. D. Hammoud[67], E. J. Hampshire[98], J. Han[144a], L. Han[115a], L. Han[63], S. Han[18a], K. Hanagaki[85], M. Hance[140], D. A. Hangal[43], H. Hanif[149], M. D. Hank[132], J. B. Hansen[44], P. H. Hansen[44], D. Harada[57], T. Harenberg[178], S. Harkusha[180], M. L. Harris[106], Y. T. Harris[25], J. Harrison[13], N. M. Harrison[123], P. F. Harrison[174], N. M. Hartman[113], N. M. Hartmann[112], R. Z. Hasan[98,138], Y. Hasegawa[147], F. Haslbeck[130], S. Hassan[17], R. Hauser[110], M. Haviernik[137], C. M. Hawkes[21], R. J. Hawkings[37], Y. Hayashi[160], D. Hayden[110], C. Hayes[109], R. L. Hayes[118], C. P. Hays[130], J. M. Hays[97], H. S. Hayward[95], F. He[63], M. He[14,115c], Y. He[49], Y. He[99], N. B. Heatley[97], V. Hedberg[101], A. L. Heggelund[129], C. Heidegger[55], K. K. Heidegger[55], J. Heilman[35], S. Heim[49], T. Heim[18a], J. G. Heinlein[132], J. J. Heinrich[127], L. Heinrich[113,ah], J. Hejbal[135], A. Held[177], S. Hellesund[17], C. M. Helling[171], S. Hellman[48a,48b], L. Henkelmann[33], A. M. Henriques Correia[37], H. Herde[101], Y. Hernández Jiménez[152], L. M. Herrmann[25], T. Herrmann[51], G. Herten[55], R. Hertenberger[112], L. Hervas[37], M. E. Hesping[103], N. P. Hessey[163a], J. Hessler[113], M. Hidaoui[36b], N. Hidic[137], E. Hill[162], S. J. Hillier[21], J. R. Hinds[110], F. Hinterkeuser[25], M. Hirose[128], S. Hirose[164], D. Hirschbuehl[178], T. G. Hitchings[104], B. Hiti[96], J. Hobbs[152], R. Hobincu[28e], N. Hod[176], M. C. Hodgkinson[146], B. H. Hodkinson[130], A. Hoecker[37], D. D. Hofer[109], J. Hofer[170], M. Holzbock[37], L. B. A. H. Hommels[33], V. Homsak[130], B. P. Honan[104], J. J. Hong[69], J. Hong[145a], T. M. Hong[133], B. H. Hooberman[169], W. H. Hopkins[6], M. C. Hoppesch[169], Y. Horii[114], M. E. Horstmann[113], S. Hou[155], M. R. Housenga[169], A. S. Howard[96], J. Howarth[60], J. Hoya[6], M. Hrabovsky[126], T. Hryn'ova[4], P. J. Hsu[66], S.-C. Hsu[143], T. Hsu[67], M. Hu[18a], Q. Hu[63], S. Huang[33], X. Huang[14,115c], Y. Huang[137], Y. Huang[115b], Y. Huang[103], Y. Huang[14], Z. Huang[104], Z. Hubacek[136], M. Huebner[25], F. Huegging[25], T. B. Huffman[130], M. Hufnagel Maranha De Faria[84a], C. A. Hugli[49], M. Huhtinen[37], S. K. Huiberts[17], R. Hulsken[107], C. E. Hultquist[18a], N. Huseynov[12,g], J. Huston[110], J. Huth[62], R. Hyneman[7], G. Iacobucci[57], G. Iakovidis[30], L. Iconomidou-Fayard[67], J. P. Iddon[37], P. Iengo[73a,73b], R. Iguchi[160], Y. Iiyama[160], T. Iizawa[130], Y. Ikegami[85], D. Iliadis[159], N. Ilic[162], H. Imam[84c], G. Inacio Goncalves[84d], S. A. Infante Cabanas[141c], T. Ingebretsen Carlson[48a,48b], J. M. Inglis[97], G. Introzzi[74a,74b], M. Iodice[78a], V. Ippolito[76a,76b], R. K. Irwin[95], M. Ishino[160], W. Islam[177], C. Issever[19], S. Istin[22a,ao], K. Itabashi[85], H. Ito[175], R. Iuppa[79a,79b], A. Ivina[176], V. Izzo[73a], P. Jacka[135], P. Jackson[1], P. Jain[49], K. Jakobs[55], T. Jakoubek[176], J. Jamieson[60], W. Jang[160], S. Jankovych[137], M. Javurkova[106], P. Jawahar[104], L. Jeanty[127], J. Jejelava[156a,af], P. Jenni[55,f], C. E. Jessiman[35], C. Jia[144a], H. Jia[171], J. Jia[152], X. Jia[14,115c], Z. Jia[115a], C. Jiang[53], Q. Jiang[65b], S. Jiggins[49], J. Jimenez Pena[13], S. Jin[115a], A. Jinaru[28b], O. Jinnouchi[142], P. Johansson[146], K. A. Johns[7], J. W. Johnson[140], F. A. Jolly[49], D. M. Jones[153], E. Jones[49], K. S. Jones[8], P. Jones[33], R. W. L. Jones[94], T. J. Jones[95], H. L. Joos[37,56], R. Joshi[123], J. Jovicevic[16], X. Ju[18a], J. J. Junggeburth[37], T. Junkermann[64a], A. Juste Rozas[13,y], M. K. Juzek[89], S. Kabana[141e], A. Kaczmarska[89], M. Kado[113], H. Kagan[123], M. Kagan[150], A. Kahn[132], C. Kahra[103], T. Kaji[160], E. Kajomovitz[157], N. Kakati[176], I. Kalaitzidou[55], S. Kandel[8], N. J. Kang[140], D. Kar[34g], K. Karava[130], E. Karentzos[25], O. Karkout[118], S. N. Karpov[40], Z. M. Karpova[40], V. Kartvelishvili[94], A. N. Karyukhin[39], E. Kasimi[159], J. Katzy[49], S. Kaur[35], K. Kawade[147], M. P. Kawale[124], C. Kawamoto[90], T. Kawamoto[63], E. F. Kay[37], F. I. Kaya[165], S. Kazakos[110], V. F. Kazanin[39], Y. Ke[152], J. M. Keaveney[34a], R. Keeler[172], G. V. Kehris[62], J. S. Keller[35], J. J. Kempster[153], O. Kepka[135], J. Kerr[163b], B. P. Kerridge[138], B. P. Kerševan[96], L. Keszeghova[29a], R. A. Khan[133], A. Khanov[125], A. G. Kharlamov[39], T. Kharlamova[39], E. E. Khoda[143], M. Kholodenko[134a], T. J. Khoo[19], G. Khoriauli[173], J. Khubua[156b,*], Y. A. R. Khwaira[131], B. Kibirige[34g], D. Kim[6], D. W. Kim[48a,48b], Y. K. Kim[41], N. Kimura[99], M. K. Kingston[56], A. Kirchhoff[56], C. Kirfel[25], F. Kirfel[25], J. Kirk[138], A. E. Kiryunin[113], S. Kita[164], C. Kitsaki[10], O. Kivernyk[25], M. Klassen[165], C. Klein[35], L. Klein[173], M. H. Klein[46], S. B. Klein[57], U. Klein[95], A. Klimentov[30], T. Klioutchnikova[37], P. Kluit[118], S. Kluth[113], E. Kneringer[80], T. M. Knight[162], A. Knue[50], M. Kobel[51], D. Kobylianskii[176], S. F. Koch[130], M. Kocian[150], P. Kodyš[137], D. M. Koeck[127], P. T. Koenig[25], T. Koffas[35], O. Kolay[51], I. Koletsou[4], T. Komarek[89], K. Köneke[56], A. X. Y. Kong[1], T. Kono[122], N. Konstantinidis[99], P. Kontaxakis[57], B. Konya[101], R. Kopeliansky[43], S. Koperny[88a], K. Korcyl[89], K. Kordas[159,e], A. Korn[99], S. Korn[56], I. Korolkov[13], N. Korotkova[39], B. Kortman[118], O. Kortner[113], S. Kortner[113], W. H. Kostecka[119], V. V. Kostyukhin[148], A. Kotsokechagia[37], A. Kotwal[52], A. Koulouris[37],

A. Kourkoumeli-Charalampidi[74a,74b], C. Kourkoumelis[9], E. Kourlitis[113], O. Kovanda[127], R. Kowalewski[172], W. Kozanecki[127], A. S. Kozhin[39], V. A. Kramarenko[39], G. Kramberger[96], P. Kramer[25], M. W. Krasny[131], A. Krasznahorkay[106], A. C. Kraus[119], J. W. Kraus[178], J. A. Kremer[49], N. B. Krengel[148], T. Kresse[51], L. Kretschmann[178], J. Kretzschmar[95], K. Kreul[19], P. Krieger[162], K. Krizka[21], K. Kroeninger[50], H. Kroha[113], J. Kroll[135], J. Kroll[132], K. S. Krowpman[110], U. Kruchonak[40], H. Krüger[25], N. Krumnack[82], M. C. Kruse[52], O. Kuchinskaia[40], S. Kuday[3a], S. Kuehn[37], R. Kuesters[55], T. Kuhl[49], V. Kukhtin[40], Y. Kulchitsky[40], S. Kuleshov[141b,141d], M. Kumar[34g], N. Kumari[49], P. Kumari[163b], A. Kupco[135], T. Kupfer[50], A. Kupich[39], O. Kuprash[55], H. Kurashige[87], L. L. Kurchaninov[163a], O. Kurdysh[4], Y. A. Kurochkin[38], A. Kurova[39], M. Kuze[142], A. K. Kvam[106], J. Kvita[126], N. G. Kyriacou[109], L. A. O. Laatu[105], C. Lacasta[170], F. Lacava[76a,76b], H. Lacker[19], D. Lacour[131], N. N. Lad[99], E. Ladygin[40], A. Lafarge[42], B. Laforge[131], T. Lagouri[179], F. Z. Lahbabi[36a], S. Lai[56], J. E. Lambert[172], S. Lammers[69], W. Lampl[7], C. Lampoudis[159,e], G. Lamprinoudis[103], A. N. Lancaster[119], E. Lançon[30], U. Landgraf[55], M. P. J. Landon[97], V. S. Lang[55], O. K. B. Langrekken[129], A. J. Lankford[166], F. Lanni[37], K. Lantzsch[25], A. Lanza[74a], M. Lanzac Berrocal[170], J. F. Laporte[139], T. Lari[72a], D. Larsen[17], F. Lasagni Manghi[24b], M. Lassnig[37], V. Latonova[135], S. D. Lawlor[146], Z. Lawrence[104], R. Lazaridou[174], M. Lazzaroni[72a,72b], H. D. M. Le[110], E. M. Le Boulicaut[179], L. T. Le Pottier[18a], B. Leban[24a,24b], M. LeBlanc[104], F. Ledroit-Guillon[61], S. C. Lee[155], T. F. Lee[95], L. L. Leeuw[34c,am], M. Lefebvre[172], C. Leggett[18a], G. Lehmann Miotto[37], M. Leigh[57], W. A. Leight[106], W. Leinonen[117], A. Leisos[159,v], M. A. L. Leite[84c], C. E. Leitgeb[19], R. Leitner[137], K. J. C. Leney[46], T. Lenz[25], S. Leone[75a], C. Leonidopoulos[53], A. Leopold[151], J. H. Lepage Bourbonnais[35], R. Les[110], C. G. Lester[33], M. Levchenko[39], J. Levêque[4], L. J. Levinson[176], G. Levrini[24a,24b], M. P. Lewicki[89], C. Lewis[143], D. J. Lewis[4], L. Lewitt[146], A. Li[30], B. Li[144a], C. Li[109], C.-Q. Li[113], H. Li[63], H. Li[144a], H. Li[104], H. Li[15], H. Li[63], H. Li[144a], J. Li[145a], K. Li[14], L. Li[145a], R. Li[179], S. Li[14,115c], S. Li[145a,145b,d], T. Li[5], X. Li[107], Z. Li[160], Z. Li[14,115c], Z. Li[63], S. Liang[14,115c], Z. Liang[14], M. Liberatore[139], B. Liberti[77a], K. Lie[65c], J. Lieber Marin[84e], H. Lien[69], H. Lin[109], L. Linden[112], R. E. Lindley[7], J. H. Lindon[2], J. Ling[62], E. Lipeles[132], A. Lipniacka[17], A. Lister[171], J. D. Little[69], B. Liu[14], B. X. Liu[115b], D. Liu[145a,145b], E. H. L. Liu[21], J. K. K. Liu[33], K. Liu[145b], K. Liu[145a,145b], M. Liu[63], M. Y. Liu[63], P. Liu[14], Q. Liu[143,145a,145b], X. Liu[63], X. Liu[144a], Y. Liu[115b,115c], Y. L. Liu[144a], Y. W. Liu[63], Z. Liu[67,l], S. L. Lloyd[97], E. M. Lobodzinska[49], P. Loch[7], E. Lodhi[162], T. Lohse[19], K. Lohwasser[146], E. Loiacono[49], J. D. Lomas[21], J. D. Long[43], I. Longarini[166], R. Longo[169], A. Lopez Solis[49], N. A. Lopez-canelas[7], N. Lorenzo Martinez[4], A. M. Lory[112], M. Losada[120a], G. Löschcke Centeno[153], O. Loseva[39], X. Lou[48a,48b], X. Lou[14,115c], A. Lounis[67], P. A. Love[94], G. Lu[14,115c], M. Lu[67], S. Lu[132], Y. J. Lu[155], H. J. Lubatti[143], C. Luci[76a,76b], F. L. Lucio Alves[115a], F. Luehring[69], B. S. Lunday[132], O. Lundberg[151], B. Lund-Jensen[151,*], N. A. Luongo[6], M. S. Lutz[37], A. B. Lux[26], D. Lynn[30], R. Lysak[135], V. Lysenko[136], E. Lytken[101], V. Lyubushkin[40], T. Lyubushkina[40], M. M. Lyukova[152], M. Firdaus M. Soberi[53], H. Ma[30], K. Ma[63], L. L. Ma[144a], W. Ma[63], Y. Ma[125], J. C. MacDonald[103], P. C. Machado De Abreu Farias[84e], R. Madar[42], T. Madula[99], J. Maeda[87], T. Maeno[30], P. T. Mafa[34c,k], H. Maguire[146], V. Maiboroda[67], A. Maio[134a,134b,134d], K. Maj[88a], O. Majersky[49], S. Majewski[127], R. Makhmanazarov[39], N. Makovec[67], V. Maksimovic[16], B. Malaescu[131], J. Malamant[129], Pa. Malecki[89], V. P. Maleev[39], F. Malek[61,q], M. Mali[96], D. Malito[98], U. Mallik[81,*], S. Maltezos[10], A. Malvezzi Lopes[84d], S. Malyukov[40], J. Mamuzic[13], G. Mancini[54], M. N. Mancini[27], G. Manco[74a,74b], J. P. Mandalia[97], S. S. Mandarry[153], I. Mandić[96], L. Manhaes de Andrade Filho[84a], I. M. Maniatis[176], J. Manjarres Ramos[92], D. C. Mankad[176], A. Mann[112], T. Manoussos[37], S. Manzoni[37], L. Mao[145a], X. Mapekula[34c], A. Marantis[159,v], R. R. Marcelo Gregorio[97], G. Marchiori[5], M. Marcisovsky[135], C. Marcon[72a], M. Marinescu[21], S. Marium[49], M. Marjanovic[124], A. Markhoos[55], M. Markovitch[67], M. K. Maroun[106], E. J. Marshall[94], Z. Marshall[18a], S. Marti-Garcia[170], J. Martin[99], T. A. Martin[138], V. J. Martin[53], B. Martin dit Latour[17], L. Martinelli[76a,76b], M. Martinez[13,y], P. Martinez Agullo[170], V. I. Martinez Outschoorn[106], P. Martinez Suarez[13], S. Martin-Haugh[138], G. Martinovicova[137], V. S. Martoiu[28b], A. C. Martyniuk[99], A. Marzin[37], D. Mascione[79a,79b], L. Masetti[103], J. Masik[104], A. L. Maslennikov[40], S. L. Mason[43], P. Massarotti[73a,73b], P. Mastrandrea[75a,75b], A. Mastroberardino[45a,45b], T. Masubuchi[128], T. T. Mathew[127], J. Matousek[137], D. M. Mattern[50], J. Maurer[28b], T. Maurin[60], A. J. Maury[67], B. Maček[96], D. A. Maximov[39], A. E. May[104], E. Mayer[42], R. Mazini[34g], I. Maznas[119], M. Mazza[110], S. M. Mazza[140], E. Mazzeo[72a,72b], J. P. Mc Gowan[172], S. P. Mc Kee[109], C. A. Mc Lean[6], C. C. McCracken[171], E. F. McDonald[108], A. E. McDougall[118], L. F. Mcelhinney[94], J. A. Mcfayden[153], R. P. McGovern[132],

R. P. Mckenzie[34g], T. C. Mclachlan[49], D. J. Mclaughlin[99], S. J. McMahon[138], C. M. Mcpartland[95], R. A. McPherson[172,ac], S. Mehlhase[112], A. Mehta[95], D. Melini[170], B. R. Mellado Garcia[34g], A. H. Melo[56], F. Meloni[49], A. M. Mendes Jacques Da Costa[104], H. Y. Meng[162], L. Meng[94], S. Menke[113], M. Mentink[37], E. Meoni[45a,45b], G. Mercado[119], S. Merianos[159], C. Merlassino[70a,70c], C. Meroni[72a,72b], J. Metcalfe[6], A. S. Mete[6], E. Meuser[103], C. Meyer[69], J.-P. Meyer[139], R. P. Middleton[138], M. Mihovilovic[67], L. Mijović[53], G. Mikenberg[176], M. Mikestikova[135], M. Mikuž[96], H. Mildner[103], A. Milic[37], D. W. Miller[41], E. H. Miller[150], L. S. Miller[35], A. Milov[176], D. A. Milstead[48a,48b], T. Min[115a], A. A. Minaenko[39], I. A. Minashvili[156b], A. I. Mincer[121], B. Mindur[88a], M. Mineev[40], Y. Mino[90], L. M. Mir[13], M. Miralles Lopez[60], M. Mironova[18a], M. Missio[117], A. Mitra[174], V. A. Mitsou[170], Y. Mitsumori[114], O. Miu[162], P. S. Miyagawa[97], T. Mkrtchyan[64a], M. Mlinarevic[99], T. Mlinarevic[99], M. Mlynarikova[37], S. Mobius[20], P. Mogg[112], M. H. Mohamed Farook[116], A. F. Mohammed[14,115c], S. Mohapatra[43], S. Mohiuddin[125], G. Mokgatitswane[34g], L. Moleri[176], B. Mondal[148], S. Mondal[136], K. Mönig[49], E. Monnier[105], L. Monsonis Romero[170], J. Montejo Berlingen[13], A. Montella[48a,48b], M. Montella[123], F. Montereali[78a,78b], F. Monticelli[93], S. Monzani[70a,70c], A. Morancho Tarda[44], N. Morange[67], A. L. Moreira De Carvalho[49], M. Moreno Llácer[170], C. Moreno Martinez[57], J. M. Moreno Perez[23b], P. Morettini[58b], S. Morgenstern[37], M. Morii[62], M. Morinaga[160], M. Moritsu[91], F. Morodei[76a,76b], P. Moschovakos[37], B. Moser[130], M. Mosidze[156b], T. Moskalets[46], P. Moskvitina[117], J. Moss[32,n], P. Moszkowicz[88a], A. Moussa[36d], Y. Moyal[176], E. J. W. Moyse[106], O. Mtintsilana[34g], S. Muanza[105], J. Mueller[133], R. Müller[37], G. A. Mullier[168], A. J. Mullin[33], J. J. Mullin[52], A. E. Mulski[62], D. P. Mungo[162], D. Munoz Perez[170], F. J. Munoz Sanchez[104], M. Murin[104], W. J. Murray[138,174], M. Muškinja[96], C. Mwewa[30], A. G. Myagkov[39,a], A. J. Myers[8], G. Myers[109], M. Myska[136], B. P. Nachman[18a], K. Nagai[130], K. Nagano[85], R. Nagasaka[160], J. L. Nagle[30,al], E. Nagy[105], A. M. Nairz[37], Y. Nakahama[85], K. Nakamura[85], K. Nakkalil[5], H. Nanjo[128], E. A. Narayanan[46], Y. Narukawa[160], I. Naryshkin[39], L. Nasella[72a,72b], S. Nasri[120b], C. Nass[25], G. Navarro[23a], J. Navarro-Gonzalez[170], A. Nayaz[19], P. Y. Nechaeva[39], S. Nechaeva[24a,24b], F. Nechansky[135], L. Nedic[130], T. J. Neep[21], A. Negri[74a,74b], M. Negrini[24b], C. Nellist[118], C. Nelson[107], K. Nelson[109], S. Nemecek[135], M. Nessi[37,h], M. S. Neubauer[169], J. Newell[95], P. R. Newman[21], Y. W. Y. Ng[169], B. Ngair[120a], H. D. N. Nguyen[111], R. B. Nickerson[130], R. Nicolaidou[139], J. Nielsen[140], M. Niemeyer[56], J. Niermann[37], N. Nikiforou[37], V. Nikolaenko[39,a], I. Nikolic-Audit[131], P. Nilsson[30], I. Ninca[49], G. Ninio[158], A. Nisati[76a], N. Nishu[2], R. Nisius[113], N. Nitika[70a,70c], J.-E. Nitschke[51], E. K. Nkadimeng[34g], T. Nobe[160], T. Nommensen[154], M. B. Norfolk[146], B. J. Norman[35], M. Noury[36a], J. Novak[96], T. Novak[96], R. Novotny[116], L. Nozka[126], K. Ntekas[166], N. M. J. Nunes De Moura Junior[84b], J. Ocariz[131], A. Ochi[87], I. Ochoa[134a], S. Oerdek[49,z], J. T. Offermann[41], A. Ogrodnik[137], A. Oh[104], C. C. Ohm[151], H. Oide[85], R. Oishi[160], M. L. Ojeda[37], Y. Okumura[160], L. F. Oleiro Seabra[134a], I. Oleksiyuk[57], S. A. Olivares Pino[141d], G. Oliveira Correa[13], D. Oliveira Damazio[30], J. L. Oliver[166], Ö. O. Öncel[55], A. P. O'Neill[20], A. Onofre[134a,134e], P. U. E. Onyisi[11], M. J. Oreglia[41], D. Orestano[78a,78b], R. Orlandini[78a,78b], R. S. Orr[162], L. M. Osojnak[132], Y. Osumi[114], G. Otero y Garzon[31], H. Otono[91], G. J. Ottino[18a], M. Ouchrif[36d], F. Ould-Saada[129], T. Ovsiannikova[143], M. Owen[60], R. E. Owen[138], V. E. Ozcan[22a], F. Ozturk[89], N. Ozturk[8], S. Ozturk[83], H. A. Pacey[130], K. Pachal[163a], A. Pacheco Pages[13], C. Padilla Aranda[13], G. Padovano[76a,76b], S. Pagan Griso[18a], G. Palacino[69], A. Palazzo[71a,71b], J. Pampel[25], J. Pan[179], T. Pan[65a], D. K. Panchal[11], C. E. Pandini[118], J. G. Panduro Vazquez[138], H. D. Pandya[1], H. Pang[139], P. Pani[49], G. Panizzo[70a,70c], L. Panwar[131], L. Paolozzi[57], S. Parajuli[169], A. Paramonov[6], C. Paraskevopoulos[54], D. Paredes Hernandez[65b], A. Pareti[74a,74b], K. R. Park[43], T. H. Park[113], F. Parodi[58a,58b], J. A. Parsons[43], U. Parzefall[55], B. Pascual Dias[42], L. Pascual Dominguez[102], E. Pasqualucci[76a], S. Passaggio[58b], F. Pastore[98], P. Patel[89], U. M. Patel[52], J. R. Pater[104], T. Pauly[37], F. Pauwels[137], C. I. Pazos[165], M. Pedersen[129], R. Pedro[134a], S. V. Peleganchuk[39], O. Penc[37], E. A. Pender[53], S. Peng[15], G. D. Penn[179], K. E. Penski[112], M. Penzin[39], B. S. Peralva[84d], A. P. Pereira Peixoto[143], L. Pereira Sanchez[150], D. V. Perepelitsa[30,al], G. Perera[106], E. Perez Codina[163a], M. Perganti[10], H. Pernegger[37], S. Perrella[76a,76b], O. Perrin[42], K. Peters[49], R. F. Y. Peters[104], B. A. Petersen[37], T. C. Petersen[44], E. Petit[105], V. Petousis[136], A. R. Petri[72a,72b], C. Petridou[159,e], T. Petru[137], A. Petrukhin[148], M. Pettee[18a], A. Petukhov[83], K. Petukhova[37], R. Pezoa[141f], L. Pezzotti[24a,24b], G. Pezzullo[179], L. Pfaffenbichler[37], A. J. Pfleger[37], T. M. Pham[177], T. Pham[108], P. W. Phillips[138], G. Piacquadio[152], E. Pianori[18a], F. Piazza[127], R. Piegaia[31], D. Pietreanu[28b], A. D. Pilkington[104], M. Pinamonti[70a,70c], J. L. Pinfold[2], B. C. Pinheiro Pereira[134a], J. Pinol Bel[13], A. E. Pinto Pinoargote[131], L. Pintucci[70a,70c], K. M. Piper[153],

A. Pirttikoski[57], D. A. Pizzi[35], L. Pizzimento[65b], M.-A. Pleier[30], V. Pleskot[137], E. Plotnikova[40], G. Poddar[97], R. Poettgen[101], L. Poggioli[131], S. Polacek[137], G. Polesello[74a], A. Poley[149,163a], A. Polini[24b], C. S. Pollard[174], Z. B. Pollock[123], E. Pompa Pacchi[124], N. I. Pond[99], D. Ponomarenko[69], L. Pontecorvo[37], S. Popa[28a], G. A. Popeneciu[28d], A. Poreba[37], D. M. Portillo Quintero[163a], S. Pospisil[136], M. A. Postill[146], P. Postolache[28c], K. Potamianos[174], P. A. Potepa[88a], I. N. Potrap[40], C. J. Potter[33], H. Potti[154], J. Poveda[170], M. E. Pozo Astigarraga[37], A. Prades Ibanez[77a,77b], J. Pretel[172], D. Price[104], M. Primavera[71a], L. Primomo[70a,70c], M. A. Principe Martin[102], R. Privara[126], T. Procter[60], M. L. Proffitt[143], N. Proklova[132], K. Prokofiev[65c], G. Proto[113], J. Proudfoot[6], M. Przybycien[88a], W. W. Przygoda[88b], A. Psallidas[47], J. E. Puddefoot[146], D. Pudzha[55], D. Pyatiizbyantseva[117], J. Qian[109], R. Qian[110], D. Qichen[104], Y. Qin[13], T. Qiu[53], A. Quadt[56], M. Queitsch-Maitland[104], G. Quetant[57], R. P. Quinn[171], G. Rabanal Bolanos[62], D. Rafanoharana[55], F. Raffaeli[77a,77b], F. Ragusa[72a,72b], J. L. Rainbolt[41], J. A. Raine[57], S. Rajagopalan[30], E. Ramakoti[39], L. Rambelli[58a,58b], I. A. Ramirez-Berend[35], K. Ran[49,115c], D. S. Rankin[132], N. P. Rapheeha[34g], H. Rasheed[28b], V. Raskina[131], D. F. Rassloff[64a], A. Rastogi[18a], S. Rave[103], S. Ravera[58a,58b], B. Ravina[37], I. Ravinovich[176], M. Raymond[37], A. L. Read[129], N. P. Readioff[146], D. M. Rebuzzi[74a,74b], A. S. Reed[113], K. Reeves[27], J. A. Reidelsturz[178], D. Reikher[127], A. Rej[50], C. Rembser[37], H. Ren[63], M. Renda[28b], F. Renner[49], A. G. Rennie[166], A. L. Rescia[49], S. Resconi[72a], M. Ressegotti[58a,58b], S. Rettie[37], W. F. Rettie[35], J. G. Reyes Rivera[110], E. Reynolds[18a], O. L. Rezanova[40], P. Reznicek[137], H. Riani[36d], N. Ribaric[52], E. Ricci[79a,79b], R. Richter[113], S. Richter[48a,48b], E. Richter-Was[88b], M. Ridel[131], S. Ridouani[36d], P. Rieck[121], P. Riedler[37], E. M. Riefel[48a,48b], J. O. Rieger[118], M. Rijssenbeek[152], M. Rimoldi[37], L. Rinaldi[24a,24b], P. Rincke[56], G. Ripellino[168], I. Riu[13], J. C. Rivera Vergara[172], F. Rizatdinova[125], E. Rizvi[97], B. R. Roberts[18a], S. S. Roberts[140], D. Robinson[33], M. Robles Manzano[103], A. Robson[60], A. Rocchi[77a,77b], C. Roda[75a,75b], S. Rodriguez Bosca[37], Y. Rodriguez Garcia[23a], A. M. Rodríguez Vera[119], S. Roe[37], J. T. Roemer[37], O. Røhne[129], R. A. Rojas[37], C. P. A. Roland[131], J. Roloff[30], A. Romaniouk[80], E. Romano[74a,74b], M. Romano[24b], A. C. Romero Hernandez[169], N. Rompotis[95], L. Roos[131], S. Rosati[76a], B. J. Rosser[41], E. Rossi[130], E. Rossi[73a,73b], L. P. Rossi[62], L. Rossini[55], R. Rosten[123], M. Rotaru[28b], B. Rottler[55], D. Rousseau[67], D. Rousso[49], S. Roy-Garand[162], A. Rozanov[105], Z. M. A. Rozario[60], Y. Rozen[157], A. Rubio Jimenez[170], V. H. Ruelas Rivera[19], T. A. Ruggeri[1], A. Ruggiero[130], A. Ruiz-Martinez[170], A. Rummler[37], Z. Rurikova[55], N. A. Rusakovich[40], H. L. Russell[172], G. Russo[76a,76b], J. P. Rutherfoord[7], S. Rutherford Colmenares[33], M. Rybar[137], P. Rybczynski[88a], E. B. Rye[129], A. Ryzhov[46], J. A. Sabater Iglesias[57], H. F.-W. Sadrozinski[140], F. Safai Tehrani[76a], S. Saha[1], M. Sahinsoy[83], A. Saibel[170], B. T. Saifuddin[124], M. Saimpert[139], M. Saito[160], T. Saito[160], A. Sala[72a,72b], D. Salamani[37], A. Salnikov[150], J. Salt[170], A. Salvador Salas[158], D. Salvatore[45a,45b], F. Salvatore[153], A. Salzburger[37], D. Sammel[55], E. Sampson[94], D. Sampsonidis[159,e], D. Sampsonidou[127], J. Sánchez[170], V. Sanchez Sebastian[170], H. Sandaker[129], C. O. Sander[49], J. A. Sandesara[106], M. Sandhoff[178], C. Sandoval[23b], L. Sanfilippo[64a], D. P. C. Sankey[138], T. Sano[90], A. Sansoni[54], L. Santi[37], C. Santoni[42], H. Santos[134a,134b], A. Santra[176], E. Sanzani[24a,24b], K. A. Saoucha[86b], J. G. Saraiva[134a,134d], J. Sardain[7], O. Sasaki[85], K. Sato[164], C. Sauer[37], E. Sauvan[4], P. Savard[162,aj], R. Sawada[160], C. Sawyer[138], L. Sawyer[100], C. Sbarra[24b], A. Sbrizzi[24a,24b], T. Scanlon[99], J. Schaarschmidt[143], U. Schäfer[103], A. C. Schaffer[46,67], D. Schaile[112], R. D. Schamberger[152], C. Scharf[19], M. M. Schefer[20], V. A. Schegelsky[39], D. Scheirich[137], M. Schernau[141e], C. Scheulen[57], C. Schiavi[58a,58b], M. Schioppa[45a,45b], B. Schlag[150], S. Schlenker[37], J. Schmeing[178], M. A. Schmidt[178], K. Schmieden[103], C. Schmitt[103], N. Schmitt[103], S. Schmitt[49], L. Schoeffel[139], A. Schoening[64b], P. G. Scholer[35], E. Schopf[148], M. Schott[25], S. Schramm[57], T. Schroer[57], H.-C. Schultz-Coulon[64a], M. Schumacher[55], B. A. Schumm[140], Ph. Schune[139], H. R. Schwartz[140], A. Schwartzman[150], T. A. Schwarz[109], Ph. Schwemling[139], R. Schwienhorst[110], F. G. Sciacca[20], A. Sciandra[30], G. Sciolla[27], F. Scuri[75a], C. D. Sebastiani[37], K. Sedlaczek[119], S. C. Seidel[116], A. Seiden[140], B. D. Seidlitz[43], C. Seitz[49], J. M. Seixas[84b], G. Sekhniaidze[73a], L. Selem[61], N. Semprini-Cesari[24a,24b], A. Semushin[180,39], D. Sengupta[57], V. Senthilkumar[170], L. Serin[67], M. Sessa[77a,77b], H. Severini[124], F. Sforza[58a,58b], A. Sfyrla[57], Q. Sha[14], E. Shabalina[56], H. Shaddix[119], A. H. Shah[33], R. Shaheen[151], J. D. Shahinian[132], D. Shaked Renous[176], M. Shamim[37], L. Y. Shan[14], M. Shapiro[18a], A. Sharma[37], A. S. Sharma[171], P. Sharma[30], P. B. Shatalov[39], K. Shaw[153], S. M. Shaw[104], Q. Shen[145a], D. J. Sheppard[149], P. Sherwood[99], L. Shi[99], X. Shi[14], S. Shimizu[85], C. O. Shimmin[179], I. P. J. Shipsey[130,*], S. Shirabe[91], M. Shiyakova[40,aa], M. J. Shochet[41], D. R. Shope[129], B. Shrestha[124], S. Shrestha[123,an], I. Shreyber[40], M. J. Shroff[172], P. Sicho[135], A. M. Sickles[169], E. Sideras Haddad[34g,167], A. C. Sidley[118], A. Sidoti[24b], F. Siegert[51],

D. Sijacki[16], F. Sili[93], J. M. Silva[53], I. Silva Ferreira[84b], M. V. Silva Oliveira[30], S. B. Silverstein[48a], S. Simion[67], R. Simoniello[37], E. L. Simpson[104], H. Simpson[153], L. R. Simpson[109], S. Simsek[83], S. Sindhu[56], P. Sinervo[162], S. N. Singh[27], S. Singh[30], S. Sinha[49], S. Sinha[104], M. Sioli[24a,24b], K. Sioulas[9], I. Siral[37], E. Sitnikova[49], J. Sjölin[48a,48b], A. Skaf[56], E. Skorda[21], P. Skubic[124], M. Slawinska[89], I. Slazyk[17], V. Smakhtin[176], B. H. Smart[138], S. Yu. Smirnov[141b], Y. Smirnov[83], L. N. Smirnova[39,a], O. Smirnova[101], A. C. Smith[43], D. R. Smith[166], E. A. Smith[41], J. L. Smith[104], M. B. Smith[35], R. Smith[150], H. Smitmanns[103], M. Smizanska[94], K. Smolek[136], P. Smolyanskiy[136], A. A. Snesarev[40], H. L. Snoek[118], S. Snyder[30], R. Sobie[172,ac], A. Soffer[158], C. A. Solans Sanchez[37], E. Yu. Soldatov[40], U. Soldevila[170], A. A. Solodkov[34g], S. Solomon[27], A. Soloshenko[40], K. Solovieva[55], O. V. Solovyanov[42], P. Sommer[51], A. Sonay[13], W. Y. Song[163b], A. Sopczak[136], A. L. Sopio[53], F. Sopkova[29b], J. D. Sorenson[116], I. R. Sotarriva Alvarez[142], V. Sothilingam[64a], O. J. Soto Sandoval[141b,141c], S. Sottocornola[69], R. Soualah[86a], Z. Soumaimi[36e], D. South[49], N. Soybelman[176], S. Spagnolo[71a,71b], M. Spalla[113], D. Sperlich[55], B. Spisso[73a,73b], D. P. Spiteri[60], L. Splendori[105], M. Spousta[137], E. J. Staats[35], R. Stamen[64a], E. Stanecka[89], W. Stanek-Maslouska[49], M. V. Stange[51], B. Stanislaus[18a], M. M. Stanitzki[49], B. Stapf[49], E. A. Starchenko[39], G. H. Stark[140], J. Stark[92], P. Staroba[135], P. Starovoitov[86b], R. Staszewski[89], G. Stavropoulos[47], A. Stefl[37], P. Steinberg[30], B. Stelzer[149,163a], H. J. Stelzer[133], O. Stelzer[163a], H. Stenzel[59], T. J. Stevenson[153], G. A. Stewart[37], J. R. Stewart[125], M. C. Stockton[37], G. Stoicea[28b], M. Stolarski[134a], S. Stonjek[113], A. Straessner[51], J. Strandberg[151], S. Strandberg[48a,48b], M. Stratmann[178], M. Strauss[124], T. Strebler[105], P. Strizenec[29b], R. Ströhmer[173], D. M. Strom[127], R. Stroynowski[46], A. Strubig[48a,48b], S. A. Stucci[30], B. Stugu[17], J. Stupak[124], N. A. Styles[49], D. Su[150], S. Su[63], W. Su[145b], X. Su[63], D. Suchy[29a], K. Sugizaki[132], V. V. Sulin[39], M. J. Sullivan[95], D. M. S. Sultan[130], L. Sultanaliyeva[39], S. Sultansoy[3b], S. Sun[177], W. Sun[14], O. Sunneborn Gudnadottir[168], N. Sur[105], M. R. Sutton[153], H. Suzuki[164], M. Svatos[135], P. N. Swallow[33], M. Swiatlowski[163a], T. Swirski[173], I. Sykora[29a], M. Sykora[137], T. Sykora[137], D. Ta[103], K. Tackmann[49,z], A. Taffard[166], R. Tafirout[163a], Y. Takubo[85], M. Talby[105], A. A. Talyshev[39], K. C. Tam[65b], N. M. Tamir[158], A. Tanaka[160], J. Tanaka[160], R. Tanaka[67], M. Tanasini[152], Z. Tao[171], S. Tapia Araya[141f], S. Tapprogge[103], A. Tarek Abouelfadl Mohamed[110], S. Tarem[157], K. Tariq[14], G. Tarna[28b], G. F. Tartarelli[72a], M. J. Tartarin[92], P. Tas[137], M. Tasevsky[135], E. Tassi[45a,45b], A. C. Tate[169], G. Tateno[160], Y. Tayalati[36e,ab], G. N. Taylor[108], W. Taylor[163b], A. S. Tegetmeier[92], P. Teixeira-Dias[98], J. J. Teoh[162], K. Terashi[160], J. Terron[102], S. Terzo[13], M. Testa[54], R. J. Teuscher[162,ac], A. Thaler[80], O. Theiner[57], T. Theveneaux-Pelzer[105], O. Thielmann[178], D. W. Thomas[98], J. P. Thomas[21], E. A. Thompson[18a], P. D. Thompson[21], E. Thomson[132], R. E. Thornberry[46], C. Tian[63], Y. Tian[57], V. Tikhomirov[83], Yu. A. Tikhonov[39], S. Timoshenko[39], D. Timoshyn[137], E. X. L. Ting[1], P. Tipton[179], A. Tishelman-Charny[30], S. H. Tlou[34g], K. Todome[142], S. Todorova-Nova[137], S. Todt[51], L. Toffolin[70a,70c], M. Togawa[85], J. Tojo[91], S. Tokár[29a], O. Toldaiev[69], G. Tolkachev[105], M. Tomoto[85,114], L. Tompkins[150,p], E. Torrence[127], H. Torres[92], E. Torró Pastor[170], M. Toscani[31], C. Tosciri[41], M. Tost[11], D. R. Tovey[146], T. Trefzger[173], P. M. Tricarico[13], A. Tricoli[30], I. M. Trigger[163a], S. Trincaz-Duvoid[131], D. A. Trischuk[27], A. Tropina[40], L. Truong[34c], M. Trzebinski[89], A. Trzupek[89], F. Tsai[152], M. Tsai[109], A. Tsiamis[159], P. V. Tsiareshka[40], S. Tsigaridas[163a], A. Tsirigotis[159,v], V. Tsiskaridze[162], E. G. Tskhadadze[156a], M. Tsopoulou[159], Y. Tsujikawa[90], I. I. Tsukerman[39], V. Tsulaia[18a], S. Tsuno[85], K. Tsuri[122], D. Tsybychev[152], Y. Tu[65b], A. Tudorache[28b], V. Tudorache[28b], S. Turchikhin[58a,58b], I. Turk Cakir[3a], R. Turra[72a], T. Turtuvshin[40,ad], P. M. Tuts[43], S. Tzamarias[159,e], E. Tzovara[103], F. Ukegawa[164], P. A. Ulloa Poblete[141b,141c], E. N. Umaka[30], G. Unal[37], A. Undrus[30], G. Unel[166], J. Urban[29b], P. Urrejola[141a], G. Usai[8], R. Ushioda[161], M. Usman[111], F. Ustuner[53], Z. Uysal[83], V. Vacek[136], B. Vachon[107], T. Vafeiadis[37], A. Vaitkus[99], C. Valderanis[112], E. Valdes Santurio[48a,48b], M. Valente[163a], S. Valentinetti[24a,24b], A. Valero[170], E. Valiente Moreno[170], A. Vallier[92], J. A. Valls Ferrer[170], D. R. Van Arneman[118], T. R. Van Daalen[143], A. Van Der Graaf[50], H. Z. Van Der Schyf[34g], P. Van Gemmeren[6], M. Van Rijnbach[37], S. Van Stroud[99], I. Van Vulpen[118], P. Vana[137], M. Vanadia[77a,77b], U. M. Vande Voorde[151], W. Vandelli[37], E. R. Vandewall[125], D. Vannicola[158], L. Vannoli[54], R. Vari[76a], E. W. Varnes[7], C. Varni[18b], D. Varouchas[67], L. Varriale[170], K. E. Varvell[154], M. E. Vasile[28b], L. Vaslin[85], M. D. Vassilev[150], A. Vasyukov[40], L. M. Vaughan[125], R. Vavricka[137], T. Vazquez Schroeder[13], J. Veatch[32], V. Vecchio[104], M. J. Veen[106], I. Veliscek[30], L. M. Veloce[162], F. Veloso[134a,134c], S. Veneziano[76a], A. Ventura[71a,71b], S. Ventura Gonzalez[139], A. Verbytskyi[113], M. Verducci[75a,75b], C. Vergis[97], M. Verissimo De Araujo[84b], W. Verkerke[118], J. C. Vermeulen[118], C. Vernieri[150], M. Vessella[166], M. C. Vetterli[149,aj], A. Vgenopoulos[103], N. Viaux Maira[141f], T. Vickey[146], O. E. Vickey Boeriu[146], G. H. A. Viehhauser[130], L. Vigani[64b], M. Vigl[113],

M. Villa[24a,24b], M. Villaplana Perez[170], E. M. Villhauer[53], E. Vilucchi[54], M. G. Vincter[35], A. Visibile[118], C. Vittori[37], I. Vivarelli[24a,24b], E. Voevodina[113], F. Vogel[112], J. C. Voigt[51], P. Vokac[136], Yu. Volkotrub[88b], E. Von Toerne[25], B. Vormwald[37], K. Vorobev[39], M. Vos[170], K. Voss[148], M. Vozak[37], L. Vozdecky[124], N. Vranjes[16], M. Vranjes Milosavljevic[16], M. Vreeswijk[118], N. K. Vu[145a,145b], R. Vuillermet[37], O. Vujinovic[103], I. Vukotic[41], I. K. Vyas[35], J. F. Wack[33], S. Wada[164], C. Wagner[150], J. M. Wagner[18a], W. Wagner[178], S. Wahdan[178], H. Wahlberg[93], C. H. Waits[124], J. Walder[138], R. Walker[112], W. Walkowiak[148], A. Wall[132], E. J. Wallin[101], T. Wamorkar[18a], A. Z. Wang[140], C. Wang[103], C. Wang[11], H. Wang[18a], J. Wang[65c], P. Wang[104], P. Wang[99], R. Wang[62], R. Wang[6], S. M. Wang[155], S. Wang[14], T. Wang[63], T. Wang[63], W. T. Wang[81], W. Wang[14], X. Wang[169], X. Wang[145a], X. Wang[49], Y. Wang[115a], Y. Wang[63], Z. Wang[109], Z. Wang[52,145a,145b], Z. Wang[109], C. Wanotayaroj[85], A. Warburton[107], R. J. Ward[21], A. L. Warnerbring[148], N. Warrack[60], S. Waterhouse[98], A. T. Watson[21], H. Watson[53], M. F. Watson[21], E. Watton[60], G. Watts[143], B. M. Waugh[99], J. M. Webb[55], C. Weber[30], H. A. Weber[19], M. S. Weber[20], S. M. Weber[64a], C. Wei[63], Y. Wei[55], A. R. Weidberg[130], E. J. Weik[121], J. Weingarten[50], C. Weiser[55], C. J. Wells[49], T. Wenaus[30], B. Wendland[50], T. Wengler[37], N. S. Wenke[113], N. Wermes[25], M. Wessels[64a], A. M. Wharton[94], A. S. White[62], A. White[8], M. J. White[1], D. Whiteson[166], L. Wickremasinghe[128], W. Wiedenmann[177], M. Wielers[138], C. Wiglesworth[44], D. J. Wilbern[124], H. G. Wilkens[37], J. J. H. Wilkinson[33], D. M. Williams[43], H. H. Williams[132], S. Williams[33], S. Willocq[106], B. J. Wilson[104], D. J. Wilson[104], P. J. Windischhofer[41], F. I. Winkel[31], F. Winklmeier[127], B. T. Winter[55], M. Wittgen[150], M. Wobisch[100], T. Wojtkowski[61], Z. Wolffs[118], J. Wollrath[37], M. W. Wolter[89], H. Wolters[134a,134c], M. C. Wong[140], E. L. Woodward[43], S. D. Worm[49], B. K. Wosiek[89], K. W. Woźniak[89], S. Wozniewski[56], K. Wraight[60], C. Wu[21], M. Wu[115b], M. Wu[117], S. L. Wu[177], S. Wu[14], X. Wu[57], X. Wu[63], Y. Wu[63], Z. Wu[4], J. Wuerzinger[113,ah], T. R. Wyatt[104], B. M. Wynne[53], S. Xella[44], L. Xia[115a], M. Xia[15], M. Xie[63], A. Xiong[127], J. Xiong[18a], D. Xu[14], H. Xu[63], L. Xu[63], R. Xu[132], T. Xu[109], Y. Xu[143], Z. Xu[53], Z. Xu[115a], B. Yabsley[154], S. Yacoob[34a], Y. Yamaguchi[85], E. Yamashita[160], H. Yamauchi[164], T. Yamazaki[18a], Y. Yamazaki[87], S. Yan[60], Z. Yan[106], H. J. Yang[145a,145b], H. T. Yang[63], S. Yang[63], T. Yang[65c], X. Yang[37], X. Yang[14], Y. Yang[160], Y. Yang[63], W.-M. Yao[18a], C. L. Yardley[153], H. Ye[56], J. Ye[14], S. Ye[30], X. Ye[63], Y. Yeh[99], I. Yeletskikh[40], B. Yeo[18b], M. R. Yexley[99], T. P. Yildirim[130], P. Yin[43], K. Yorita[175], S. Younas[28b], C. J. S. Young[37], C. Young[150], N. D. Young[127], Y. Yu[63], J. Yuan[14,115c], M. Yuan[109], R. Yuan[145a,145b], L. Yue[99], M. Zaazoua[63], B. Zabinski[89], I. Zahir[36a], Z. K. Zak[89], T. Zakareishvili[170], S. Zambito[57], J. A. Zamora Saa[141d], J. Zang[160], D. Zanzi[55], R. Zanzottera[72a,72b], O. Zaplatilek[136], C. Zeitnitz[178], H. Zeng[14], J. C. Zeng[169], D. T. Zenger Jr.[27], O. Zenin[39], T. Ženiš[29a], S. Zenz[97], S. Zerradi[36a], D. Zerwas[67], M. Zhai[14,115c], D. F. Zhang[146], J. Zhang[144a], J. Zhang[6], K. Zhang[14,115c], L. Zhang[63], L. Zhang[115a], P. Zhang[14,115c], R. Zhang[177], S. Zhang[92], T. Zhang[160], X. Zhang[145a], Y. Zhang[143], Y. Zhang[99], Y. Zhang[63], Y. Zhang[115a], Z. Zhang[18a], Z. Zhang[144a], Z. Zhang[67], H. Zhao[143], T. Zhao[144a], Y. Zhao[35], Z. Zhao[63], Z. Zhao[63], A. Zhemchugov[40], J. Zheng[115a], K. Zheng[169], X. Zheng[63], Z. Zheng[150], D. Zhong[169], B. Zhou[109], H. Zhou[7], N. Zhou[145a], Y. Zhou[15], Y. Zhou[115a], Y. Zhou[7], C. G. Zhu[144a], J. Zhu[109], X. Zhu[145b], Y. Zhu[145a], Y. Zhu[63], X. Zhuang[14], K. Zhukov[69], N. I. Zimine[40], J. Zinsser[64b], M. Ziolkowski[148], L. Živković[16], A. Zoccoli[24a,24b], K. Zoch[62], T. G. Zorbas[146], O. Zormpa[47], W. Zou[43], L. Zwalinski[37]

[1] Department of Physics, University of Adelaide, Adelaide, Australia
[2] Department of Physics, University of Alberta, Edmonton, AB, Canada
[3] [(a)]Department of Physics, Ankara University, Ankara, Türkiye; [(b)]Division of Physics, TOBB University of Economics and Technology, Ankara, Türkiye
[4] LAPP, Université Savoie Mont Blanc, CNRS/IN2P3, Annecy, France
[5] APC, Université Paris Cité, CNRS/IN2P3, Paris, France
[6] High Energy Physics Division, Argonne National Laboratory, Argonne, IL, USA
[7] Department of Physics, University of Arizona, Tucson, AZ, USA
[8] Department of Physics, University of Texas at Arlington, Arlington, TX, USA
[9] Physics Department, National and Kapodistrian University of Athens, Athens, Greece
[10] Physics Department, National Technical University of Athens, Zografou, Greece
[11] Department of Physics, University of Texas at Austin, Austin, TX, USA
[12] Institute of Physics, Azerbaijan Academy of Sciences, Baku, Azerbaijan

[13] Institut de Física d'Altes Energies (IFAE), Barcelona Institute of Science and Technology, Barcelona, Spain
[14] Institute of High Energy Physics, Chinese Academy of Sciences, Beijing, China
[15] Physics Department, Tsinghua University, Beijing, China
[16] Institute of Physics, University of Belgrade, Belgrade, Serbia
[17] Department for Physics and Technology, University of Bergen, Bergen, Norway
[18] [(a)]Physics Division, Lawrence Berkeley National Laboratory, Berkeley, CA, USA; [(b)]University of California, Berkeley, CA, USA
[19] Institut für Physik, Humboldt Universität zu Berlin, Berlin, Germany
[20] Albert Einstein Center for Fundamental Physics and Laboratory for High Energy Physics, University of Bern, Bern, Switzerland
[21] School of Physics and Astronomy, University of Birmingham, Birmingham, UK
[22] [(a)]Department of Physics, Bogazici University, Istanbul, Türkiye; [(b)]Department of Physics Engineering, Gaziantep University, Gaziantep, Türkiye; [(c)]Department of Physics, Istanbul University, Istanbul, Türkiye
[23] [(a)]Facultad de Ciencias y Centro de Investigaciónes, Universidad Antonio Nariño, Bogotá, Colombia; [(b)]Departamento de Física, Universidad Nacional de Colombia, Bogotá, Colombia
[24] [(a)]Dipartimento di Fisica e Astronomia A. Righi, Università di Bologna, Bologna, Italy; [(b)]INFN Sezione di Bologna, Bologna, Italy
[25] Physikalisches Institut, Universität Bonn, Bonn, Germany
[26] Department of Physics, Boston University, Boston, MA, USA
[27] Department of Physics, Brandeis University, Waltham, MA, USA
[28] [(a)]Transilvania University of Brasov, Brasov, Romania; [(b)]Horia Hulubei National Institute of Physics and Nuclear Engineering, Bucharest, Romania; [(c)]Department of Physics, Alexandru Ioan Cuza University of Iasi, Iasi, Romania; [(d)]Physics Department, National Institute for Research and Development of Isotopic and Molecular Technologies, Cluj-Napoca, Romania; [(e)]National University of Science and Technology Politechnica, Bucharest, Romania; [(f)]West University in Timisoara, Timisoara, Romania; [(g)]Faculty of Physics, University of Bucharest, Bucharest, Romania
[29] [(a)]Faculty of Mathematics, Physics and Informatics, Comenius University, Bratislava, Slovak Republic; [(b)]Department of Subnuclear Physics, Institute of Experimental Physics of the Slovak Academy of Sciences, Kosice, Slovak Republic
[30] Physics Department, Brookhaven National Laboratory, Upton, NY, USA
[31] Departamento de Física, y CONICET, Facultad de Ciencias Exactas y Naturales, Instituto de Física de Buenos Aires (IFIBA), Universidad de Buenos Aires, Buenos Aires, Argentina
[32] California State University, Fresno, CA, USA
[33] Cavendish Laboratory, University of Cambridge, Cambridge, UK
[34] [(a)]Department of Physics, University of Cape Town, Cape Town, South Africa; [(b)]iThemba Labs, Western Cape, South Africa; [(c)]Department of Mechanical Engineering Science, University of Johannesburg, Johannesburg, South Africa; [(d)]National Institute of Physics, University of the Philippines Diliman (Philippines), Quezon City, Philippines; [(e)]Department of Physics, University of South Africa, Pretoria, South Africa; [(f)]University of Zululand, KwaDlangezwa, South Africa; [(g)]School of Physics, University of the Witwatersrand, Johannesburg, South Africa
[35] Department of Physics, Carleton University, Ottawa, ON, Canada
[36] [(a)]Faculté des Sciences Ain Chock, Université Hassan II de Casablanca, Casablanca, Morocco; [(b)]Faculté des Sciences, Université Ibn-Tofail, Kénitra, Morocco; [(c)]Faculté des Sciences Semlalia, Université Cadi Ayyad, LPHEA-Marrakech, Marrakech, Morocco; [(d)]LPMR, Faculté des Sciences, Université Mohamed Premier, Oujda, Morocco; [(e)]Faculté des sciences, Université Mohammed V, Rabat, Morocco; [(f)]Institute of Applied Physics, Mohammed VI Polytechnic University, Ben Guerir, Morocco
[37] CERN, Geneva, Switzerland
[38] Affiliated with an Institute Formerly Covered by a Cooperation Agreement with CERN, Geneva, Switzerland
[39] Affiliated with an Institute Covered by a Cooperation Agreement with CERN, Geneva, Switzerland
[40] Affiliated with an International Laboratory Covered by a Cooperation Agreement with CERN, Geneva, Switzerland
[41] Enrico Fermi Institute, University of Chicago, Chicago, IL, USA
[42] LPC, Université Clermont Auvergne, CNRS/IN2P3, Clermont-Ferrand, France
[43] Nevis Laboratory, Columbia University, Irvington, NY, USA
[44] Niels Bohr Institute, University of Copenhagen, Copenhagen, Denmark

[45] [(a)]Dipartimento di Fisica, Università della Calabria, Rende, Italy; [(b)]INFN Gruppo Collegato di Cosenza, Laboratori Nazionali di Frascati, Frascati, Italy
[46] Physics Department, Southern Methodist University, Dallas, TX, USA
[47] National Centre for Scientific Research "Demokritos", Agia Paraskevi, Greece
[48] [(a)]Department of Physics, Stockholm University, Stockholm, Sweden; [(b)]Oskar Klein Centre, Stockholm, Sweden
[49] Deutsches Elektronen-Synchrotron DESY, Hamburg and Zeuthen, Germany
[50] Fakultät Physik , Technische Universität Dortmund, Dortmund, Germany
[51] Institut für Kern- und Teilchenphysik, Technische Universität Dresden, Dresden, Germany
[52] Department of Physics, Duke University, Durham, NC, USA
[53] SUPA-School of Physics and Astronomy, University of Edinburgh, Edinburgh, UK
[54] INFN e Laboratori Nazionali di Frascati, Frascati, Italy
[55] Physikalisches Institut, Albert-Ludwigs-Universität Freiburg, Freiburg, Germany
[56] II. Physikalisches Institut, Georg-August-Universität Göttingen, Göttingen, Germany
[57] Département de Physique Nucléaire et Corpusculaire, Université de Genève, Geneva, Switzerland
[58] [(a)]Dipartimento di Fisica, Università di Genova, Genoa, Italy; [(b)]INFN Sezione di Genova, Genoa, Italy
[59] II. Physikalisches Institut, Justus-Liebig-Universität Giessen, Giessen, Germany
[60] SUPA-School of Physics and Astronomy, University of Glasgow, Glasgow, UK
[61] LPSC, Université Grenoble Alpes, CNRS/IN2P3, Grenoble INP, Grenoble, France
[62] Laboratory for Particle Physics and Cosmology, Harvard University, Cambridge, MA, USA
[63] Department of Modern Physics and State Key Laboratory of Particle Detection and Electronics, University of Science and Technology of China, Hefei, China
[64] [(a)]Kirchhoff-Institut für Physik, Ruprecht-Karls-Universität Heidelberg, Heidelberg, Germany; [(b)]Physikalisches Institut, Ruprecht-Karls-Universität Heidelberg, Heidelberg, Germany
[65] [(a)]Department of Physics, Chinese University of Hong Kong, Shatin, N.T., Hong Kong, China; [(b)]Department of Physics, University of Hong Kong, Hong Kong, China; [(c)]Department of Physics and Institute for Advanced Study, Hong Kong University of Science and Technology, Clear Water Bay, Kowloon, Hong Kong, China
[66] Department of Physics, National Tsing Hua University, Hsinchu, Taiwan
[67] IJCLab, Université Paris-Saclay, CNRS/IN2P3, 91405 Orsay, France
[68] Centro Nacional de Microelectrónica (IMB-CNM-CSIC), Barcelona, Spain
[69] Department of Physics, Indiana University, Bloomington, IN, USA
[70] [(a)]INFN Gruppo Collegato di Udine, Sezione di Trieste, Udine, Italy; [(b)]ICTP, Trieste, Italy; [(c)]Dipartimento Politecnico di Ingegneria e Architettura, Università di Udine, Udine, Italy
[71] [(a)]INFN Sezione di Lecce, Lecce, Italy; [(b)]Dipartimento di Matematica e Fisica, Università del Salento, Lecce, Italy
[72] [(a)]INFN Sezione di Milano, Milan, Italy; [(b)]Dipartimento di Fisica, Università di Milano, Milan, Italy
[73] [(a)]INFN Sezione di Napoli, Naples, Italy; [(b)]Dipartimento di Fisica, Università di Napoli, Naples, Italy
[74] [(a)]INFN Sezione di Pavia, Pavia, Italy; [(b)]Dipartimento di Fisica, Università di Pavia, Pavia, Italy
[75] [(a)]INFN Sezione di Pisa, Pisa, Italy; [(b)]Dipartimento di Fisica E. Fermi, Università di Pisa, Pisa, Italy
[76] [(a)]INFN Sezione di Roma, Rome, Italy; [(b)]Dipartimento di Fisica, Sapienza Università di Roma, Rome, Italy
[77] [(a)]INFN Sezione di Roma Tor Vergata, Rome, Italy; [(b)]Dipartimento di Fisica, Università di Roma Tor Vergata, Rome, Italy
[78] [(a)]INFN Sezione di Roma Tre, Rome, Italy; [(b)]Dipartimento di Matematica e Fisica, Università Roma Tre, Rome, Italy
[79] [(a)]INFN-TIFPA, Povo, Italy; [(b)]Università degli Studi di Trento, Trento, Italy
[80] Department of Astro and Particle Physics, Universität Innsbruck, Innsbruck, Austria
[81] University of Iowa, Iowa City, IA, USA
[82] Department of Physics and Astronomy, Iowa State University, Ames, IA, USA
[83] Istinye University, Sariyer, Istanbul, Türkiye
[84] [(a)]Departamento de Engenharia Elétrica, Universidade Federal de Juiz de Fora (UFJF), Juiz de Fora, Brazil; [(b)]Universidade Federal do Rio De Janeiro COPPE/EE/IF, Rio de Janeiro, Brazil; [(c)]Instituto de Física, Universidade de São Paulo, São Paulo, Brazil; [(d)]Rio de Janeiro State University, Rio de Janeiro, Brazil; [(e)]Federal University of Bahia, Bahia, Brazil
[85] KEK, High Energy Accelerator Research Organization, Tsukuba, Japan
[86] [(a)]Khalifa University of Science and Technology, Abu Dhabi, United Arab Emirates; [(b)]University of Sharjah, Sharjah, United Arab Emirates

[87] Graduate School of Science, Kobe University, Kobe, Japan
[88] [(a)]Faculty of Physics and Applied Computer Science, AGH University of Krakow, Kraków, Poland; [(b)]Marian Smoluchowski Institute of Physics, Jagiellonian University, Kraków, Poland
[89] Institute of Nuclear Physics Polish Academy of Sciences, Kraków, Poland
[90] Faculty of Science, Kyoto University, Kyoto, Japan
[91] Research Center for Advanced Particle Physics and Department of Physics, Kyushu University, Fukuoka, Japan
[92] L2IT, Université de Toulouse, CNRS/IN2P3, UPS, Toulouse, France
[93] Instituto de Física La Plata, Universidad Nacional de La Plata and CONICET, La Plata, Argentina
[94] Physics Department, Lancaster University, Lancaster, UK
[95] Oliver Lodge Laboratory, University of Liverpool, Liverpool, UK
[96] Department of Experimental Particle Physics, Jožef Stefan Institute and Department of Physics, University of Ljubljana, Ljubljana, Slovenia
[97] Department of Physics and Astronomy, Queen Mary University of London, London, UK
[98] Department of Physics, Royal Holloway University of London, Egham, UK
[99] Department of Physics and Astronomy, University College London, London, UK
[100] Louisiana Tech University, Ruston, LA, USA
[101] Fysiska institutionen, Lunds universitet, Lund, Sweden
[102] Departamento de Física Teorica C-15 and CIAFF, Universidad Autónoma de Madrid, Madrid, Spain
[103] Institut für Physik, Universität Mainz, Mainz, Germany
[104] School of Physics and Astronomy, University of Manchester, Manchester, UK
[105] CPPM, Aix-Marseille Université, CNRS/IN2P3, Marseille, France
[106] Department of Physics, University of Massachusetts, Amherst, MA, USA
[107] Department of Physics, McGill University, Montreal, QC, Canada
[108] School of Physics, University of Melbourne, Victoria, Australia
[109] Department of Physics, University of Michigan, Ann Arbor, MI, USA
[110] Department of Physics and Astronomy, Michigan State University, East Lansing, MI, USA
[111] Group of Particle Physics, University of Montreal, Montreal, QC, Canada
[112] Fakultät für Physik, Ludwig-Maximilians-Universität München, Munich, Germany
[113] Max-Planck-Institut für Physik (Werner-Heisenberg-Institut), Munich, Germany
[114] Graduate School of Science and Kobayashi-Maskawa Institute, Nagoya University, Nagoya, Japan
[115] [(a)]Department of Physics, Nanjing University, Nanjing, China; [(b)]School of Science, Shenzhen Campus of Sun Yat-sen University, Shenzhen, China; [(c)]University of Chinese Academy of Science (UCAS), Beijing, China
[116] Department of Physics and Astronomy, University of New Mexico, Albuquerque, NM, USA
[117] Institute for Mathematics, Astrophysics and Particle Physics, Radboud University/Nikhef, Nijmegen, The Netherlands
[118] Nikhef National Institute for Subatomic Physics and University of Amsterdam, Amsterdam, The Netherlands
[119] Department of Physics, Northern Illinois University, DeKalb, IL, USA
[120] [(a)]New York University Abu Dhabi, Abu Dhabi, United Arab Emirates; [(b)]United Arab Emirates University, Al Ain, United Arab Emirates
[121] Department of Physics, New York University, New York, NY, USA
[122] Ochanomizu University, Otsuka, Bunkyo-ku, Tokyo, Japan
[123] Ohio State University, Columbus, OH, USA
[124] Homer L. Dodge Department of Physics and Astronomy, University of Oklahoma, Norman, OK, USA
[125] Department of Physics, Oklahoma State University, Stillwater, OK, USA
[126] Joint Laboratory of Optics, Palacký University, Olomouc, Czech Republic
[127] Institute for Fundamental Science, University of Oregon, Eugene, OR, USA
[128] Graduate School of Science, University of Osaka, Osaka, Japan
[129] Department of Physics, University of Oslo, Oslo, Norway
[130] Department of Physics, Oxford University, Oxford, UK
[131] LPNHE, Sorbonne Université, Université Paris Cité, CNRS/IN2P3, Paris, France
[132] Department of Physics, University of Pennsylvania, Philadelphia, PA, USA
[133] Department of Physics and Astronomy, University of Pittsburgh, Pittsburgh, PA, USA
[134] [(a)]Laboratório de Instrumentação e Física Experimental de Partículas-LIP, Lisbon, Portugal; [(b)]Departamento de Física, Faculdade de Ciências, Universidade de Lisboa, Lisbon, Portugal; [(c)]Departamento de Física, Universidade de Coimbra,

Coimbra, Portugal; [d]Centro de Física Nuclear da Universidade de Lisboa, Lisbon, Portugal; [e]Departamento de Física, Escola de Ciências, Universidade do Minho, Braga, Portugal; [f]Departamento de Física Teórica y del Cosmos, Universidad de Granada, Granada, Spain; [g]Departamento de Física, Instituto Superior Técnico, Universidade de Lisboa, Lisbon, Portugal
[135] Institute of Physics of the Czech Academy of Sciences, Prague, Czech Republic
[136] Czech Technical University in Prague, Prague, Czech Republic
[137] Charles University, Faculty of Mathematics and Physics, Prague, Czech Republic
[138] Particle Physics Department, Rutherford Appleton Laboratory, Didcot, UK
[139] IRFU, CEA, Université Paris-Saclay, Gif-sur-Yvette, France
[140] Santa Cruz Institute for Particle Physics, University of California Santa Cruz, Santa Cruz, CA, USA
[141] [a]Departamento de Física, Pontificia Universidad Católica de Chile, Santiago, Chile; [b]Millennium Institute for Subatomic physics at high energy frontier (SAPHIR), Santiago, Chile; [c]Instituto de Investigación Multidisciplinario en Ciencia y Tecnología, y Departamento de Física, Universidad de La Serena, La Serena, Chile; [d]Department of Physics, Universidad Andres Bello, Santiago, Chile; [e]Instituto de Alta Investigación, Universidad de Tarapacá, Arica, Chile; [f]Departamento de Física, Universidad Técnica Federico Santa María, Valparaíso, Chile
[142] Department of Physics, Institute of Science, Tokyo, Japan
[143] Department of Physics, University of Washington, Seattle, WA, USA
[144] [a]Institute of Frontier and Interdisciplinary Science and Key Laboratory of Particle Physics and Particle Irradiation (MOE), Shandong University, Qingdao, China; [b]School of Physics, Zhengzhou University, Zhengzhou, China
[145] [a]State Key Laboratory of Dark Matter Physics, School of Physics and Astronomy, Key Laboratory for Particle Astrophysics and Cosmology (MOE), SKLPPC, Shanghai Jiao Tong University, Shanghai, China; [b]State Key Laboratory of Dark Matter Physics, Tsung-Dao Lee Institute, Shanghai Jiao Tong University, Shanghai, China
[146] Department of Physics and Astronomy, University of Sheffield, Sheffield, UK
[147] Department of Physics, Shinshu University, Nagano, Japan
[148] Department Physik, Universität Siegen, Siegen, Germany
[149] Department of Physics, Simon Fraser University, Burnaby, BC, Canada
[150] SLAC National Accelerator Laboratory, Stanford, CA, USA
[151] Department of Physics, Royal Institute of Technology, Stockholm, Sweden
[152] Departments of Physics and Astronomy, Stony Brook University, Stony Brook, NY, USA
[153] Department of Physics and Astronomy, University of Sussex, Brighton, UK
[154] School of Physics, University of Sydney, Sydney, Australia
[155] Institute of Physics, Academia Sinica, Taipei, Taiwan
[156] [a]E. Andronikashvili Institute of Physics, Iv. Javakhishvili Tbilisi State University, Tbilisi, Georgia; [b]High Energy Physics Institute, Tbilisi State University, Tbilisi, Georgia; [c]University of Georgia, Tbilisi, Georgia
[157] Department of Physics, Technion, Israel Institute of Technology, Haifa, Israel
[158] Raymond and Beverly Sackler School of Physics and Astronomy, Tel Aviv University, Tel Aviv, Israel
[159] Department of Physics, Aristotle University of Thessaloniki, Thessaloniki, Greece
[160] International Center for Elementary Particle Physics and Department of Physics, University of Tokyo, Tokyo, Japan
[161] Graduate School of Science and Technology, Tokyo Metropolitan University, Tokyo, Japan
[162] Department of Physics, University of Toronto, Toronto, ON, Canada
[163] [a]TRIUMF, Vancouver, BC, Canada; [b]Department of Physics and Astronomy, York University, Toronto, ON, Canada
[164] Division of Physics and Tomonaga Center for the History of the Universe, Faculty of Pure and Applied Sciences, University of Tsukuba, Tsukuba, Japan
[165] Department of Physics and Astronomy, Tufts University, Medford, MA, USA
[166] Department of Physics and Astronomy, University of California Irvine, Irvine, CA, USA
[167] University of West Attica, Athens, Greece
[168] Department of Physics and Astronomy, University of Uppsala, Uppsala, Sweden
[169] Department of Physics, University of Illinois, Urbana, IL, USA
[170] Instituto de Física Corpuscular (IFIC), Centro Mixto Universidad de Valencia - CSIC, Valencia, Spain
[171] Department of Physics, University of British Columbia, Vancouver, BC, Canada
[172] Department of Physics and Astronomy, University of Victoria, Victoria, BC, Canada
[173] Fakultät für Physik und Astronomie, Julius-Maximilians-Universität Würzburg, Würzburg, Germany
[174] Department of Physics, University of Warwick, Coventry, UK

[175] Waseda University, Tokyo, Japan
[176] Department of Particle Physics and Astrophysics, Weizmann Institute of Science, Rehovot, Israel
[177] Department of Physics, University of Wisconsin, Madison, WI, USA
[178] Fakultät für Mathematik und Naturwissenschaften, Fachgruppe Physik, Bergische Universität Wuppertal, Wuppertal, Germany
[179] Department of Physics, Yale University, New Haven, CT, USA
[180] Yerevan Physics Institute, Yerevan, Armenia

[a] Also at Affiliated with an Institute Covered by a Cooperation Agreement with CERN, Geneva, Switzerland
[b] Also at An-Najah National University, Nablus, Palestine
[c] Also at Borough of Manhattan Community College, City University of New York, New York, NY, USA
[d] Also at Center for High Energy Physics, Peking University, Beijing, China
[e] Also at Center for Interdisciplinary Research and Innovation (CIRI-AUTH), Thessaloniki, Greece
[f] Also at CERN, Geneva, Switzerland
[g] Also at CMD-AC UNEC Research Center, Azerbaijan State University of Economics (UNEC), Baku, Azerbaijan
[h] Also at Département de Physique Nucléaire et Corpusculaire, Université de Genève, Geneva, Switzerland
[i] Also at Departament de Fisica de la Universitat Autonoma de Barcelona, Barcelona, Spain
[j] Also at Department of Financial and Management Engineering, University of the Aegean, Chios, Greece
[k] Also at Department of Mathematical Sciences, University of South Africa, Johannesburg, South Africa
[l] Also at Department of Modern Physics and State Key Laboratory of Particle Detection and Electronics, University of Science and Technology of China, Hefei, China
[m] Also at Department of Physics, Bolu Abant Izzet Baysal University, Bolu, Türkiye
[n] Also at Department of Physics, California State University, Sacramento, USA
[o] Also at Department of Physics, King's College London, London, UK
[p] Also at Department of Physics, Stanford University, Stanford, CA, USA
[q] Also at Department of Physics, Stellenbosch University, Stellenbosch, South Africa
[r] Also at Department of Physics, University of Fribourg, Fribourg, Switzerland
[s] Also at Department of Physics, University of Thessaly, Vólos, Greece
[t] Also at Department of Physics, Westmont College, Santa Barbara, USA
[u] Also at Faculty of Physics, Sofia University, 'St. Kliment Ohridski', Sofia, Bulgaria
[v] Also at Hellenic Open University, Patras, Greece
[w] Also at Henan University, Kaifeng, China
[x] Also at Imam Mohammad Ibn Saud Islamic University, Riyadh, Saudi Arabia
[y] Also at Institucio Catalana de Recerca i Estudis Avancats, ICREA, Barcelona, Spain
[z] Also at Institut für Experimentalphysik, Universität Hamburg, Hamburg, Germany
[aa] Also at Institute for Nuclear Research and Nuclear Energy (INRNE) of the Bulgarian Academy of Sciences, Sofia, Bulgaria
[ab] Also at Institute of Applied Physics, Mohammed VI Polytechnic University, Ben Guerir, Morocco
[ac] Also at Institute of Particle Physics (IPP), Edmonton, Canada
[ad] Also at Institute of Physics and Technology, Mongolian Academy of Sciences, Ulaanbaatar, Mongolia
[ae] Also at Institute of Physics, Azerbaijan Academy of Sciences, Baku, Azerbaijan
[af] Also at Institute of Theoretical Physics, Ilia State University, Tbilisi, Georgia
[ag] Also at National Institute of Physics, University of the Philippines Diliman (Philippines), Quezon City, Philippines
[ah] Also at Technical University of Munich, Munich, Germany
[ai] Also at The Collaborative Innovation Center of Quantum Matter (CICQM), Beijing, China
[aj] Also at TRIUMF, Vancouver, BC, Canada
[ak] Also at Università di Napoli Parthenope, Naples, Italy
[al] Also at Department of Physics, University of Colorado Boulder, Colorado, USA
[am] Also at University of the Western Cape, Cape Town, South Africa
[an] Also at Washington College, Chestertown, MD, USA
[ao] Also at Physics Department, Yeditepe University, Istanbul, Türkiye
* Deceased